

NAVAL POSTGRADUATE SCHOOL MONTEREY, CALIFORNIA



19990504 088

THESIS

ADRIATIC SEA SURFACE TEMPERATURE: SATELLITE
AND DRIFTER OBSERVATIONS, MAY TO OCTOBER,
1995

by

Jason A. Vogt

March 1999

Thesis Advisor:
Second Reader:

Pierre-Marie Poulain
Philip A. Durkee

Approved for public release; distribution is unlimited.

REPORT DOCUMENTATION PAGE			Form Approved OMB No. 0704-0188	
Public reporting burden for this collection of information is estimated to average 1 hour per response, including the time for reviewing instruction, searching existing data sources, gathering and maintaining the data needed, and completing and reviewing the collection of information. Send comments regarding this burden estimate or any other aspect of this collection of information, including suggestions for reducing this burden, to Washington headquarters Services, Directorate for Information Operations and Reports, 1215 Jefferson Davis Highway, Suite 1204, Arlington, VA 22202-4302, and to the Office of Management and Budget, Paperwork Reduction Project (0704-0188) Washington DC 20503.				
1. AGENCY USE ONLY (Leave blank)		2. REPORT DATE March 1999		3. REPORT TYPE AND DATES COVERED Master's Thesis
4. TITLE AND SUBTITLE ADRIATIC SEA SURFACE TEMPERATURE: SATELLITE AND DRIFTER OBSERVATIONS, MAY TO OCTOBER, 1995				5. FUNDING NUMBERS
6. AUTHOR(S) Vogt, Jason A.				
7. PERFORMING ORGANIZATION NAME(S) AND ADDRESS(ES) Naval Postgraduate School Monterey, CA 93943-5000				8. PERFORMING ORGANIZATION REPORT NUMBER
9. SPONSORING / MONITORING AGENCY NAME(S) AND ADDRESS(ES)				10. SPONSORING / MONITORING AGENCY REPORT NUMBER
11. SUPPLEMENTARY NOTES The views expressed in this thesis are those of the author and do not reflect the official policy or position of the Department of Defense or the U.S. Government.				
12a. DISTRIBUTION / AVAILABILITY STATEMENT Approved for public release; distribution is unlimited.				12b. DISTRIBUTION CODE
13. ABSTRACT (maximum 200 words) The Adriatic Sea is the northernmost semi-enclosed basin of the Mediterranean Sea and has been the subject of various oceanographic studies since the 19th century. Substantial changes in water properties (such as temperature) and in circulation, both spatially and temporally (seasonal) occur as a result of extreme forcings by the local winds and by the fresh water discharge by rivers. In recent years, extensive measurements have been made, primarily through remote sensing techniques. In particular, satellite infrared data were used to study the surface thermal features and associated circulation. In order to improve upon previous results, this study focuses on a period of 6 months (May to October, 1995) in which the full resolution (1.25x1.25 km) satellite images are used to describe and study the variability of the sea surface temperature (SST) and circulation from meso- (days) to seasonal (months) scales. The satellite infrared temperatures are compared to simultaneous and collocated in-situ drifter temperature measurements. They are corrected by removing biases obtained by regression analysis. The corrected images are used to produce maps representing daily, three-day, weekly and monthly Adriatic SSTs. Selected SST composites augmented with drifter overlays disclose important quantitative features of the Adriatic surface waters. The spatial structure and temporal variability of the surface fields are presented and discussed.				
14. SUBJECT TERMS Adriatic, SST, Oceanography, AVHRR, MCSST, Remote sensing				15. NUMBER OF PAGES 102
				16. PRICE CODE
17. SECURITY CLASSIFICATION OF REPORT Unclassified		18. SECURITY CLASSIFICATION OF THIS PAGE Unclassified		19. SECURITY CLASSIFICATION OF ABSTRACT Unclassified
				20. LIMITATION OF ABSTRACT UL

NSN 7540-01-280-5500

Standard Form 298 (Rev. 2-89)
Prescribed by ANSI Std. Z39-18

Approved for public release; distribution is unlimited.

**ADRIATIC SEA SURFACE TEMPERATURE:
SATELLITE AND DRIFTER OBSERVATIONS,
MAY TO OCTOBER, 1995**

Jason A. Vogt
Lieutenant, United States Navy
B.S., United States Naval Academy, 1991

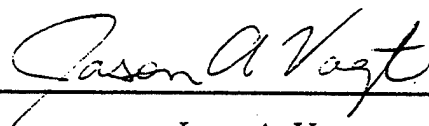
Submitted in partial fulfillment of the
requirements for the degree of

MASTER OF SCIENCE IN PHYSICAL OCEANOGRAPHY

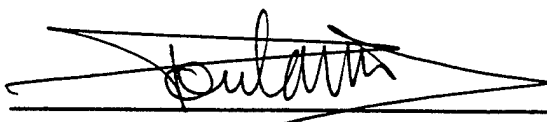
from the

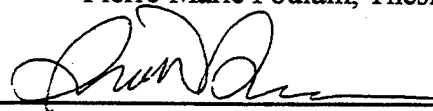
**NAVAL POSTGRADUATE SCHOOL
March 1999**

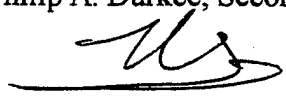
Author:


Jason A. Vogt

Approved by:


Pierre-Marie Poulain, Thesis Advisor


Philip A. Durkee, Second Reader


Roland W. Garwood, Chairman
Department of Oceanography

ABSTRACT

The Adriatic Sea is the northernmost semi-enclosed basin of the Mediterranean Sea and has been the subject of various oceanographic studies since the 19th century. Substantial changes in water properties (such as temperature) and in circulation, both spatially and temporally (seasonal) occur as a result of extreme forcings by the local winds and by the fresh water discharge by rivers. In recent years, extensive measurements have been made, primarily through remote sensing techniques. In particular, satellite infrared data were used to study the surface thermal features and associated circulation.

In order to improve upon previous results, this study focuses on a period of 6 months (May to October, 1995) in which the full resolution (1.25x1.25 km) satellite images are used to describe and study the variability of the sea surface temperature (SST) and circulation from meso- (days) to seasonal (months) scales. The satellite infrared temperatures are compared to simultaneous and collocated in-situ drifter temperature measurements. They are corrected by removing biases obtained by regression analysis. The corrected images are used to produce maps representing daily, three-day, weekly and monthly Adriatic SSTs. Selected SST composites augmented with drifter overlays disclose important quantitative features of the Adriatic surface waters. The spatial structure and temporal variability of the surface fields are presented and discussed.

TABLE OF CONTENTS

I.	INTRODUCTION	1
II.	BACKGROUND	3
	A. TOPOGRAPHY	3
	B. WEATHER	3
	C. SEA SURFACE TEMPERATURE	4
	D. SURFACE CIRCULATION	6
III.	DATA AND METHODS	11
	A. AVHRR	11
	B. MCSST	11
	C. DRIFTER DATA	12
	D. IMAGE PROCESSING	13
	E. DRIFTER VS. SATELLITE TEMPERATURE REGRESSION	16
	F. COMPOSITING	17
	1. One and Three Day Composites	17
	2. Weekly and Monthly Composites	19
IV.	RESULTS	51
	A. MONTHLY COMPOSITES	51
	B. WEEKLY COMPOSITES WITH DRIFTER TRACKS	52
	C. SELECTED 3 DAY AND 1 DAY COMPOSITES WITH DRIFTER TRACKS	57
	1. Period 8-10 July 1995	58
	2. Period 17-19 October 1995	58
V.	DISCUSSION AND CONCLUSIONS	81
VI.	RECOMMENDATIONS	83
	LIST OF REFERENCES	85
	INITIAL DISTRIBUTION LIST	87

LIST OF FIGURES

1.	Adriatic Sea coastline and topography	7
2.	Seasonal surface temperature (CC) maps of the Adriatic Sea. The contour interval is 0.5°C. The field is plotted for expected error less than 30% (from Artegiani et al., 1997)	8
3.	Composite diagram of the low-pass filtered drifter trajectories. Star and solid circle symbols are depicted at the deployment and last "good" transmission sites, respectively (from Poulain, 1999)	9
4.	Map of surface mean currents in 0.250 x 0.25° bins. Gray shades indicate regions deeper than 200, 1000, and 1200 meters (from Poulain, 1999)	9
5.	Schematic diagram of the surface drifter used. The drifter design is similar to the CODE drifter. Four drag-producing vanes provide adherence to the water whereas a small antenna protrudes above sea level for satellite tracking and SET data transmission (from Poulain, 1999)	20
6.	Time distribution of the 664 AVHRR images (images per day)	21
7.	Attitude of Adriatic Sea images (rotation and location of 250x750 grid)	22
8.	Percentage of masked pixels for the cloud/land-masked images	23
9.	Time distribution of AVHRR images (GMT time of day (hours) vs. time of year, for each satellite)	24
10.	(a) Maximum and minimum temperature values for NOAA 09 images. (b) mean and median temperature values for NOAA 09 images	25
11.	(a) Maximum and minimum temperature values for NOAA 12 images. (b) Mean and median temperature values for NOAA 12 images	26
12.	(a) Maximum and minimum temperature values for NOAA 14 images. (b) Mean and median temperature values for NOAA 14 images	27
13.	Flow diagram for determining contemporaneous/collocated drifter and satellite SETs	28
14.	NOAA 09 satellite temperature vs. drifter temperature. Straight lines corresponding to the regression analysis results are overlaid	29
15.	Same as Figure 14 but for NOAA 12 (Day)	30
16.	Same as Figure 14 but for NOAA 12 (Night)	31
17.	Same as Figure 14 but for NOAA 14 (Day)	32
18.	Same as Figure 14 but for NOAA 14 (Night)	33
19.	Composite results based on uncorrected data for July 8, 1995; (a) mean, (b) median, (c) standard deviation, (d) count of images used in composite images	34
20.	Same as Figure 19, but for three-day period (July 8-10, 1995)	35
21.	Same as Figure 19, but for October 20, 1995	36
22.	Same as Figure 19, but for three-day period (October 18-20, 1995)	37

23. Composite results based on data corrected by the median difference for July 8, 1995; (a) mean, (b) median, (c) standard deviation, (d) count of images used in composite images	38
24. Same as Figure 23, but for three-day period (July 8-10, 1995)	39
25. Same as Figure 23, but for October 20, 1995	40
26. Same as Figure 23, but for three-day period (October 18-20, 1995)	41
27. Median temperatures for each of the images (computed over the common pixels only) and "median of medians" temperature during the time periods considered. (a) July 8, 1995, (b) July 8-10, 1995, (c) October 20, 1995, (d) October 18-20, 1994	42
28. For July 8, 1995; (a) Median of satellite corrected images. (b) "Median of medians" correction to (a) . (c) Count of images used	43
29. Same as Figure 28, but for three-day period (July 8-10, 1995)	44
30. Same as Figure 28, but for October 20, 1995	45
31. Same as Figure 28, but for three-day period (October 18-20, 1995)	46
32. 1 and 3 day image compositing flow diagram	47
33. Weekly and monthly image compositing flow diagram	48
34. Composite based on data corrected by the median difference for September 19-25, 1995; (a) mean, (b) median, (c) standard deviation, (d) count of images used in composite images	49
35. Same as Figure 34, but for June, 1995	50
36. SET composite images for (a) May, 1995, (b) June, 1995, (c) July, 1995, (d) August, 1995, (e) September, 1995, (f) October, 1995	60
37. Spatial mean and standard deviation interval of the weekly temperature composites over the Adriatic Sea	62
38. Weekly composite images for (a) May 9-15, 1995, (b) May 16-22, 1995, (c) May 23-29, 1995. The spatial mean was removed and the SET anomaly was normalized by the standard deviation. Weekly drifter trajectories are superimposed, with star (circle) symbols at beginning (end)	63
39. Same as Figure 40, but for (a) May 30 - June 5, 1995, (b) June 6-12, 1995, (c) June 13-19, 1995	64
40. Same as Figure 40, but for (a) June 20-26, 1995, (b) June 27 - July 3, 1995, (c) July 4-10, 1995	65
41. Same as Figure 40, but for (a) July 11-17, 1995, (b) July 18-24, 1995, (c) July 25-31, 1995	66
42. Same as Figure 40, but for (a) August 1-7, 1995, (b) August 8-14, 1995, (c) August 15-21, 1995	66
43. Same as Figure 40, but for (a) August 22-28, 1995, (b) August 29 - September 4, 1995, (c) September 5-11, 1995	68

44. Same as Figure 40, but for (a) September 12-18, 1995, (b) September 19-25, 1995, (c) September 26 - October 2, 1995	69
45. Same as Figure 40, but for (a) October 3-9, 1995, (b) October 10-16, 1995, (c) October 17-23, 1995	70
46. Comparison of weekly mean temperatures at (a) PO River, (b) Istria Peninsula, (c) Gargano Peninsula, (d) Albanian Coast, (e) Otranto Strait (western boundary), (f) Otranto Strait (eastern boundary)	71
47. "Median of median" composite in the southern Adriatic and Otranto Strait region with simultaneous drifters overlaid for period July 8, 1995. Drifter tracks over the same time period are overlaid, with star (circle) symbols at beginning (end) 72	
48. Same as Figure 47, but for July 9, 1995	73
49. Same as Figure 47, but for July 10, 1995	74
50. Same as Figure 47, but for July 8-10, 1995	75
51. Same as Figure 47, but for October 17, 1995	76
52. Same as Figure 47, but for October 18, 1995	77
53. Same as Figure 47, but for October 19, 1995	78
54. Same as Figure 47, but for October 17-19, 1995	79

LIST OF TABLES

1. MCSST Algorithm coefficients to be used with:	
$MCSST = aT_4 + b (T_4 - T_5 + c (T_4 - T_5) (\sec(\theta) - 1) + d$	12
2. Cloud Masking Tests	14
3. Results of the linear regression analysis: Satellite Vs. drifter SST	16
4. Comparison statistics between smoothed drifter and composite satellite SSTs in southern Adriatic and Otranto Strait region	57

I. INTRODUCTION

The Adriatic Sea is the northernmost semi-enclosed basin of the Mediterranean Sea and has been the subject of various oceanographic studies since the 19th century. Substantial changes in water properties (such as temperature) and in circulation, both spatially and temporally (seasonal) occur as a result of extreme forcings by the local winds and by the fresh water discharge by rivers. In recent years, extensive measurements have been made, primarily through remote sensing techniques. These satellite data were used to identify basin-wide and sub-basin scale sea surface temperature (SST) features and associated circulation patterns (Gacic et al., 1997). Limitations in the resolution of the thermal maps used (18x18 km in weekly averages) resulted in seasonal and monthly comparisons only.

In order to improve upon previous results, this study focuses on a shorter time period, May to October, 1995, which is observed in more detail by using satellite images at full resolution of about 1.25x1.25 km. Additionally, these images were compared and corrected with simultaneous and collocated in situ drifter temperature measurements. Temperature estimates were compared by performing linear regressions. This comparison indicated the multichannel SST algorithms mostly overestimated the SST with respect to the in situ measurements. Composite images representing daily, three day, weekly, and monthly composite maps of the SST in the Adriatic were produced. Images were created using raw data, as well as data corrected by removing biases obtained from the regression analyses. The thermal composites augmented with the tracks of satellite tracked surface drifters, disclose quantitative aspects of the surface thermal and circulation fields in the Adriatic from the meso- to the seasonal scales. Specifically, the addition of drifters provides a presentation of flow speed and direction in the thermal field.

This thesis is organized into five chapters. Chapter II provides a detailed background to allow the reader a better understanding of the regional characteristics, the basis for this study, and the tools that were required to complete it. Chapter III discusses the means with which data were collected, organized, manipulated, and presented. The complete results of these methods for the time period of May to October, 1995 are presented in Chapter IV. Discussion, summaries and conclusions make up Chapter V.

II. BACKGROUND

This chapter describes the topography, weather, surface thermal structure and circulation of the Adriatic Sea.

A. TOPOGRAPHY

The Adriatic Sea (Figure 1) is an elongated semi-enclosed ocean basin having an average length and width of 783 km and 243 km respectively. Its major axis lies in the northwest-southeast direction. It is located in the central Mediterranean between the Italian peninsula and the Balkans, and is commonly divided into three regions, north, middle and south.

The northern Adriatic is very shallow with an average depth of only 70 m. A smooth bottom gradually slopes to 100 m and then drops quickly to 200 m just south of Ancona, Italy (Orlic et al., 1992). The middle component of the Adriatic begins here and ends at the Palagruza Sill, a shoal area west of Dubrovnik. The Jabuka Pit, a 280 m deep basin, is the prominent bottom topographic feature at the northern end of the middle Adriatic (Orlic et al., 1992). The southern Adriatic then begins with the Palagruza Sill to the north and ends at the Otranto Strait, where the Adriatic Sea meets the Ionian Sea and the rest of the Mediterranean. This southern area is steep sided with a maximum depth of 1200 m found in its center, known as the South Adriatic Pit. The Otranto Strait has a maximum sill depth of almost 800 m, but generally is an average of 325 m across the 75 km strait. From here, the bottom again deepens as it enters the Ionian Sea (Orlic et al., 1992, Gacic et al., 1997). Islands abruptly rise from deep coastal water all along the rugged eastern coastline of the Adriatic while regular isobaths parallel the western shore (Orlic et al., 1992).

B. WEATHER

Because the Adriatic is a semi-enclosed basin, meteorological conditions strongly influence its surface temperature and circulatory characteristics. The basin is situated between the sub-tropical high pressure zone and the mid-latitude or westerly belt, in which atmospheric disturbances generally move from west to east. Generally, weather systems are dominated by the mid-latitude belt. However, a summer subtropical high pressure zone subverts the westerlies dissipating most disturbances. Mesoscale atmospheric events such as

local winds, gravity waves, etc. may modify the regional weather patterns on time scales ranging from a few days to a week (Orlic et al., 1992).

The high and rocky coastlines in the north and east enhance wind effects on the sea surface. Northeasterly dry winds, known as Bora, can be quite strong (gusts up to 50 m/s) and mostly occur in winter. These Bora events can stir the entire water column over the northern Adriatic region, resulting in a vertically homogeneous medium. The southeasterly Sirocco winds also dominate the winter months. Etesian winds from the northwest blow during the summer months, especially in the south where 53% of all winds are Etesian. Summer air temperatures range between 22-26°C. In the winter the range is from an average of 2°C in the north to an average of 10°C in the south (Orlic et al., 1992). Maximum precipitation occurs during the late fall and minimum precipitation occurs during the summer months. The inland precipitation can exceed 1000 mm/yr, heightening the importance of river runoff to the general circulation of the Adriatic Sea (Orlic et al., 1992).

C. SEA SURFACE TEMPERATURE

The sea surface temperature (SST) of the Adriatic proves to be very seasonal in variability. Figure 2 shows the Adriatic Sea surface temperature maps for the four seasons derived from 41 years of in situ observations (Artegiani et al., 1997). They demonstrate seasonal temperature changes of over 10°C due to the heat exchanged with the atmosphere and other inputs such as rivers. In winter the temperature field exhibits a sharply defined frontal area in the north and along the west coast separating cold waters (as low as 8°C) along the coast from almost uniformly warm (12-15°C) in the rest of the basin. In summer the SST appears more uniform throughout the Adriatic Sea, with smaller cold and warm sub-regions developing all through the basin. During transition periods between winter and summer smaller spatial structures and local thermal front areas have been recognized. During the winter, the temperature gradient associated with the fresh and cold water discharged by the Po River provides a large-scale frontal area dividing the western and eastern parts of the basin along the longitudinal axis as far south as the southern Adriatic. Artegiani et al. (1997) speculates this offshore frontal area retreats toward the western

coastlines during the winter, forming a well-defined frontal jet along the Italian coast.

River discharge into the Adriatic basin significantly influences the surface thermal and velocity fields, particularly the Po River in the north and several rivers along the Albanian coast in the south. Maximum runoff occurs in the autumn following heavy precipitation inland and in the spring after the snow melts. The annual mean runoff from the Po River is 1700 cubic meters per second (Orlic et al., 1992), with no other rivers significantly contributing to the Adriatic along the northern or western coasts. Rivers along the east coast supply an annual mean runoff of 1150 cubic meters per second along the Albanian coast (Orlic et al., 1992). The effects of the Po are seasonal with the freshwater input bringing much colder water into the basin in the winter that brings the northern Adriatic to a temperature colder than the Otranto Strait by as much as 5°C (Gacic et al., 1997). This cold water spreads along the Italian shore in a well defined coastal layer that can be traced as far south as the middle of the southern Adriatic (Figure 2). As the Po inputs warm through the spring and summer, the cold water layer is succeeded by a warm water pool situated in front of the river mouth.

Gacic et al. (1997) provided the first systematic analysis of long-term and seasonal variations of the basin-wide surface thermal structure of the Adriatic Sea using low-resolution advanced very high resolution radiometer (AVHRR) satellite data. A spatial resolution of 18 km allowed analysis of basin and sub-basin sea surface temperature features averaged over monthly and seasonal periods occurring from 1984 through 1992. The seasonal SST maps derived from the AVHRR data are in good agreement with the thermal maps of Artegiani et al. (1997). The analysis of AVHRR satellite SST data showed the absence of any permanent sea surface thermal features in the Adriatic. Instead, the variability of the basin-wide thermal pattern revealed four distinct seasons as well as several recurrent features previously assumed to be constant. Four seasons are unique to the Adriatic, where comparison to the eastern and western Mediterranean find only two main seasonal patterns present.

Seasonal elements perceived by Gacic et al. (1997) included the south Adriatic SST minimum only being evident in late autumn and early winter. Additionally, the surface thermal pattern over the middle Adriatic undergoes especially large seasonal variations, changing from a local SST maximum in spring to a minimum in autumn. The warm plume of

Ionian Surface Water meanders in the southeastern Adriatic and is most prominent in autumn. However, the cold coastal layer along the western shore is most pronounced in winter, a reflection of the colder Po River water spreading along the west coast. Gacic et al. (1997) also described the summer surface thermal structure as characterized by relatively cold and distinct water patches along the eastern shore in the middle and south Adriatic due to coastal upwelling. All of these features were found to not only vary from season to season, but also from year to year.

D. SURFACE CIRCULATION

Overall the circulation of the Adriatic is represented by a basin-wide cyclonic (counter-clockwise) gyre with northward flow along the eastern portion and southward flow along the western coast. Figure 3 demonstrates this cyclonic surface circulation as exhibited by drifter trajectories following the general circulation of the Adriatic during the period December 1994 to March 1996 (Poulain, 1999). A wide current on the eastern side is more pronounced in the winter, while a south bound current on the western side dominates the summer months (Orlic et al., 1992). Smaller cyclonic gyres are encountered in each of the three Adriatic subsections. These smaller gyres are not permanent features, but rather can be labeled as seasonal (Poulain, 1999). Topography influences the flow, particularly around the Jabuka Pit and the South Adriatic Pit. Additionally, the effect of the Po River influences the circulation in the Northern Adriatic. Seasonal variations in the wind and river runoff as well as high frequency wind forcing and density-driven currents and tides (near the northern end of the basin) also disturb the mean flow. Poulain (1999) determined mean currents and graphically expressed the sub-tidal velocity variance, demonstrating the substantial mesoscale and seasonal surface circulation variability (Figure 4).

Thermal infrared images (Gacic et al., 1997) have shown upwelling areas in the southern Adriatic. Created by north and northeasterly winds, these upwelling events affect the general current pattern causing the currents to meander rather than follow the normal north bound circulation pattern. Strong, short duration local winds can also alter the general flow, although this is not frequently seen (Gacic et al., 1997; Poulain, 1999).

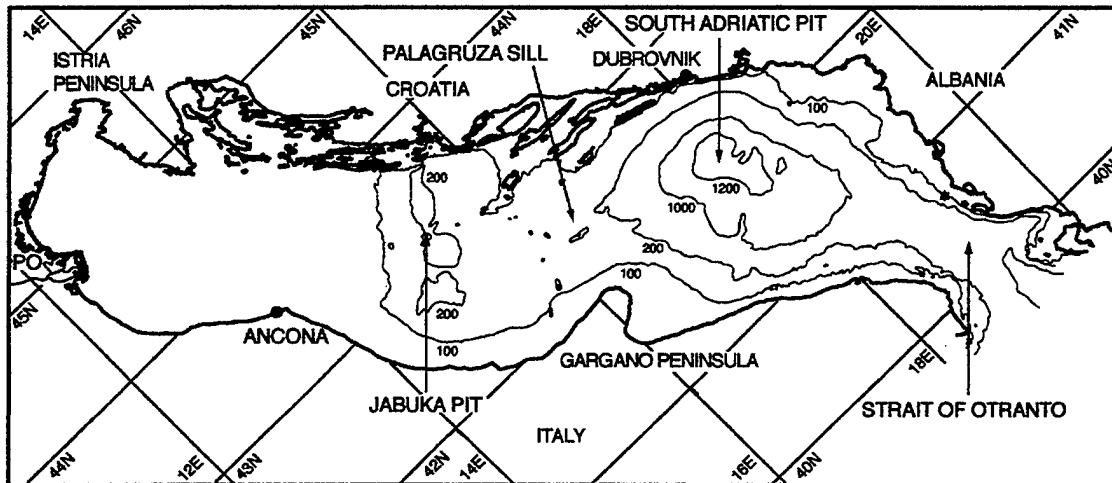


Figure 1. Adriatic Sea coastline and topography.

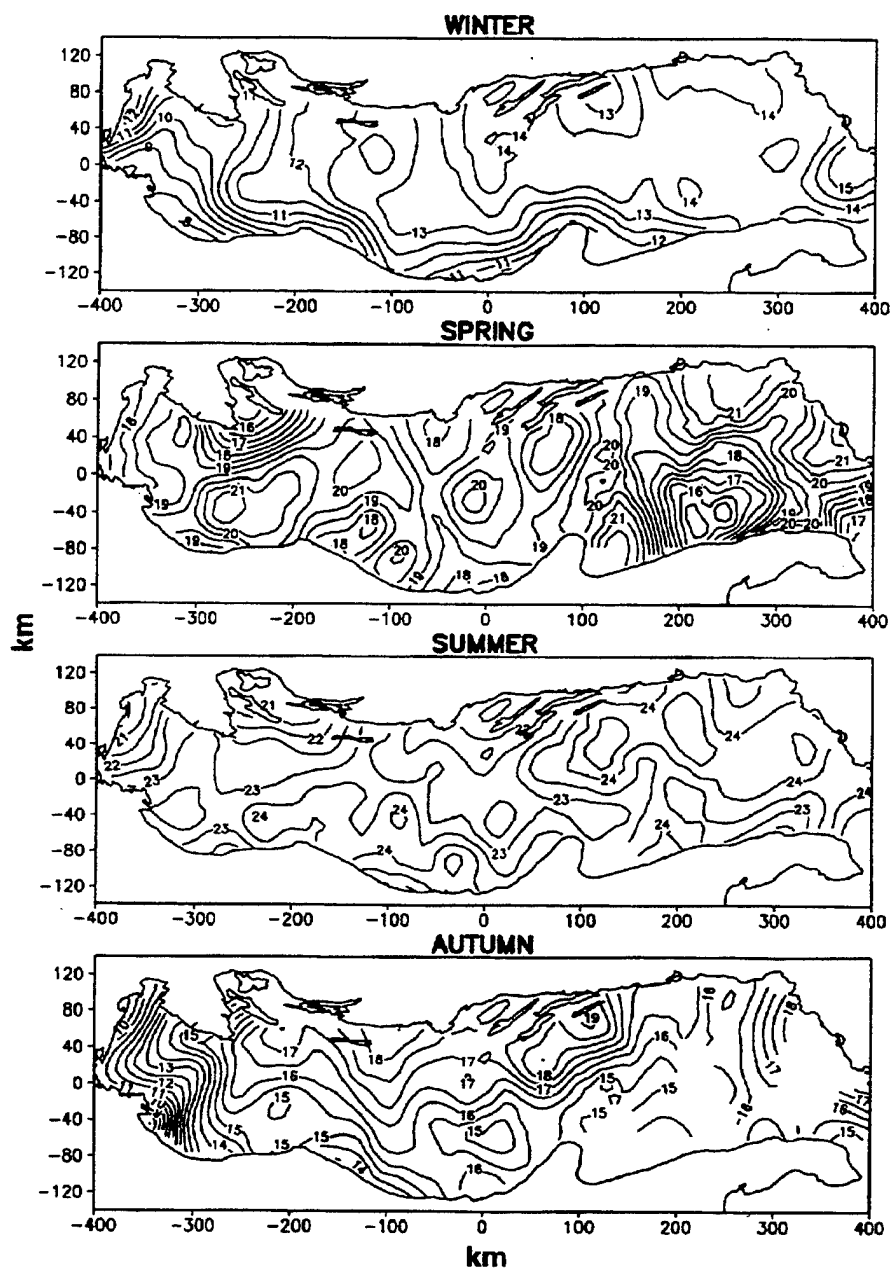


Figure 2. Seasonal surface temperature ($^{\circ}\text{C}$) maps of the Adriatic Sea. The contour interval is 0.5°C . The field is plotted for expected error less than 30% (from Artegiani et al., 1997).

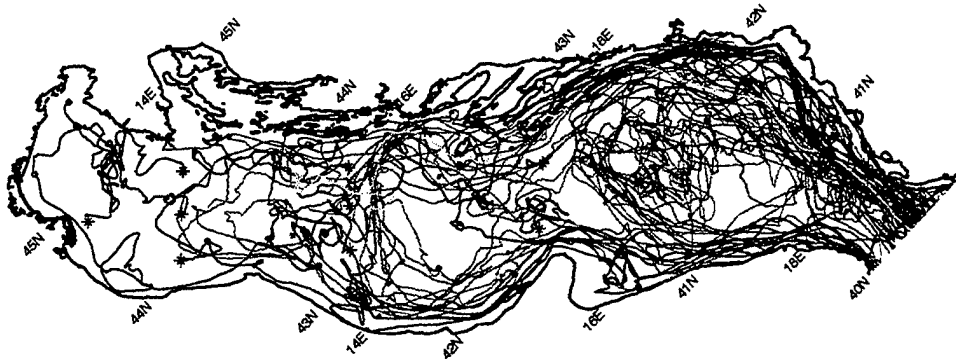


Figure 3. Composite diagram of the low-pass filtered drifter trajectories. Star and solid circle symbols are depicted at the deployment and last "good" transmission sites, respectively (from Poulain, 1999).

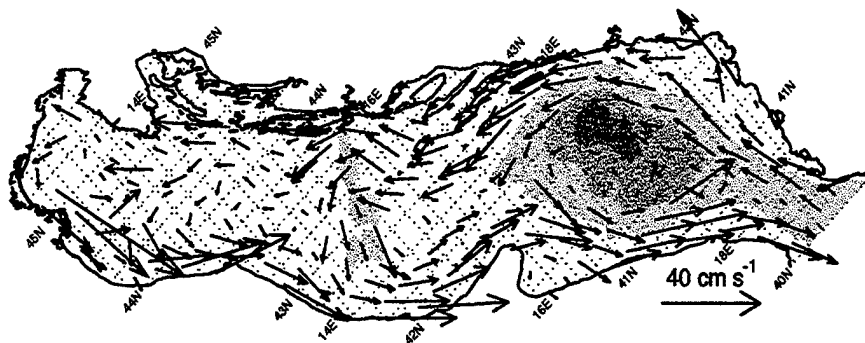


Figure 4. Map of surface mean currents in $0.25^\circ \times 0.25^\circ$ bins. Gray shades indicate regions deeper than 200, 1000, and 1200 meters (from Poulain, 1999).

III. DATA AND METHODS

A. AVHRR

The Advanced Very High Resolution Radiometer (AVHRR) on board the NOAA satellites is a scanning radiometer with five spectral channels, monitoring the visible and near-infrared spectra at 0.62 μm , (channel 1) and 0.91 μm (channel 2), and in the thermal infrared spectrum at 3.74 μm (channel 3), 10.8 μm (channel 4) and 12.0 μm (channel 5). The satellites travel at altitudes of about 820 km on near-polar sun-synchronous orbits. The AVHRR scan angle is 112°, resulting in a swath width on the earth of 2970 km with a ground resolution (pixel size) of 1.1x1.1 km² at the sub-satellite point degrading to 1.5x4.0 km² at the swath edges (Poulain et al., 1998).

The full resolution (1.1 km) AVHRR data are transmitted continuously in High Resolution Picture Transmit (HRPT) mode to ground stations in view of the satellite. For the time period of this study, a receiving station was installed on board the NRV Alliance to collect SST images of the Adriatic Sea. Additionally, AVHRR images were collected on land at NATO SACLANT Undersea research Centre, La Spezia, Italy (Poulain et al., 1998). The data acquisition subsystem was programmed to automatically capture all satellite overpasses in view of the ground station with a minimum satellite elevation of 20°.

B. MCSST

The Multichannel Sea Surface Temperature (MCSST) split window equations provided by NOAA can be used to estimate the sea surface temperature from the AVHRR radiance data. Split-window indicates the use of data specifically from the AVHRR channels 4 and 5 to both calculate temperature and correct for atmospheric attenuation due to water vapor. The MCSST algorithm is described in McClain et al. (1985), and has the form:

$$\text{MCSST} = a T_4 + b (T_4 - T_5) + c (T_4 - T_5)(\sec(\theta) - 1) + d$$

where MCSST is the SST in Kelvin, T_4 and T_5 are channel 4 and 5 brightness temperatures in °C, θ is the satellite zenith angle (the angle between the local zenith of the pixel and the satellite view path to the pixel), a , b , c , and d are linear regression coefficients

obtained from global drifting buoy temperature measurements. These coefficients vary for each satellite and also vary for day versus night computations in the case of two of the satellites used in this study. The coefficients, provided by NOAA, are listed in Table 1.

satellite	a	b	c	d	remark
NOAA-9	0.9731	2.6353	0	265.479	day/night
NOAA-12	0.963563	2.579211	0.242598	263.006	day
	0.967077	2.384376	0.480788	263.94	night
NOAA-14	1.017342	2.139588	0.779706	278.43	day
	1.029088	2.275385	0.752567	282.24	night

Table 1. MCSST Algorithm Coefficients to be used with:

$$\text{MCSST} = a T_4 + b (T_4 - T_5) + c (T_4 - T_5)(\sec(\theta) - 1) + d$$

Global estimates of accuracy achieved with MCSST algorithms have been computed by Strong and McClain (1984). Comparisons with data from ships-of-opportunity, moored buoys, and drifting buoys for the period November 1981 to August 1982 resulted in RMS differences of 1.81, 1.05, and 0.68°C, respectively. Of the MCSST algorithms, the split-window equations provide the greatest accuracy as they do not use channel 3 data, which can have random noise of 1-1.5°C and is susceptible to solar reflection at dawn or dusk.

The NOAA-9 satellite is no longer used operationally, therefore its calibration constants are not maintained up-to-date by NOAA. Consequently, NOAA-9 images used in this work may have an offset of several degrees compared to the immediately preceding or following NOAA-12 and NOAA-14 images (Poulain et al., 1998).

C. DRIFTER DATA

More than 60 drifters were deployed in the Adriatic Sea by SACLANT to study the spatial characteristics and the temporal variability of its surface circulation. Most of the drifters were released in the eastern side of the Otranto Strait during five deployment episodes (December 1994, May 1995, July 1995, August 1995, and October 1995). Additionally, ten drifters were released in the northern and middle Adriatic in May 1995. The drifters provided surface current and temperature data from December 1994 to March 1996 (Poulain, 1999). The surface drifters used are similar to the one used in the Coastal Ocean Dynamics Experiment (CODE) (Davis, 1985). It consists of a one meter

long tube with four drag-producing vanes extending radially from the tube over its entire length (Figure 5). A small antenna for satellite tracking and data transmission is attached on the top of the tube and extends about 37 cm above the sea level. A thermistor is embedded in the main tubular hull at about 40 cm under the sea level for measuring sea surface temperature (SST). The thermistor is calibrated to $\pm 0.1^{\circ}\text{C}$ in the range of -5 to 39°C (Poulain, 1999).

The drifters were tracked by the Argos system carried by the NOAA satellites. The drifter emits a fixed frequency (401.65 MHz) signal, as well as SST and battery voltages, every 90 seconds. For each satellite overpass, the drifter location is calculated from the Doppler shift of the signal provided by the relative motion of the satellite (accuracy of a few hundred meters).

The raw position and temperature data were edited, objectively interpolated and low-pass filtered (Poulain et al., 1996; Hansen and Poulain, 1996). Velocity components were then estimated from centered finite differences of the interpolated latitudes and longitudes. The processed drifter data made available to us consisted of the edited data and the smoothed time series of latitude, longitude, SST, and the zonal and meridional components of velocity, sampled at uniform six hour intervals.

D. IMAGE PROCESSING

The images were originally processed at the University of Hawaii Satellite Oceanography Laboratory. Processing included calibration, navigation, cloud detection, remapping to a common grid, and production of a CD-ROM disk in which these results were published (Poulain et al. 1998). The processed data includes 664 images over a six month period from May to October, 1995 (Figure 6). Each image consists of a 250×750 pixel representation of the Adriatic. The pixel size is $1.25 \text{ km} \times 1.25$. These images were rotated 45° counterclockwise and centered at 43°N 16°E as shown in Figure 7 (Poulain et al., 1998).

Detection of clear versus cloud contaminated pixels has a large effect on satellite-derived SST accuracy. In order to determine which pixels were useful, the data were subjected to a sequence of tests to identify and eliminate cloudy areas. Six tests were applied to each pixel of the entire domain of every image. The tests are summarized in Table 2.

Test number	Test	Remark
1	sun reflection > 25°	
2	$T_{\min} < SST < T_{\max}$	
3	std dev $T_4 \leq 0.3^{\circ}\text{C}$	
4	std dev Ch 2 $\leq 0.2\%$	Daytime only
5	$\text{abs}(T_3 - T_4) \leq 3.0^{\circ}\text{C}$	
6	land mask	
7	Ch 1/Ch 2 ≥ 1.35	Daytime only

Table 2. Cloud Masking Tests.

The specular reflection of sunlight on a smooth sea surface results in a decreased channel 1 to channel 2 ratio, even for clear pixels. Over those areas the channel 3 values are also much larger than those of channel 4. This situation could also result from the presence of low, warm clouds (fog) or high cirrostratus; it is therefore not possible to tell whether such a pixel is clear or cloudy. Consequently, the first test flagged all pixels where the sun reflection angle was less than 25°, to allow selective use of the fifth and seventh tests.

The second test compares the calculated MCSST value to those expected from the climatology of the region. The SST climatology for the Adriatic and Ionian seas issued by the University of Liege, Belgium, was used. The ranges used are: winter, 7.9-17.0°C; spring, 14.6-20.7°C; summer, 21.6-26.3°C; fall, 14.8-22.6°C. This seasonal cycle was interpolated to a fortnightly time step, and the resulting ranges were broadened by lowering the minima by 1°C and increasing the maxima by 1°C.

The third test is based on the variations in temperature due to the uneven cloud-top heights of most convective clouds, which are detectable when comparing channel 4 brightness temperatures between neighboring pixels (called a textural test). To determine pass/fail criteria the standard deviation of each 3x3 pixel array was calculated and the value recorded at the center pixel. A maximum standard deviation of 0.3°C was selected for clear pixels.

The fourth test uses channel 2 values for a textural test. The nonuniform nature of most cloud tops causes variations in reflectance

received by the visible and near-infrared channels in daytime. Pixels of daytime images with a standard deviation of more than 0.2% albedo fail.

A fifth test to detect stratiform clouds is based on differences between the infrared channels. The three infrared wavelengths have different sensitivities to emitted surface radiation, emitted atmospheric radiation, reflected solar radiation, and absorption by water vapor. In this Mediterranean region of relatively low atmospheric moisture, a maximum difference of 3°C between channel 3 and channel 4 was selected for clear pixels.

Approximately 50% of the 250x750 image corresponds to land region around the Adriatic Sea. These pixels were eliminated using a land mask (test 6).

The seventh test compares the radiance ratio of the visible to near-infrared (channels 1 and 2) for those pixels where the mean sun zenith angle is less than 80°. Differences between channel 1 and 2 values are very small for clouds. In contrast, over clear sea surface molecular and aerosol scattering result in increased radiance at shorter wavelengths. A minimum threshold of 1.35 for cloud-free sea surface was selected.

The data were recorded as black and white GIF images available on the CD-ROM disk. Because MATLAB is incapable of reading GIF images, the data were converted to XWD binary files. A linear mapping was then applied using MATLAB to convert the digital count (0-255) to sea surface temperatures in degrees Celsius:

$$\text{byte_value} = (\text{temperature_degree_C} - 5) * 10 ,$$
$$\text{temperature_degree_C} = (\text{byte_value}/10) + 5 .$$

The percentage of non-masked pixels in each image (Figure 8) is a good measure of its usefulness. The masking that was applied to each image uses all seven tests of table 2 and is due to both cloud cover and ground masking. Images with approximately 52% of non-masked pixels correspond to full thermal fields of the Adriatic basin (no cloud cover on the water).

Passes occurred approximately twice a day for each satellite. Figure 9 shows the distribution of images for the satellites occurring at roughly the same time each day (near 9 and 21 GMT for NOAA 9, near 6

and 18 GMT for NOAA 12, and near 0 and 12 GMT for NOAA 14). Additionally, each pass was analyzed for mean, median, maximum and minimum temperature values of the masked images (Figures 10, 11, 12). For each satellite, a seasonal temperature variation is evident.

E. DRIFTER VS SATELLITE TEMPERATURE REGRESSION

In order to determine if any additional corrections were necessary to improve the accuracy of the satellite-derived SSTs, a comparison analysis was performed between collocated and simultaneous in situ edited drifter temperature data and satellite MCSST retrievals for the 664 images (Figure 13). Each image time period was compared to more than 60 drifter data sets to determine if data existed within ten minutes of the satellite image interval. If there was coincidence between a drifter and image time, and the drifter laid within the Adriatic Sea, the image was inspected for the cloud-free pixel closest to the drifter location. When that cloud-free pixel was among the closest four pixels, the image latitude, longitude, and SST were recorded along with the drifter latitude, longitude, SST and drifter identification. If a drifter SST was available but no location was available (due to weak signal), the drifter data set was examined to determine if the immediately preceding and subsequent data points could be utilized to interpolate the drifter position.

The comparisons were divided into categories defined by the satellite that produced the image and time of day, corresponding to the 5 MCSST algorithms shown in Table 1. If corresponding satellite and drifter SST points were found, they were plotted in Figures 14 through 18. Statistical analysis was conducted for each category with results listed in Table 3.

satellite	time	number of points	correlation coefficient	mean diff	standard dev	median diff
9	all	84	0.9751	-0.4792	1.6655	-0.7528
12	day	147	0.9869	0.7433	0.5235	0.7433
	night	240	0.9685	0.5192	0.9014	0.4773
14	day	237	0.9752	1.1103	0.7105	1.1103
	night	84	0.9751	0.5109	0.6830	0.5109

Table 3. Results of the linear regression analysis: Satellite Vs drifter SST.

A linear regression was applied to each group of drifter and satellite SST points. The regression curves are plotted on Figures 14 through 18. Additionally, the regression was "forced" to a slope of one to determine the mean differences between the drifter and satellite temperatures. The median difference was also estimated.

F. COMPOSITING

1. One and Three Day Composites

In order to create composite images, each satellite image was read and processed as described above, and then placed into a three dimensional matrix hereafter referred to as the "cube". The cube has dimensions of 250 pixels by 750 pixels by the number of satellite images existing during the time period being composed. The cube was then manipulated to statistically determine the mean, median, and standard deviation at each pixel within the 250x750 region characterizing the Adriatic, as well as provide a count of how many images provided cloud free data (Figures 19 through 22).

To better explain the compositing procedure, examples were taken from two time periods; middle July and late October, 1995. Figure 8 shows two relatively clear periods in the data set near days 190 through 220 and again from 250 to 295. A significant number of images in these periods exhibit minimal cloud coverage (roughly 50 to 60% masked images). Thus, the compositing examples correspond to ideal conditions with mostly clear images. The periods used to describe the one and three day compositing technique are 08 July and 20 October, and 08 to 10 July and 18 to 20 October.

Corrections were made to individual images in the cube to reduce differences between satellites and time of day, and to improve the SST accuracy for each image. The median temperature differences (Table 3) were applied to the individual images within the cube. This "corrected cube" was then manipulated as before to determine a corrected mean, median, and standard deviation (Figures 23 through 26). As expected, the count of images remained unchanged from Figures 19 through 22 and Figures 23 through 26. By correcting each satellite image, the corrected mean and median values decreased slightly as the images were calibrated. The correction caused the temperature standard deviation over the composite to decrease.

An additional correction was applied to all images in an effort to further decrease offsets between images. By determining how many cloud-free pixels were common to all images, a direct comparison was made from image to image using these corresponding common pixels. The median SST over the common cloud-free pixels was retrieved for each image, then the median of these medians over the time period considered was computed. By applying a correction to each image using the difference between the individual image common pixel median and the median of all image common pixel medians, the "median of the medians" (Figure 27), a median composite was produced with less dependence on any individual image or difference based on satellite, SST algorithm, or time of day. Figures 28 through 31 compare the corrected medians (identical to medians found in Figures 23-26) to the "median of medians" correction results.

It should be noted that the values of Figure 27 do not necessarily represent the median temperatures of the composite. Varying numbers of pixels common to all images affect the median of the common median values. For example, Figure 28 (representing July 08) compares approximately 32,000 pixels from each image while Figure 29 (July 08 through 10) corrects the images based on the median of only two pixels. Hence, if no cloud-free pixels are common to all images, no correction is made. Figures 30 and 31 are corrected images for October 20 and October 18 to 20 using approximately 30,000 and 2200 pixels respectively.

The "median of the medians" composite was used for one and three day comparisons during this study, and is summarized in Figure 32.

Examination of Figure 30 shows the usefulness of the "median of the medians" technique. For the most part, the "median of the median" method results in small temperature corrections in the final composite images. Comparing Figure 30a to 30b demonstrates slight differences in composites created from the same images, particularly what appears to be a front in the southern Adriatic running across the basin (A). Figure 30c shows the same line across the Adriatic (A), but as a result of a satellite pass not including the entire southern basin. The difference provided by compositing four versus five images leaves the appearance of a possible thermal front where none exists. The "median of the medians" allows a correction to be made to each image with respect to the other images. By correcting the composite with the "median of the medians", features unique to a single image can be reduced or eliminated in the

composite, providing a better "undistorted" combination as seen in Figure 30b.

2. Weekly and Monthly Composites

Composites were also created for time periods of seven days and for each month of the data set. The composites were obtained in the same manner described for the one and three day compositing, with the exception of the omission of the "median of the medians" technique. Because the likelihood of finding common cloud-free pixels in all images compared for periods of a week or more is small, weekly and monthly compositing only corrects the individual images with the mean difference (Table 3) and simply combines the image. Figure 33 graphically shows the steps taken to complete the weekly and monthly composite images, while Figures 34 and 35 present the results for weekly and monthly compositions.

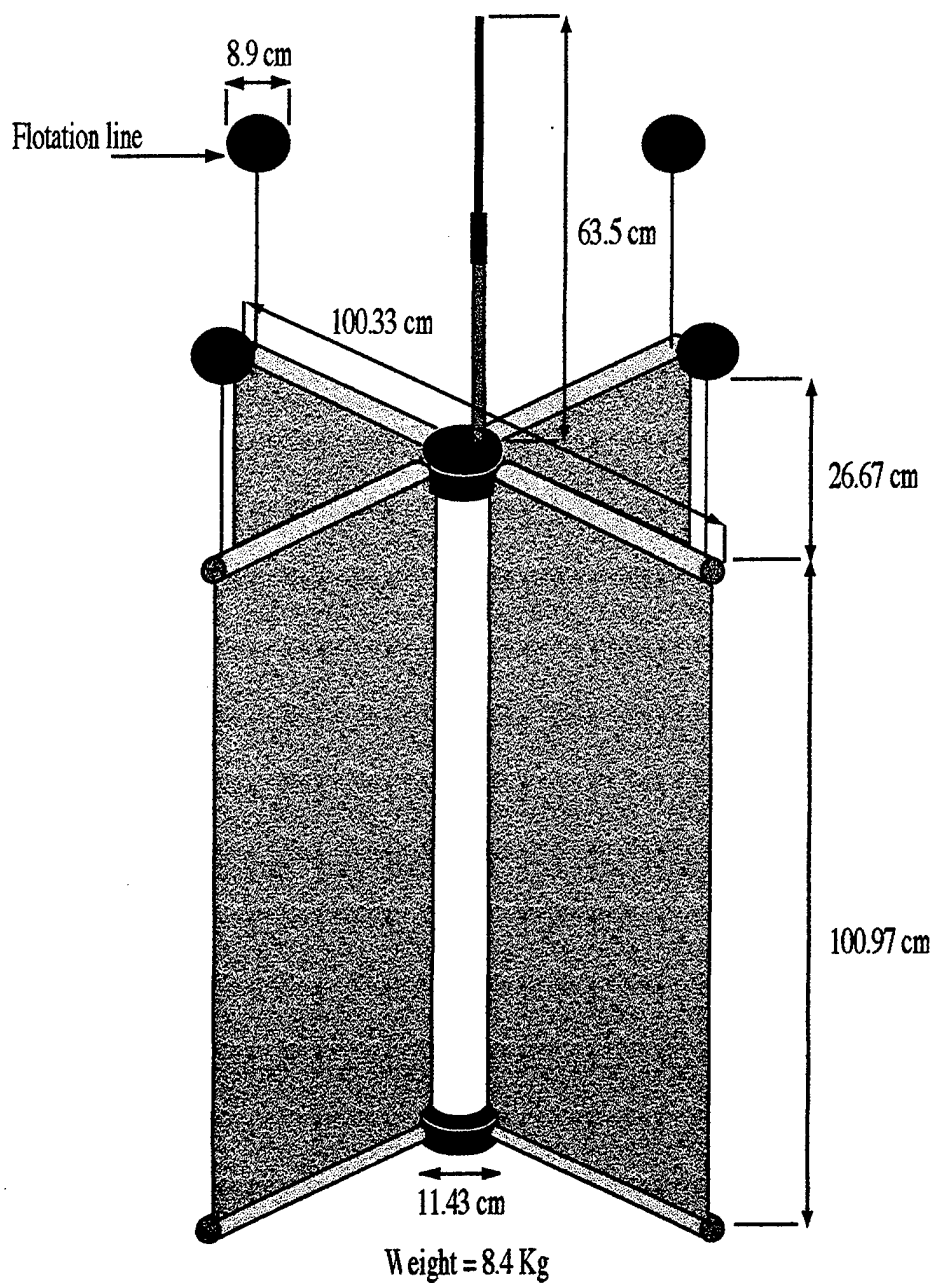


Figure 5. Schematic diagram of the surface drifter used. The drifter design is similar to the CODE drifter. Four drag-producing vanes provide adherence to the water whereas a small antenna protrudes above sea level for satellite tracking and SST data transmission (from Poulain, 1999).

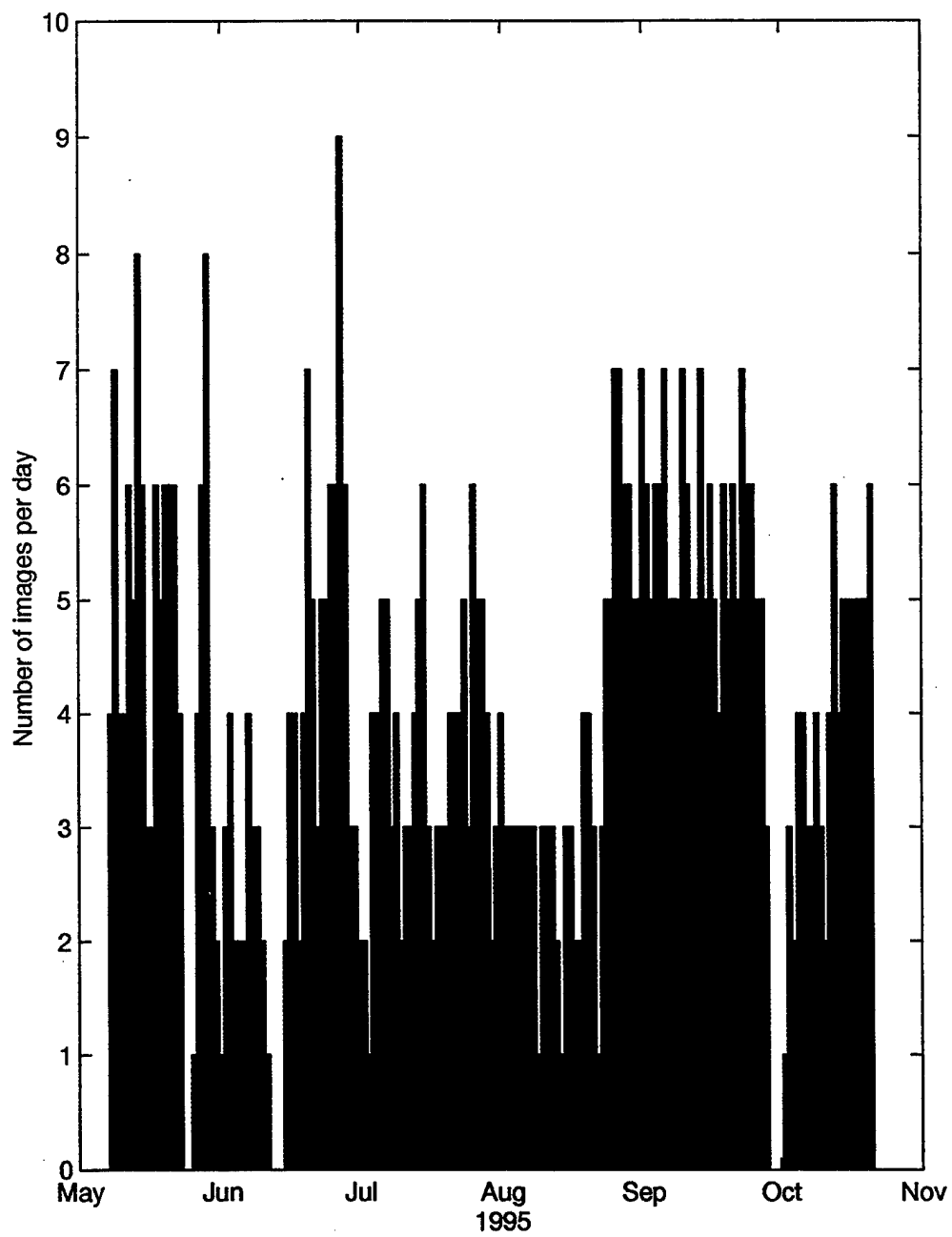


Figure 6. Time distribution of the 664 AVHRR images (images per day)

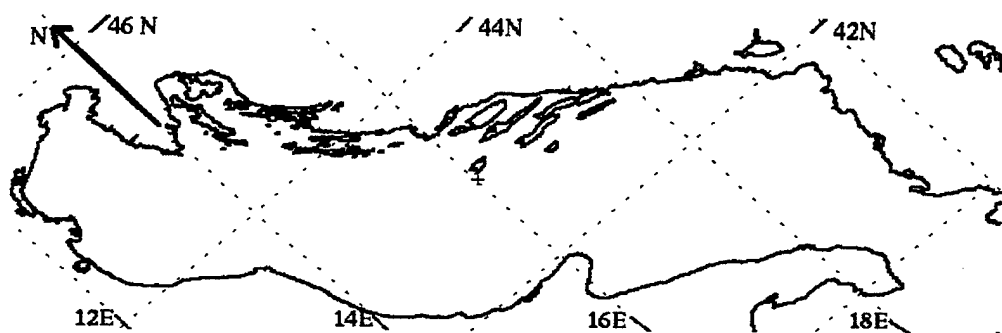


Figure 7. Attitude of Adriatic Sea images
(rotation and location of 250 x 750 grid).

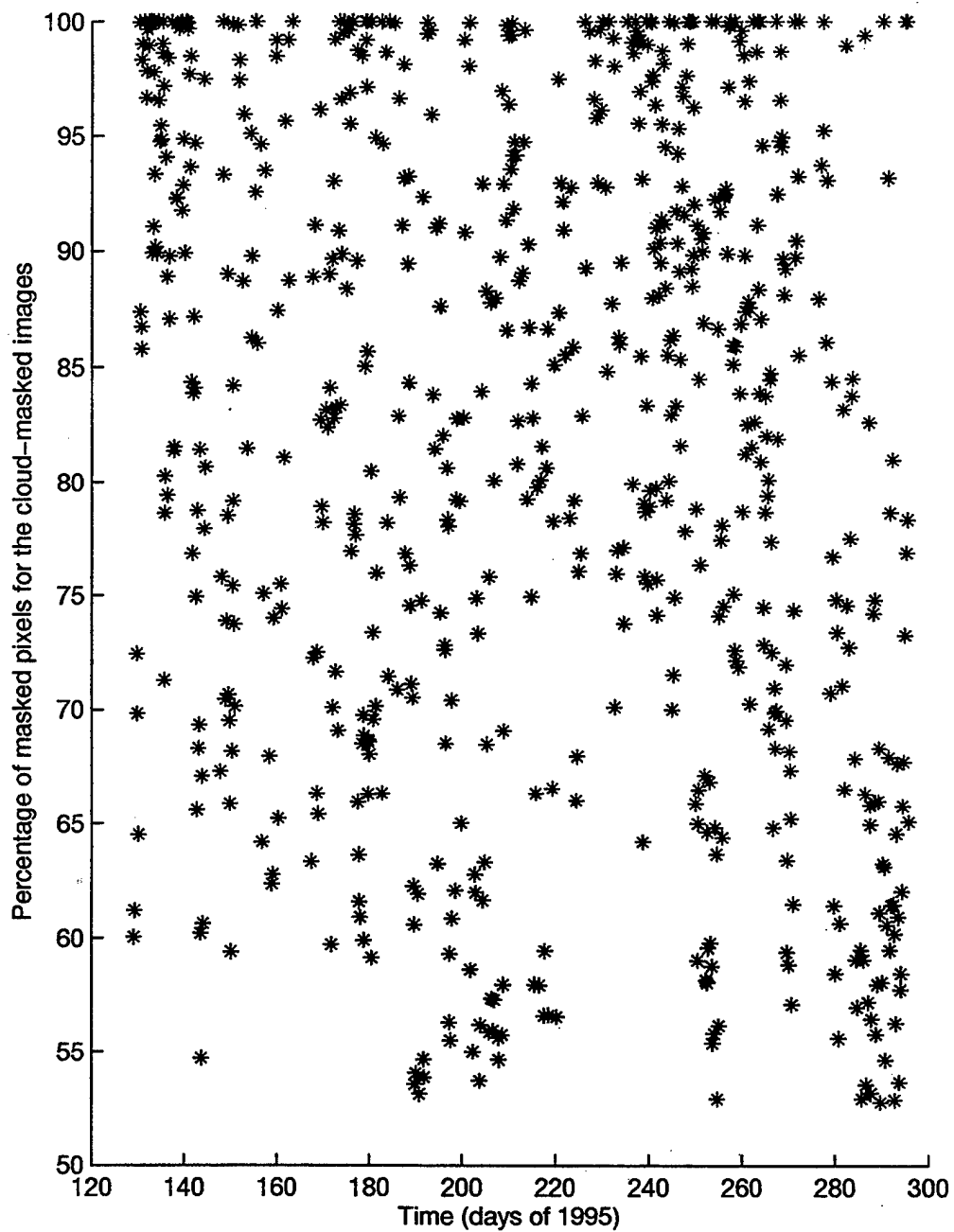


Figure 8. Percentage of masked pixels for the cloud/land-masked images

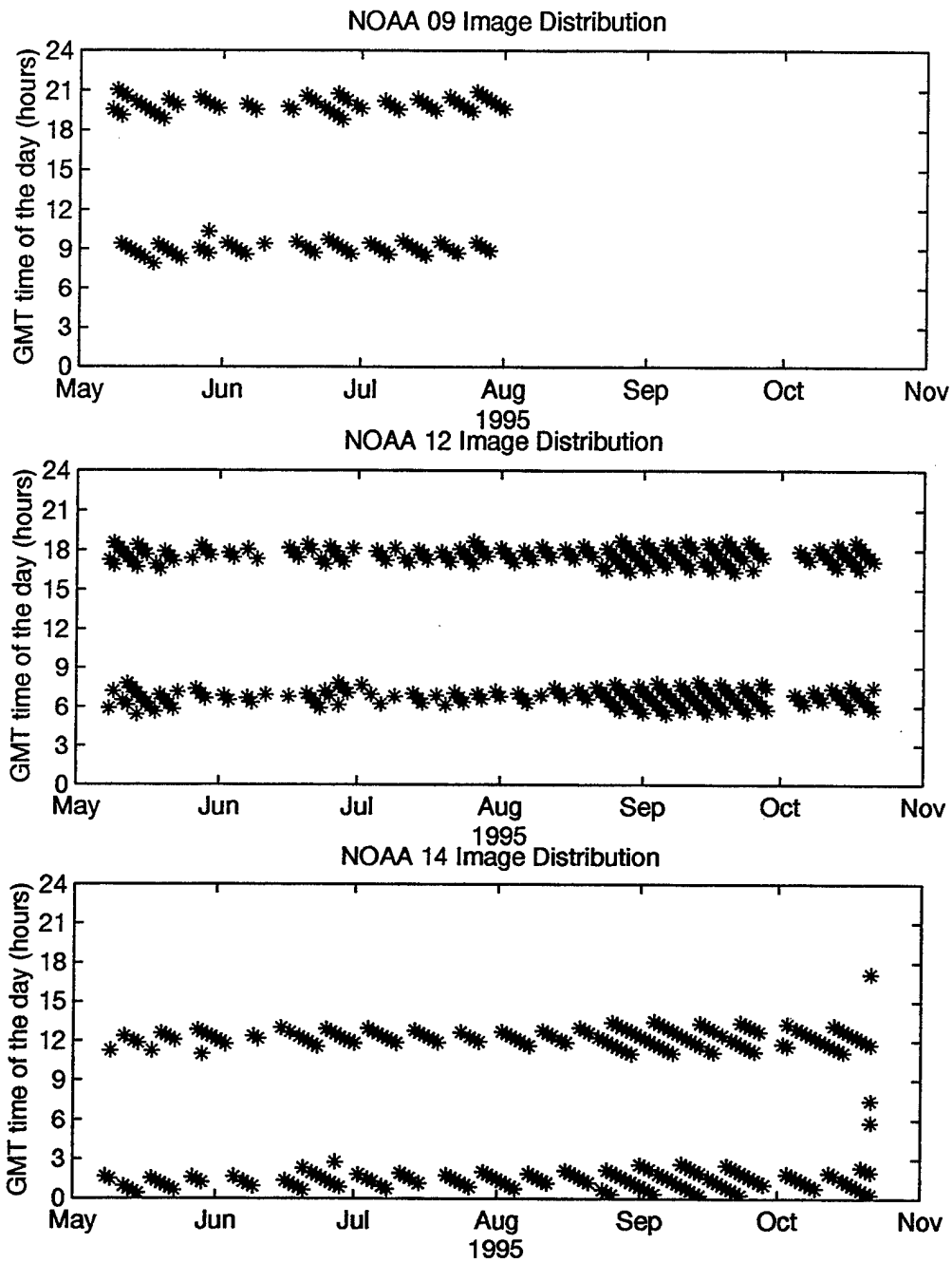


Figure 9. Time distribution of AVHRR images (GMT time of day (hours) vs. time of year, for each satellite).

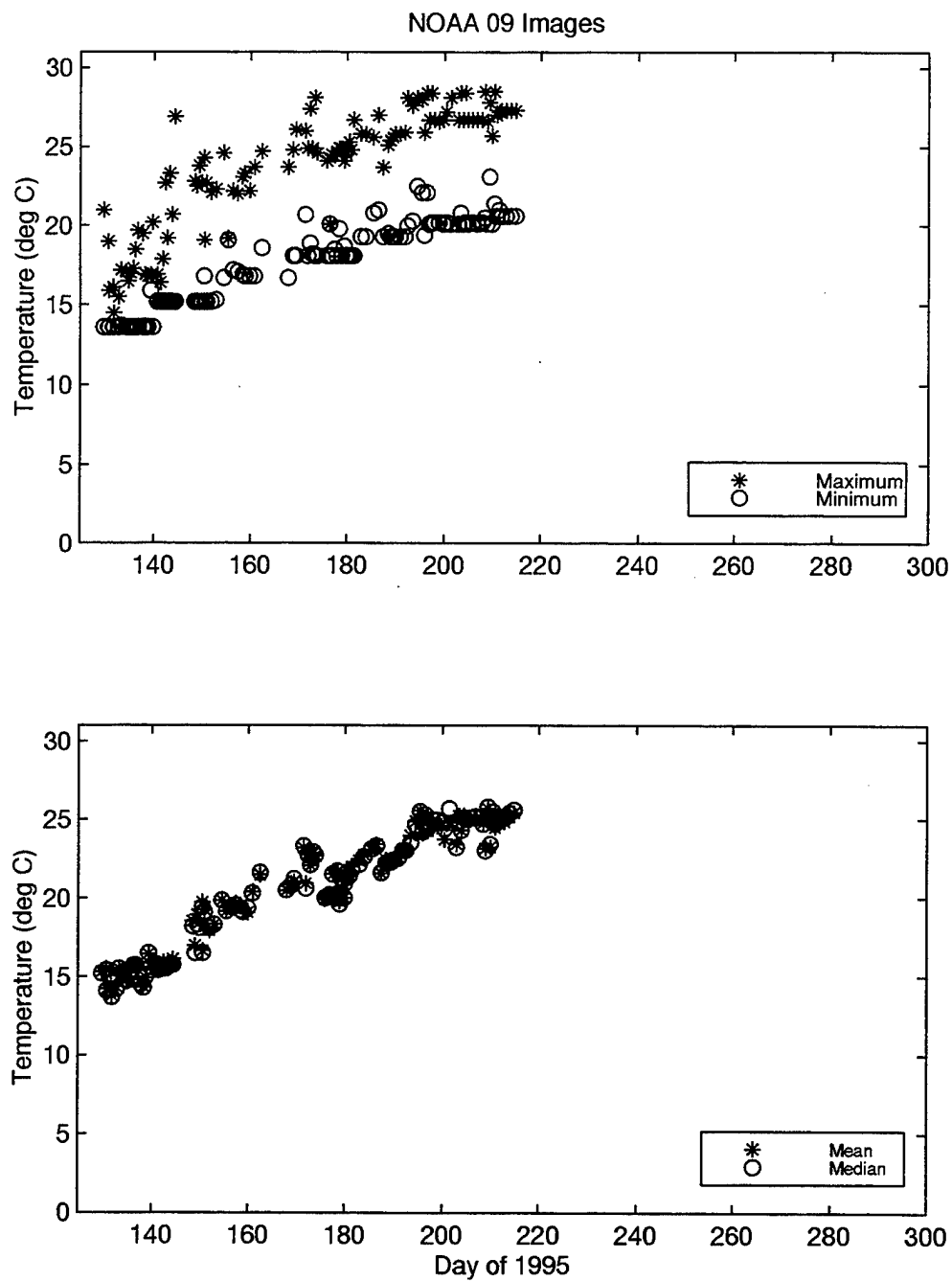


Figure 10. (a) Maximum and minimum temperature values for NOAA 9 images.
(b) Mean and median temperature values for NOAA 9 images.

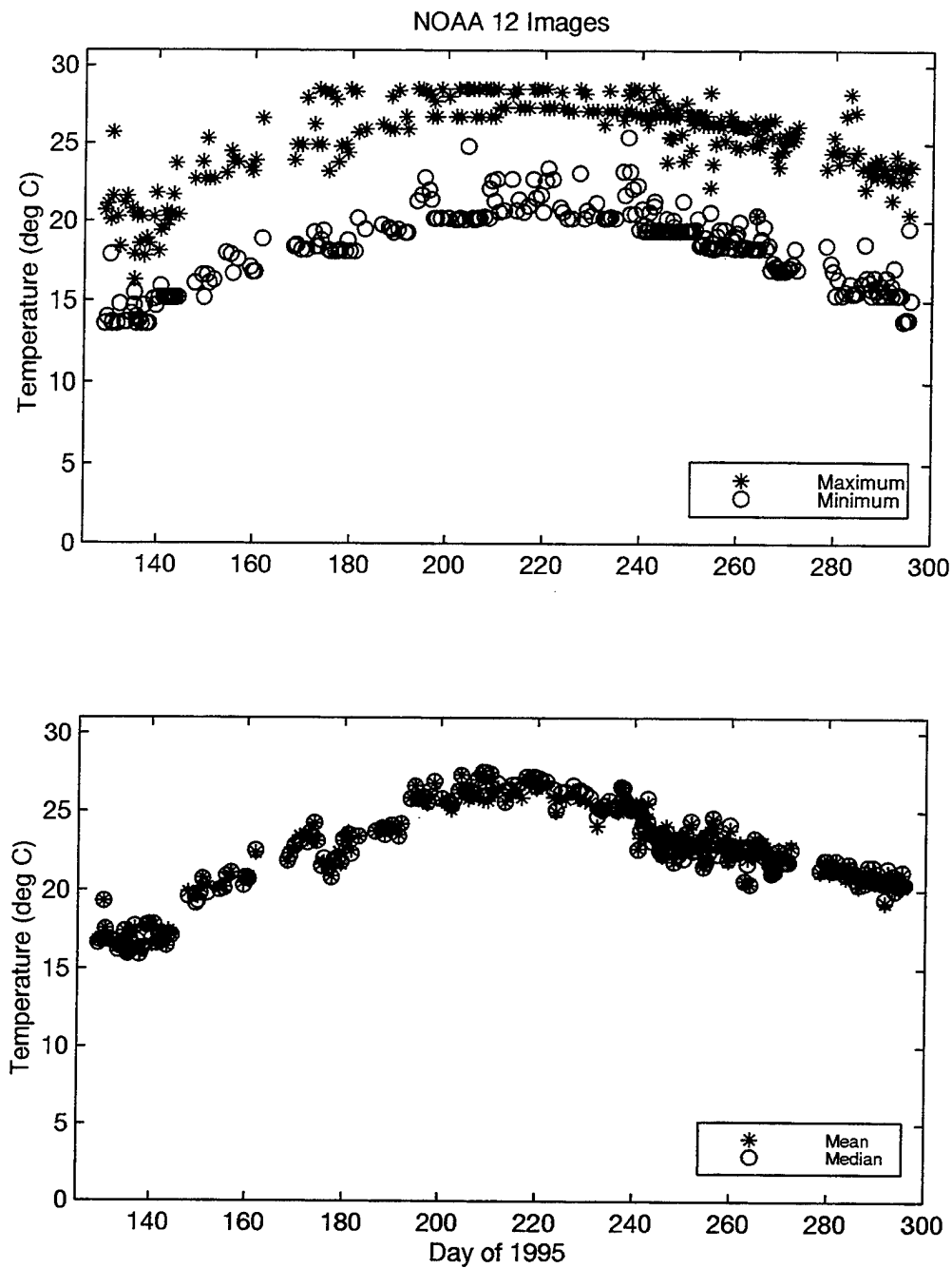


Figure 11. (a) Maximum and minimum temperature values for NOAA 12 images. (b) Mean and median temperature values for NOAA 12 images.

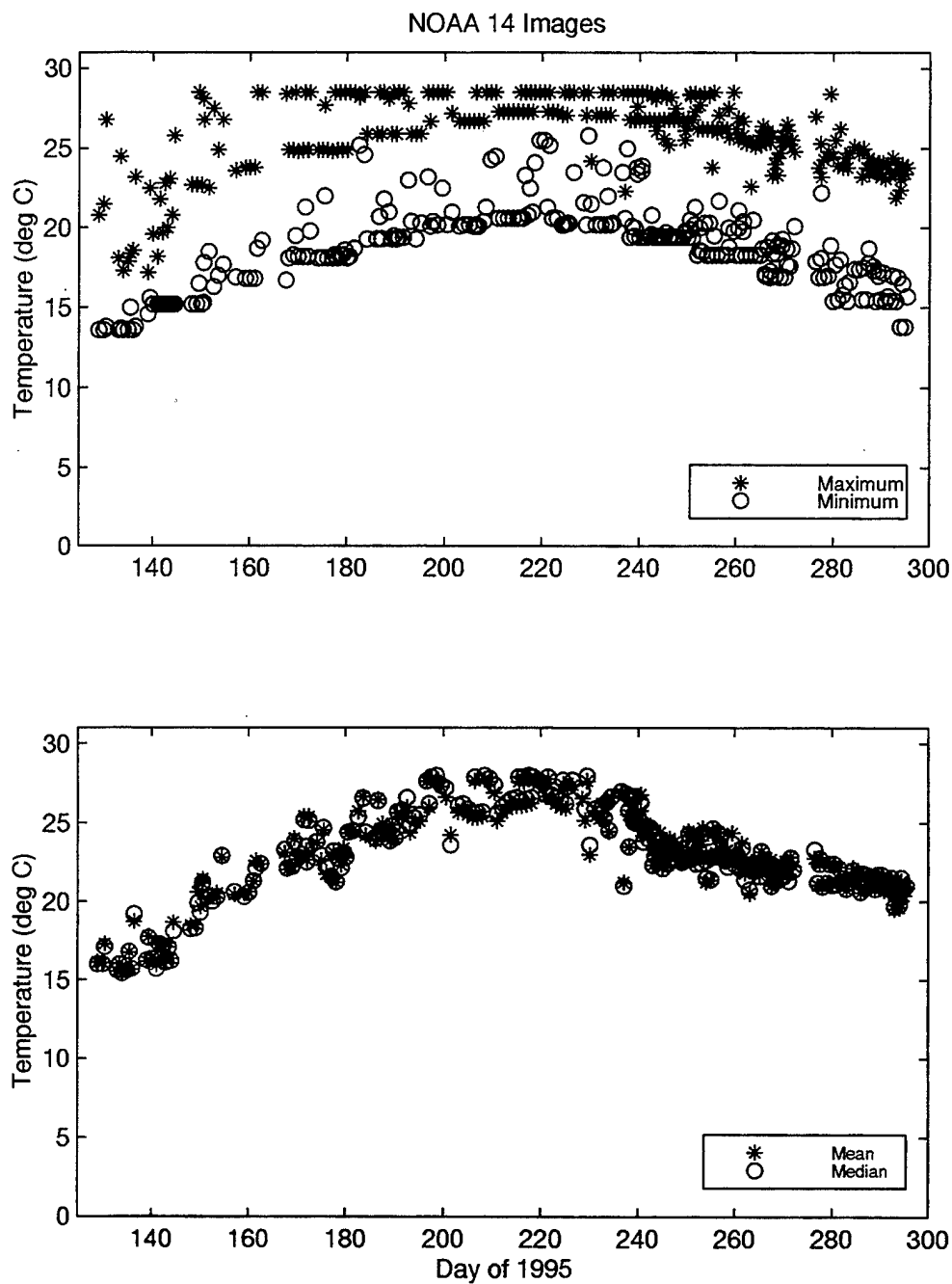


Figure 12. (a) Maximum and minimum temperature values for NOAA 14 images. (b) Mean and median temperature values for NOAA 14 images.

Determine Contemporaneous/Collocated Drifter vs Satellite SSTs

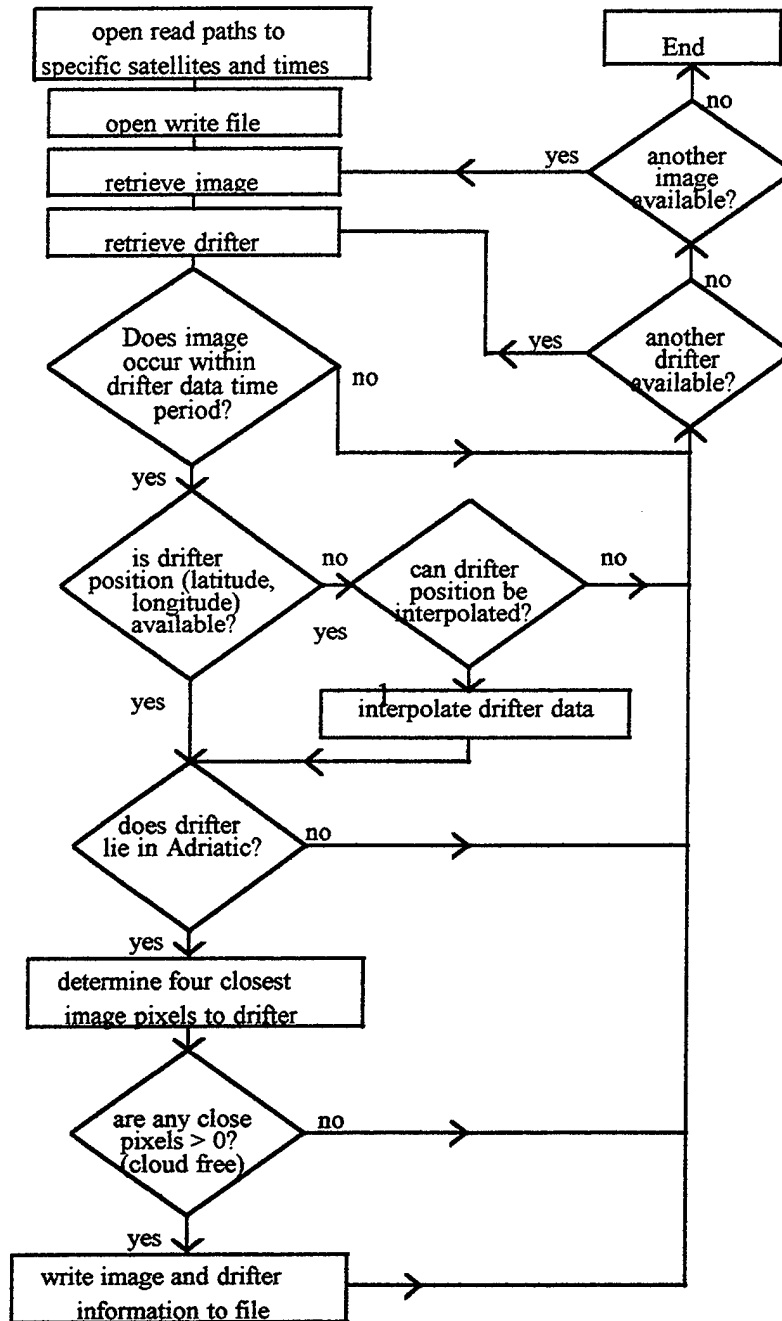


Figure 13. Flow diagram for determining contemporaneous/collocated drifter and satellite SSTs.

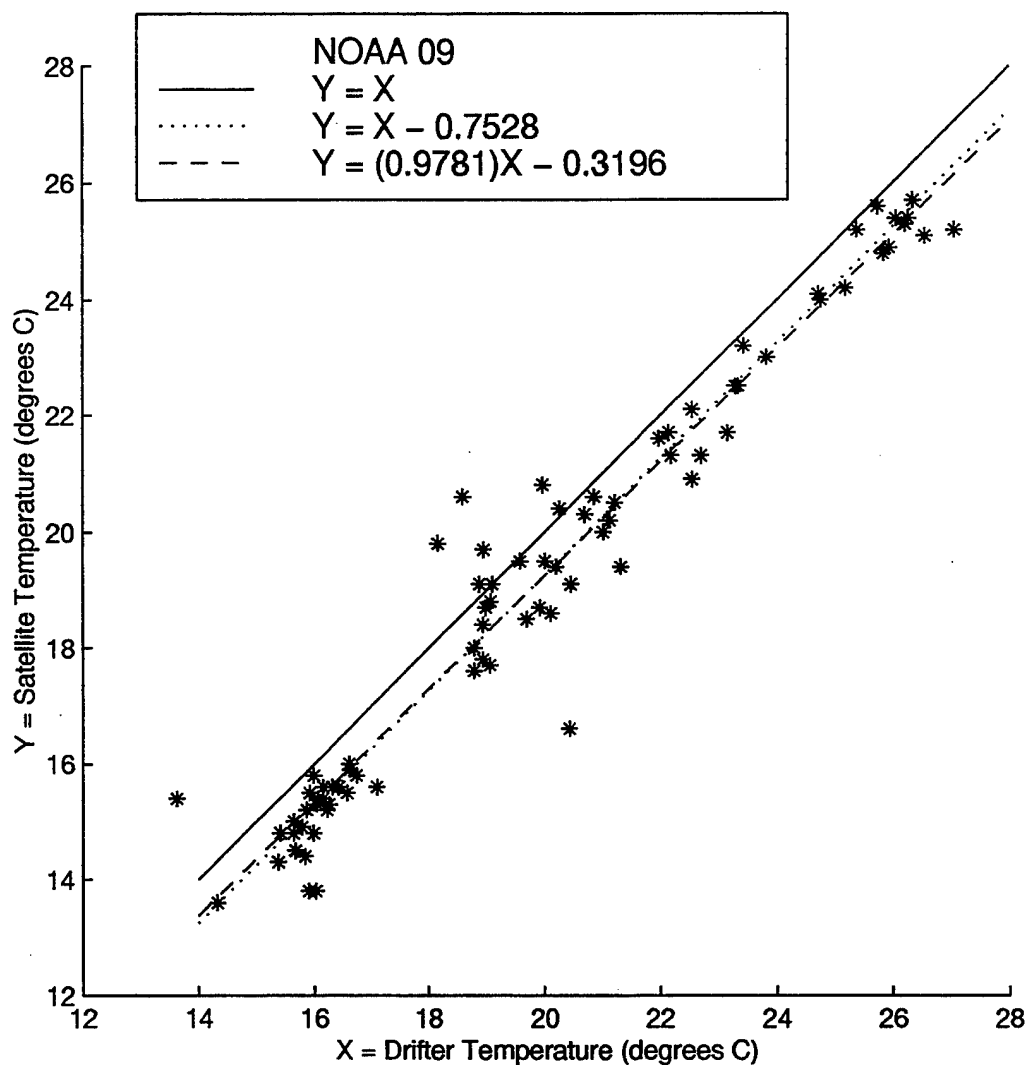


Figure 14. NOAA 09 satellite temperature vs. drifter temperature. Straight lines corresponding to the regression analysis results are overlaid.

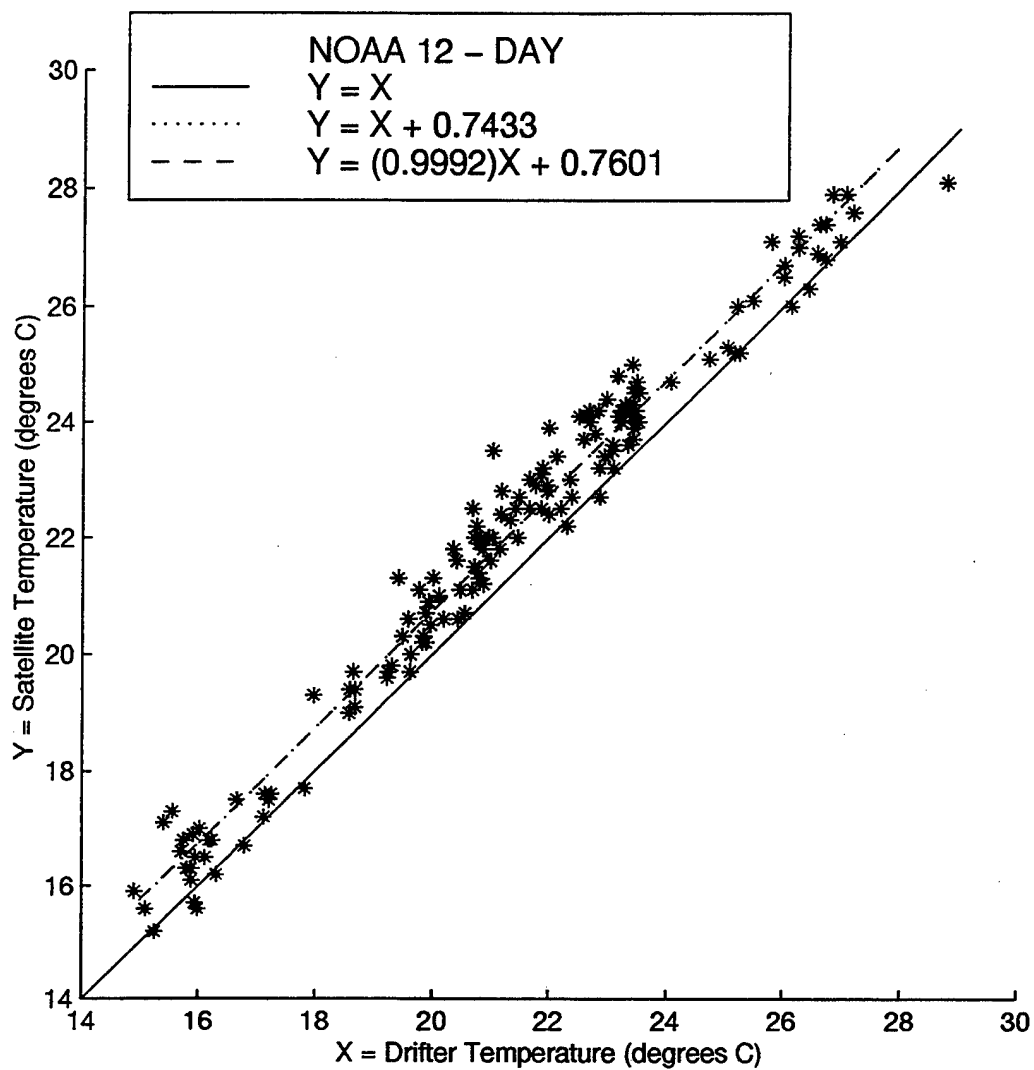


Figure 15. Same as Figure 14 but for NOAA 12 (Day).

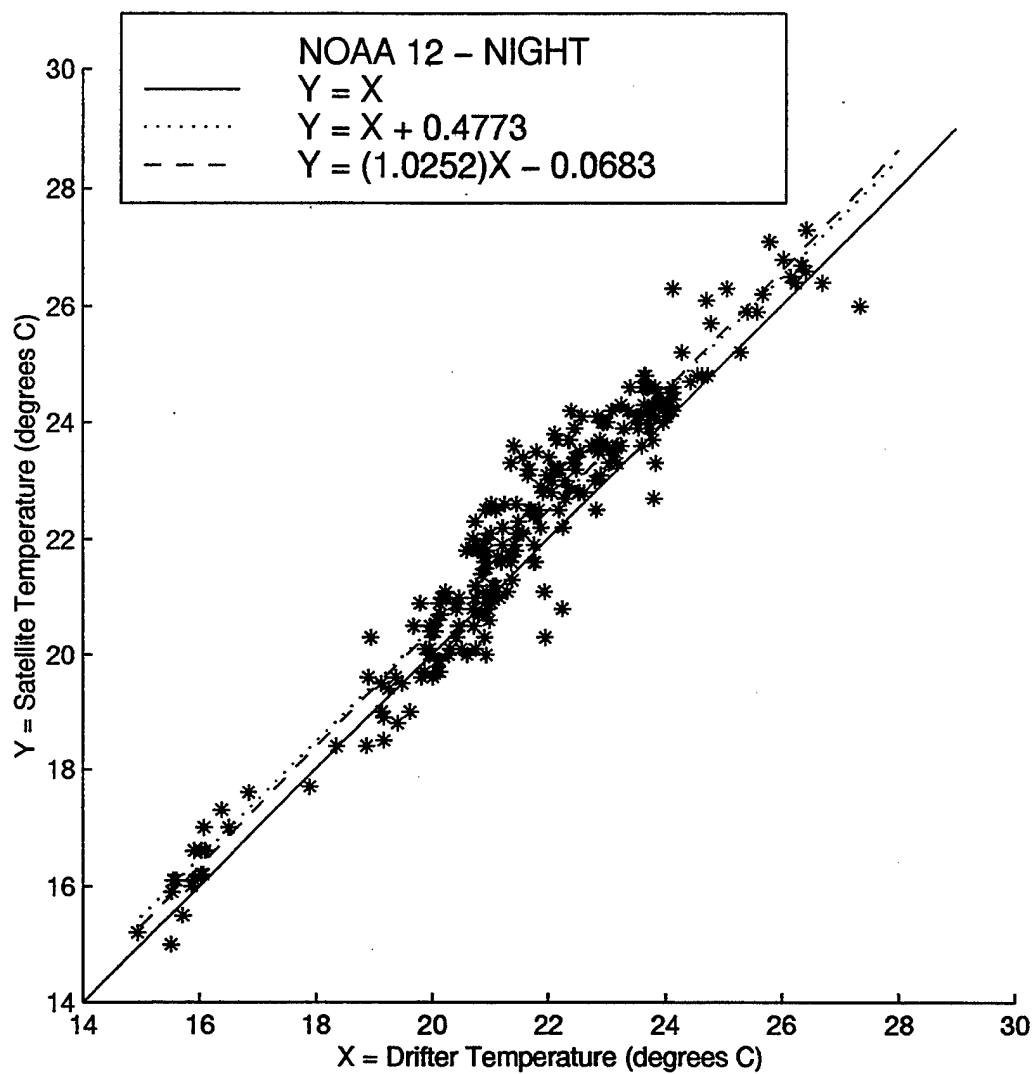


Figure 16. Same as Figure 14 but for NOAA 12 (Night).

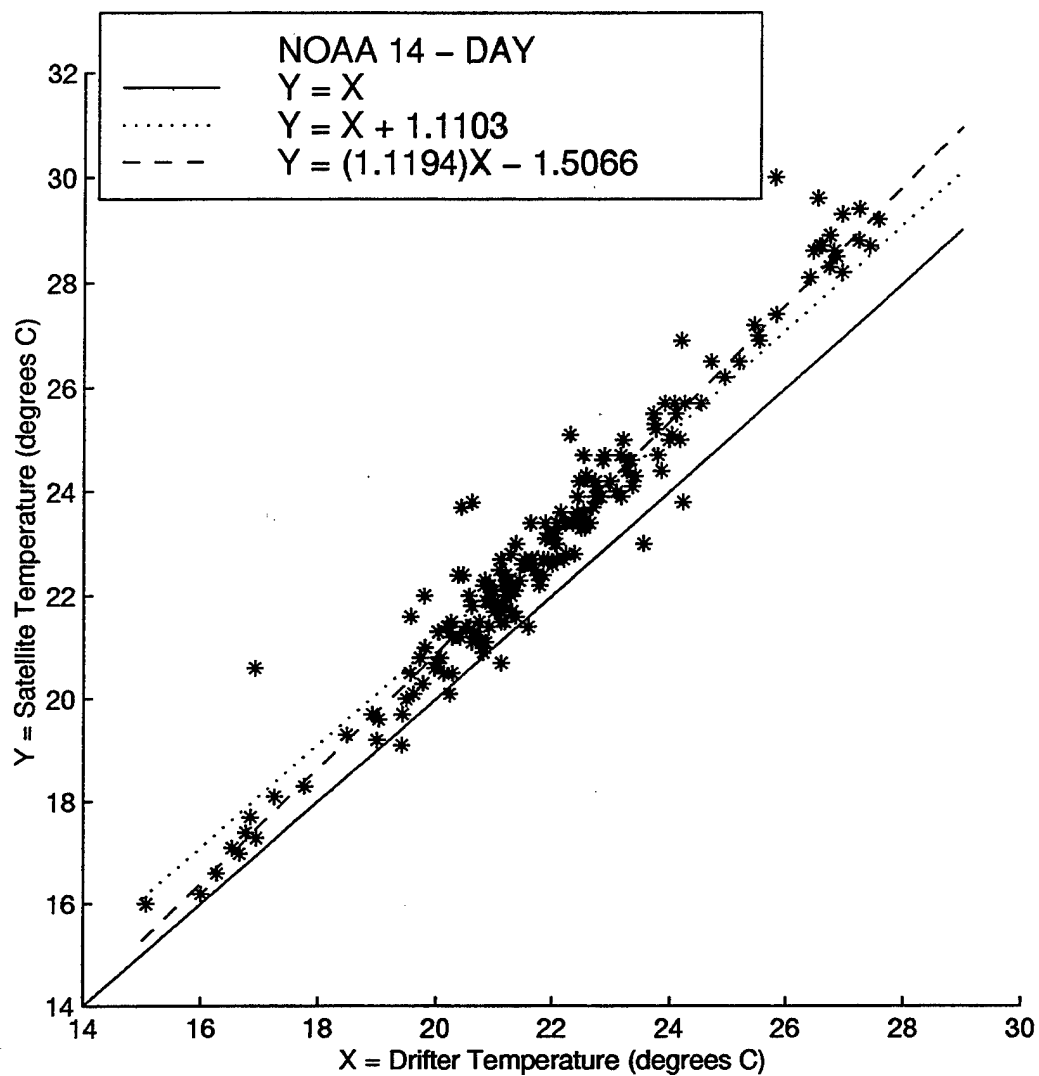


Figure 17. Same as Figure 14 but for NOAA 14 (Day).

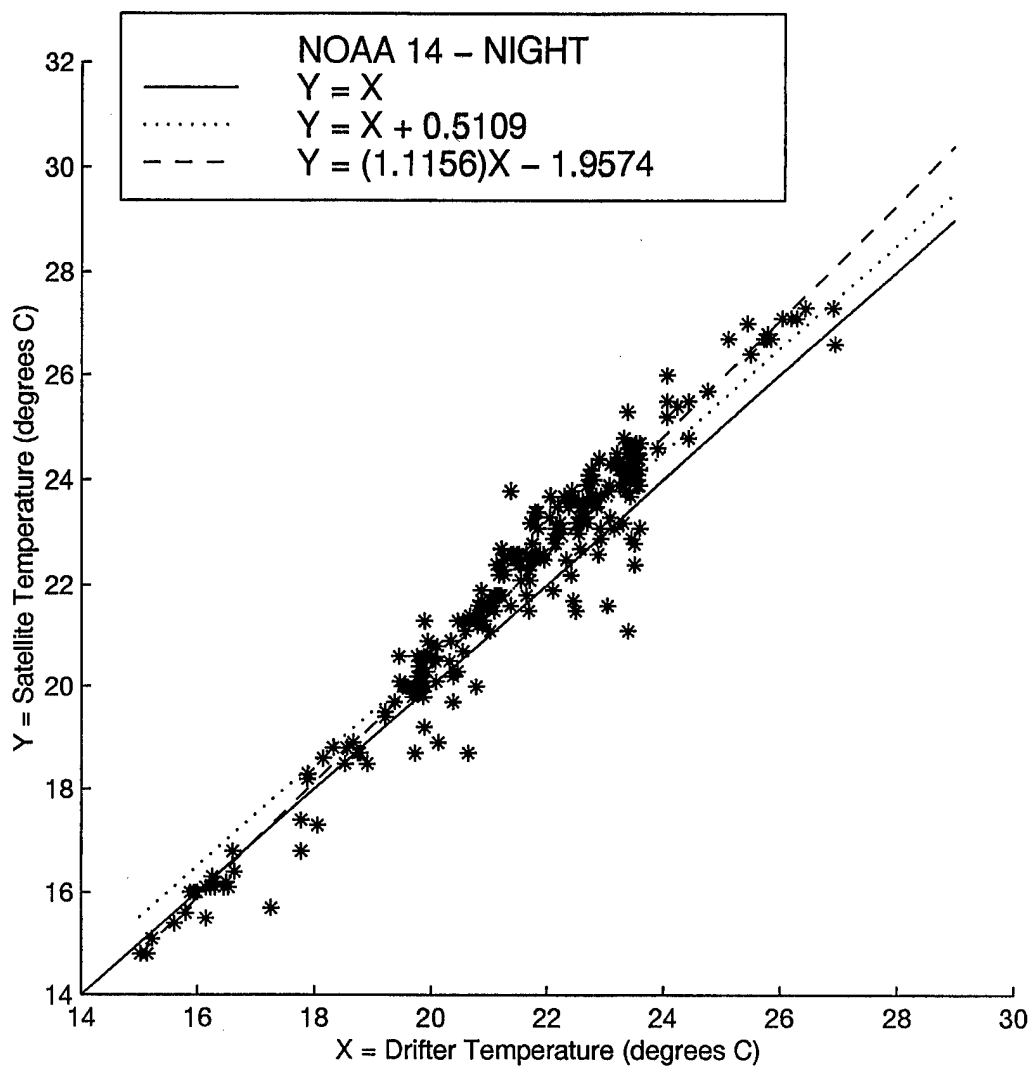


Figure 18. Same as Figure 14 but for NOAA 14 (Night).

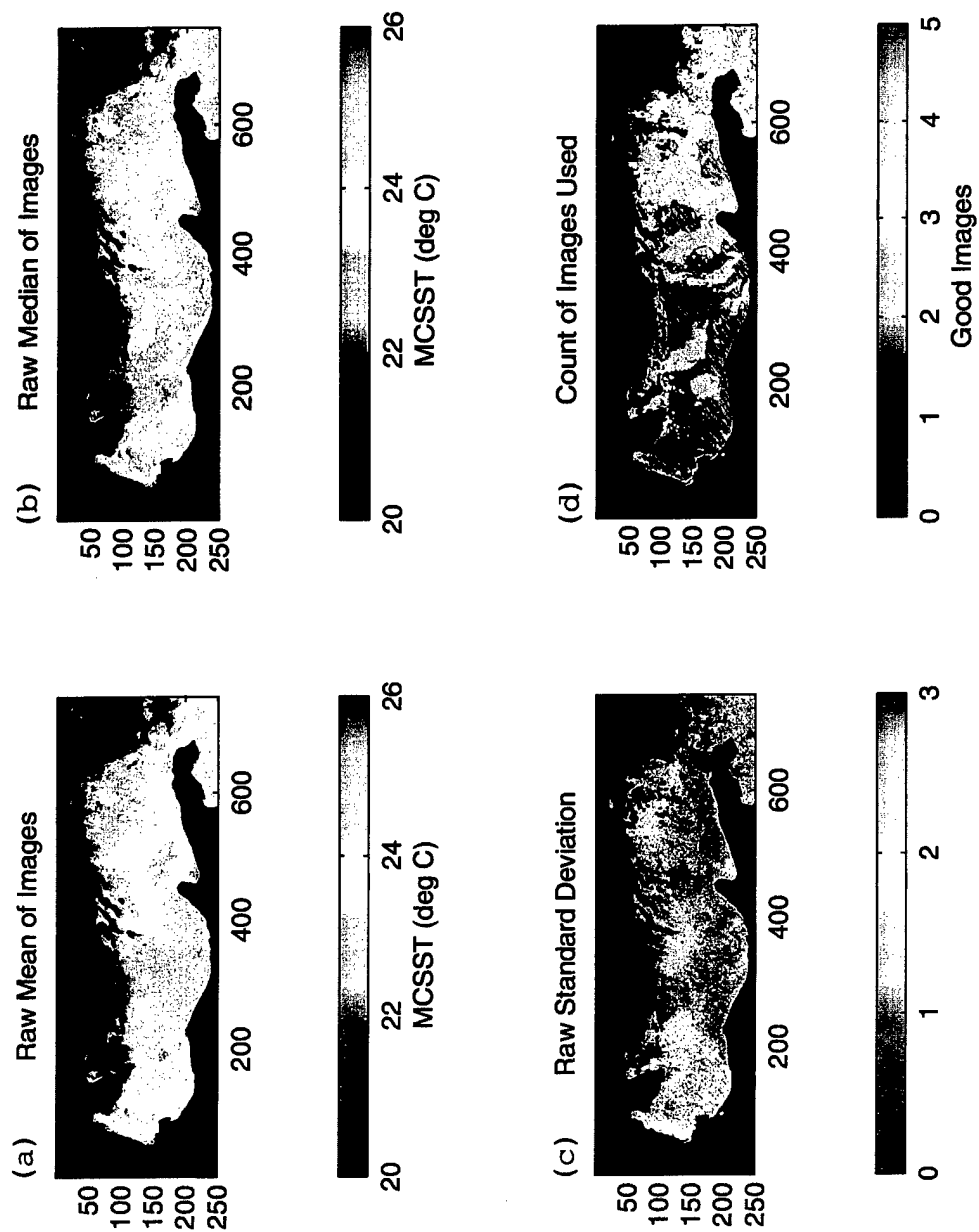


Figure 19. Composite results based on uncorrected data for July 8, 1995; (a) mean, (b) median, (c) standard deviation, (d) count of images used in composite images.

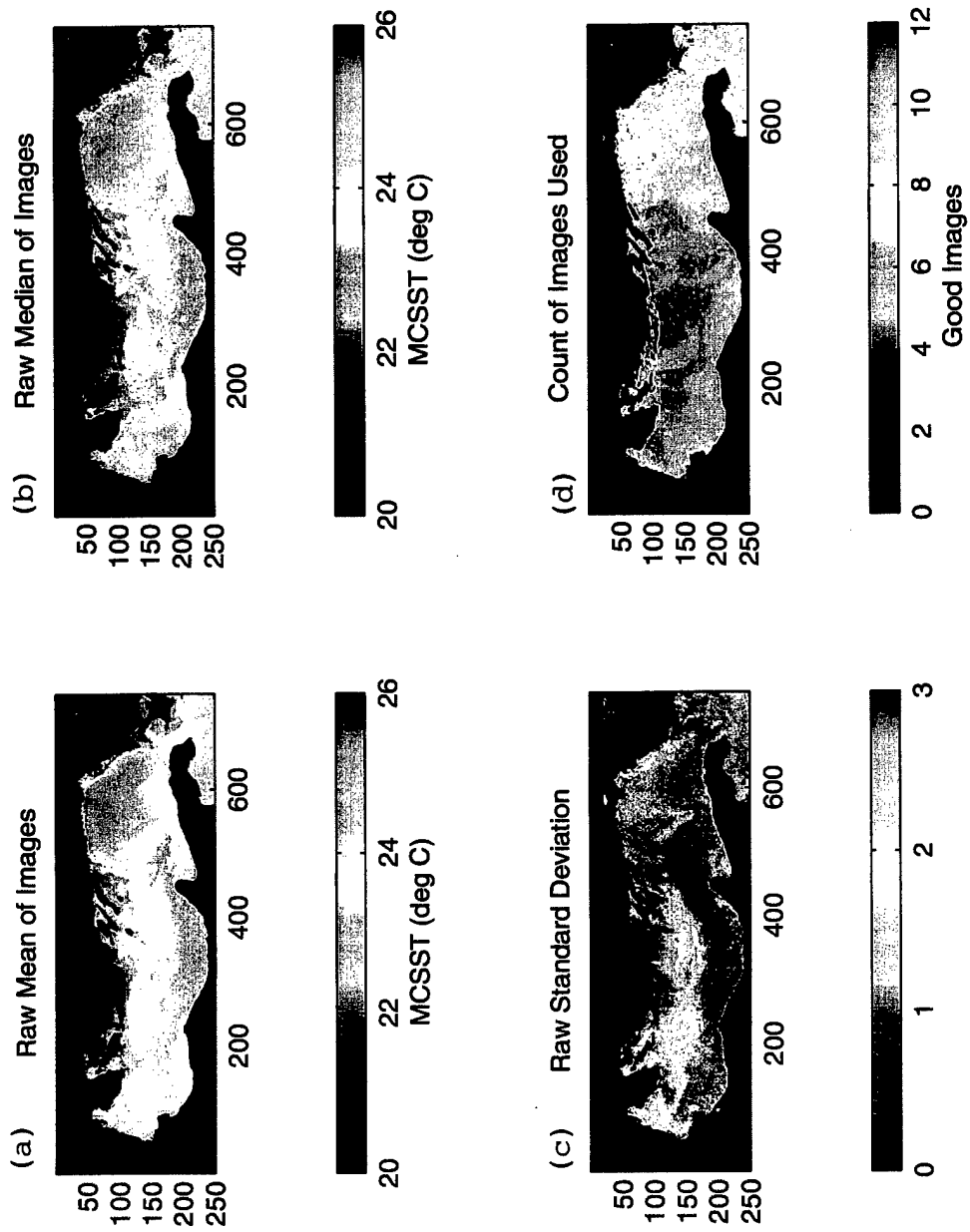


Figure 20. Same as Figure 19, but for three-day period (July 8-10, 1995).

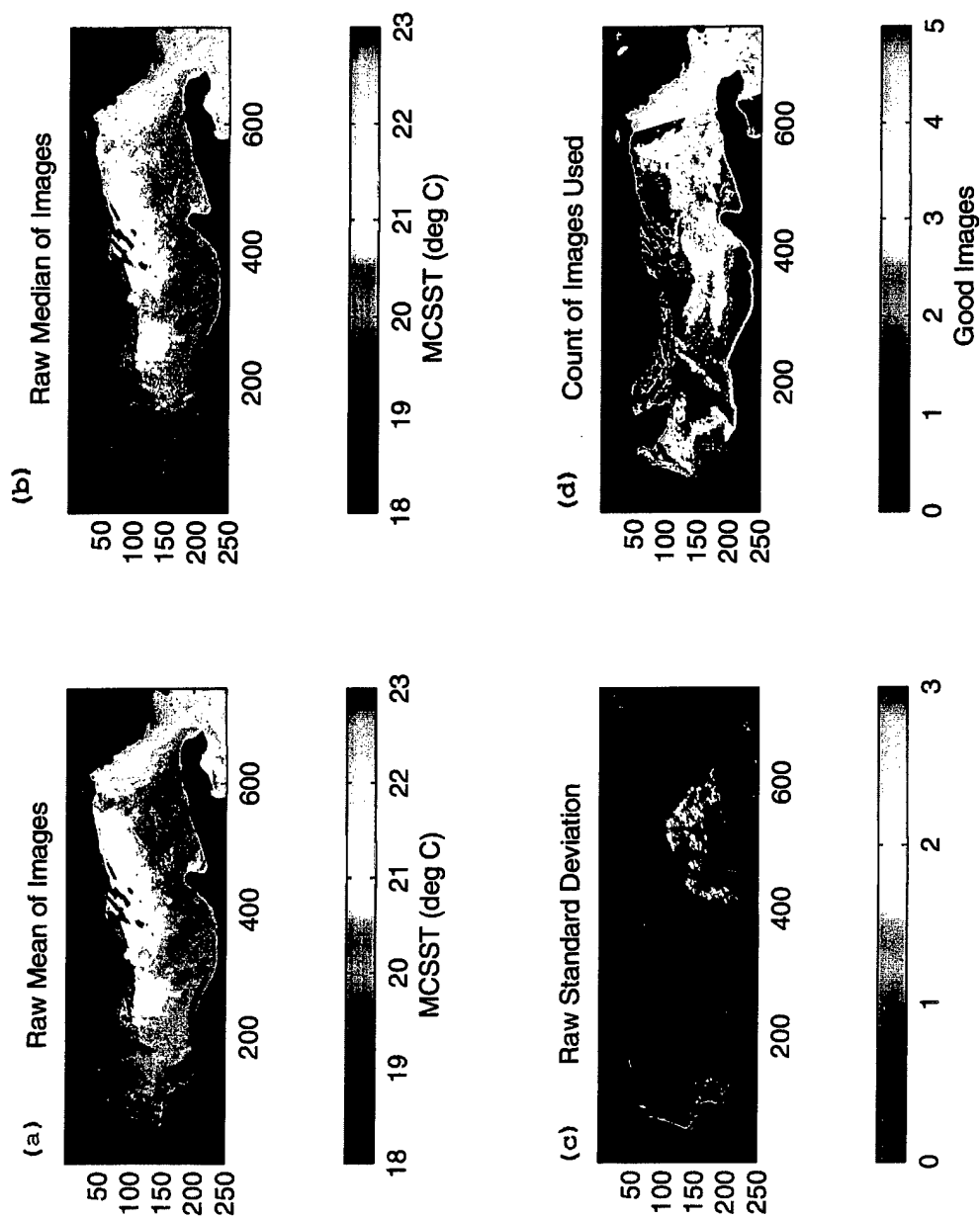


Figure 21. Same as Figure 19, but for October 20, 1995

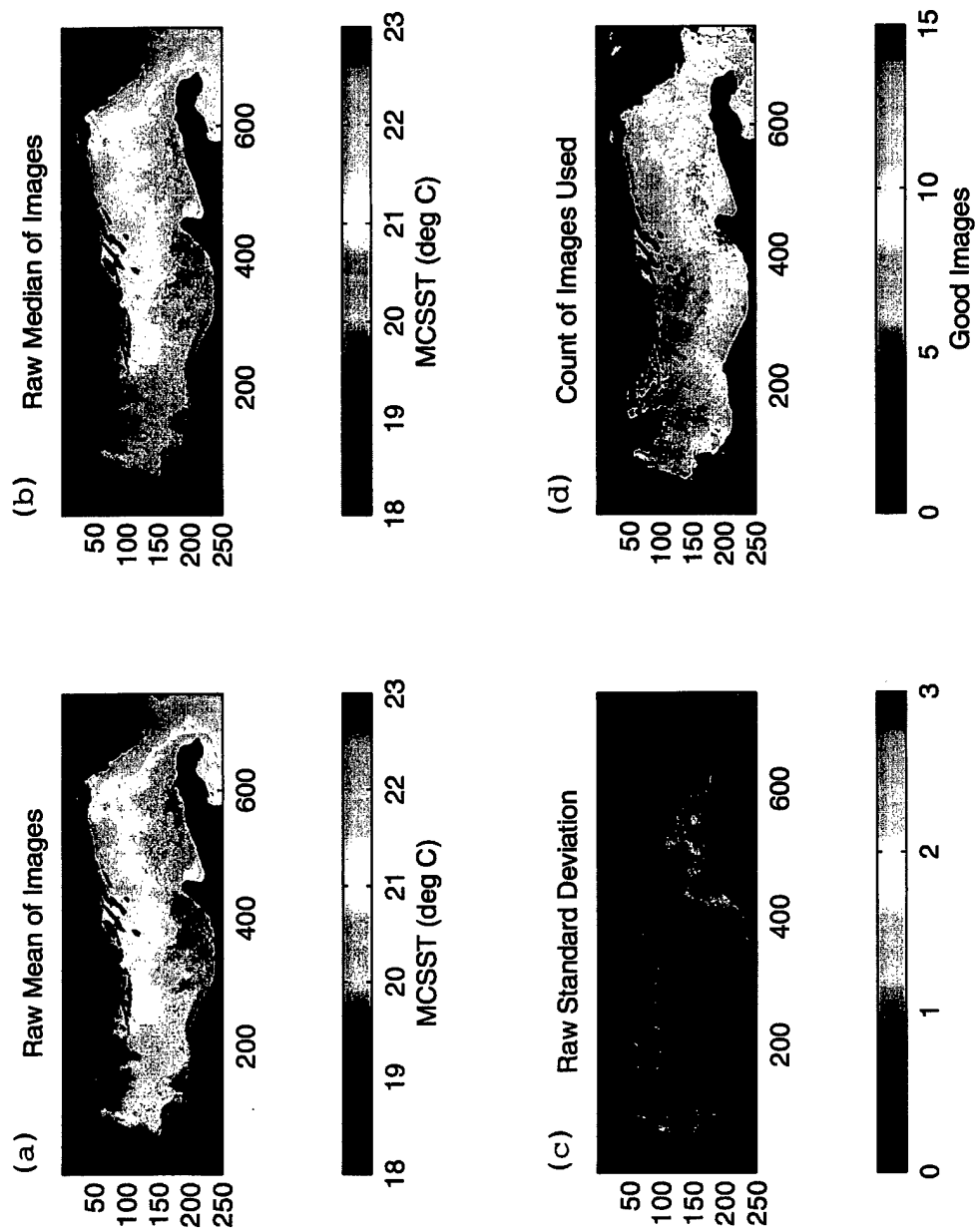


Figure 22. Same as Figure 19, but for three-day period (October 18-20, 1995).

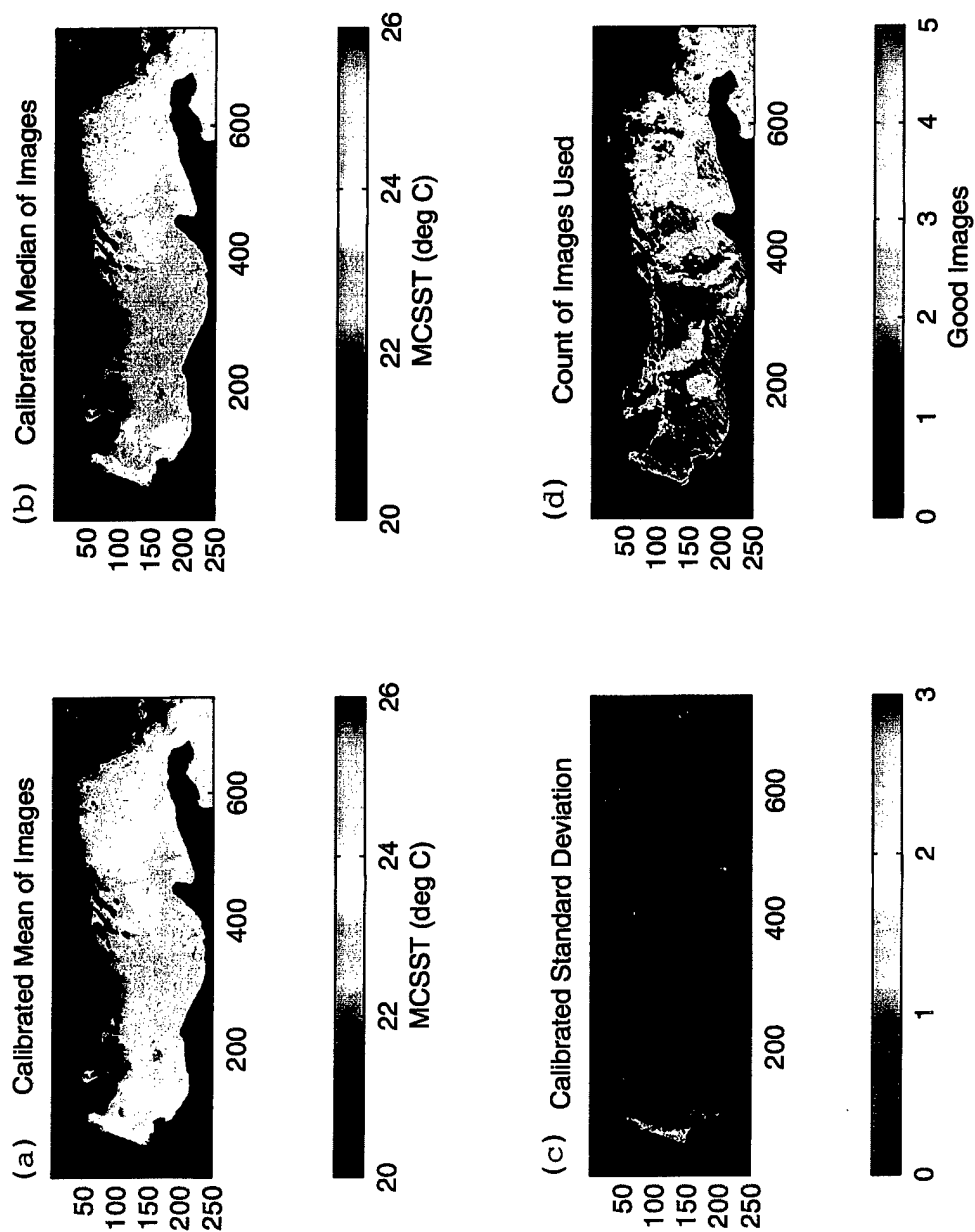


Figure 23. Composite results based on data corrected by the median difference for July 8, 1995; (a) mean, (b) median, (c) standard deviation, (d) count of images used in composite images.

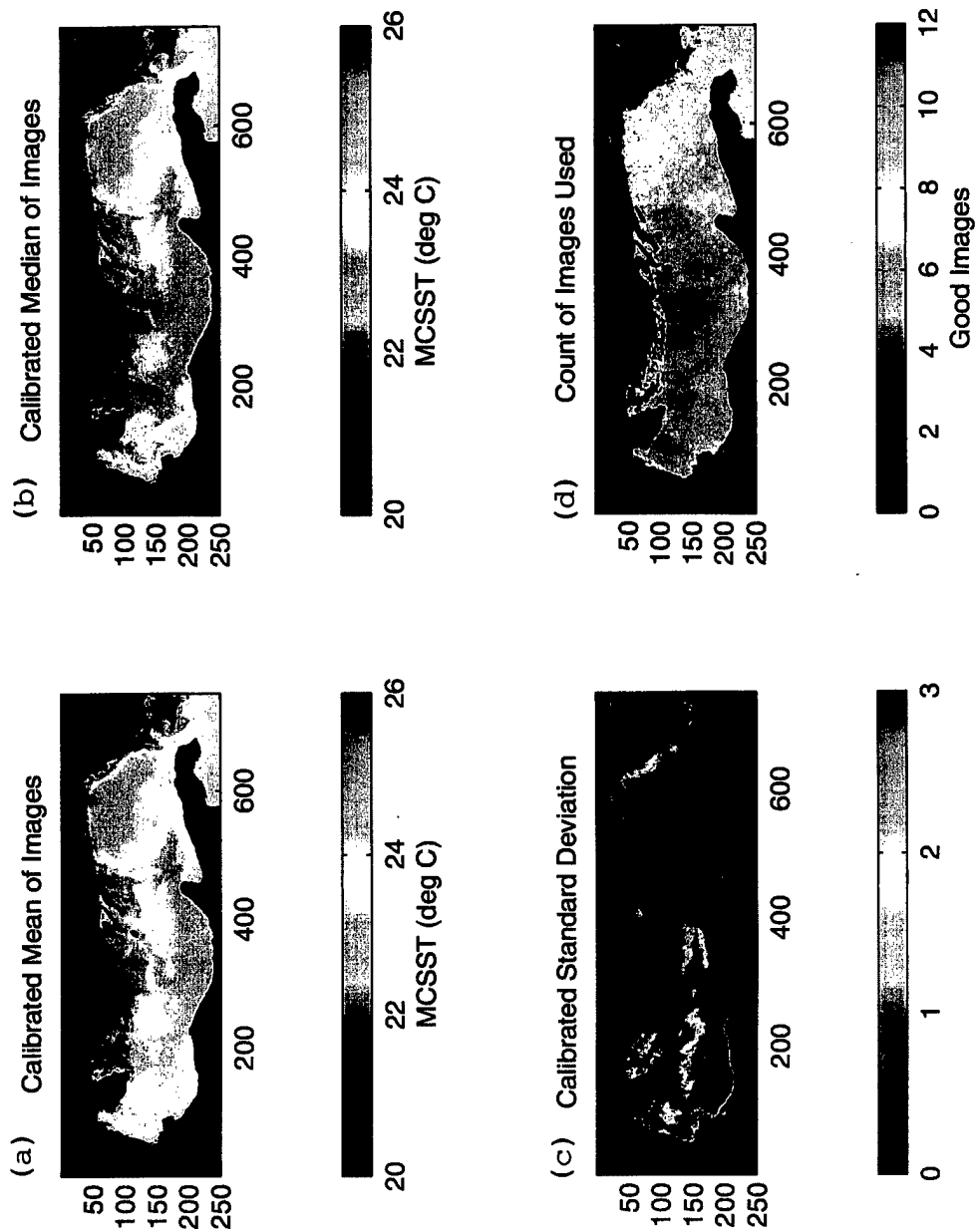


Figure 24. Same as Figure 23, but for three-day period (July 8-10, 1995).

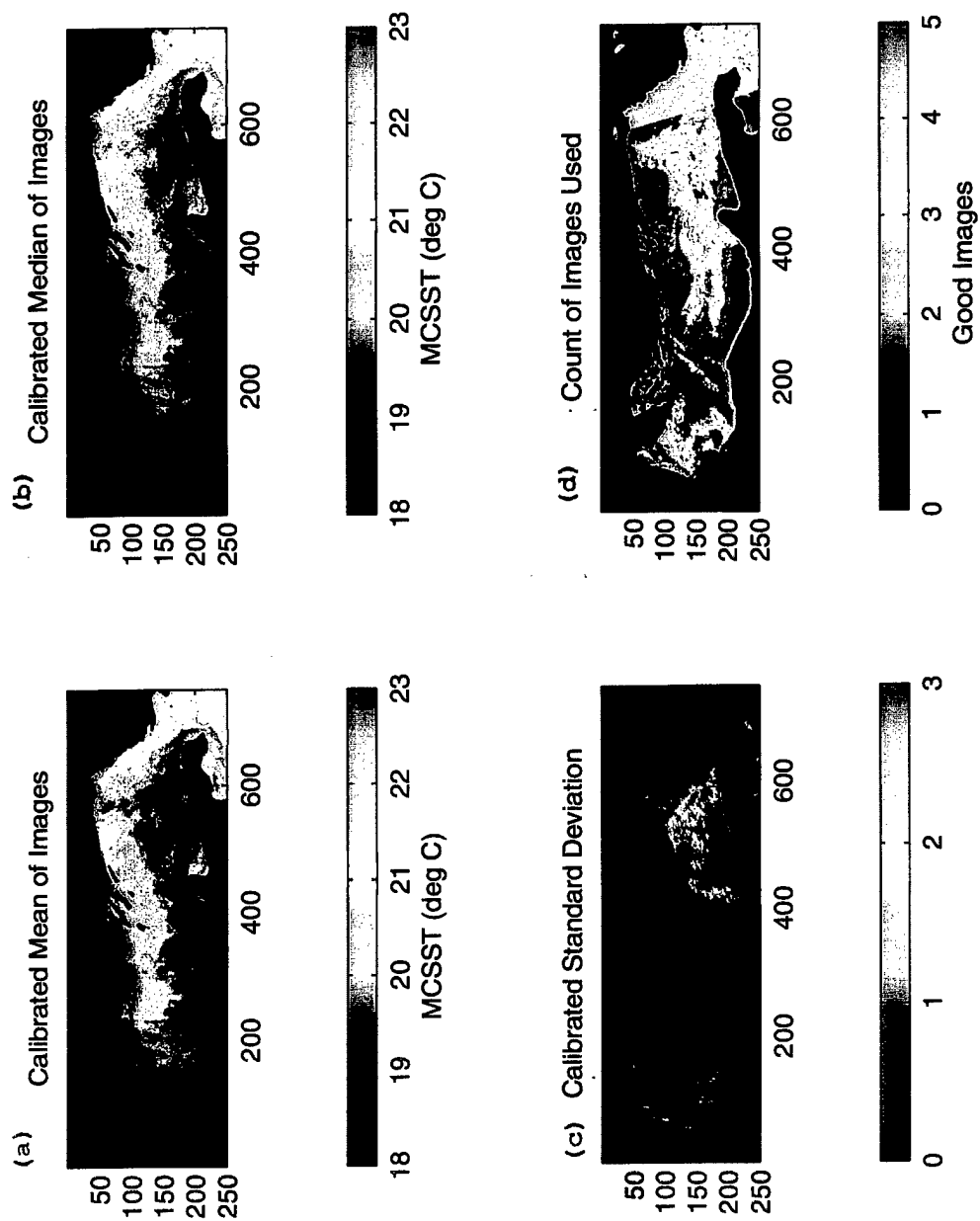


Figure 25. Same as Figure 23, but for October 20, 1995.

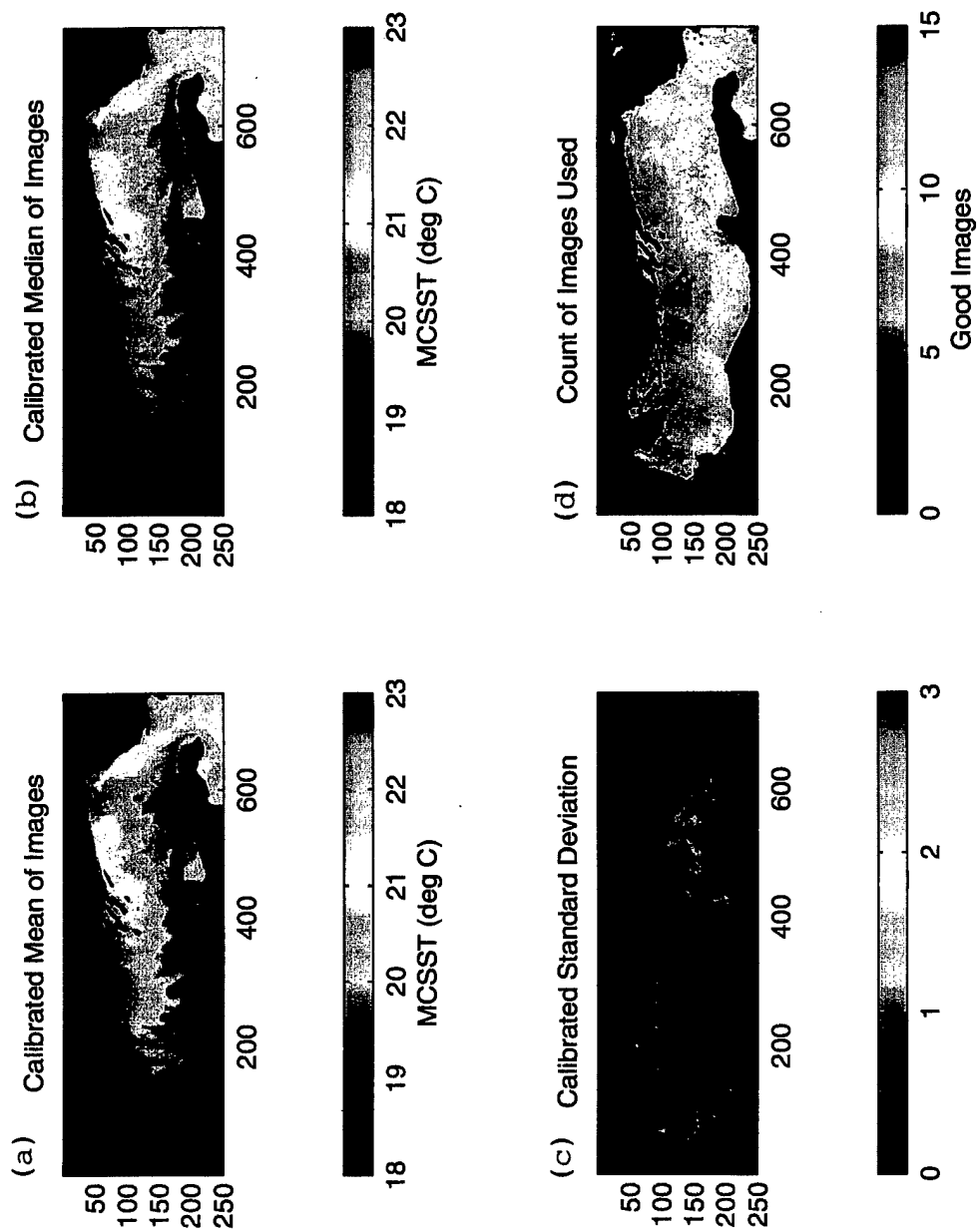


Figure 26. Same as Figure 23, but for three-day period (October 18-20, 1995).

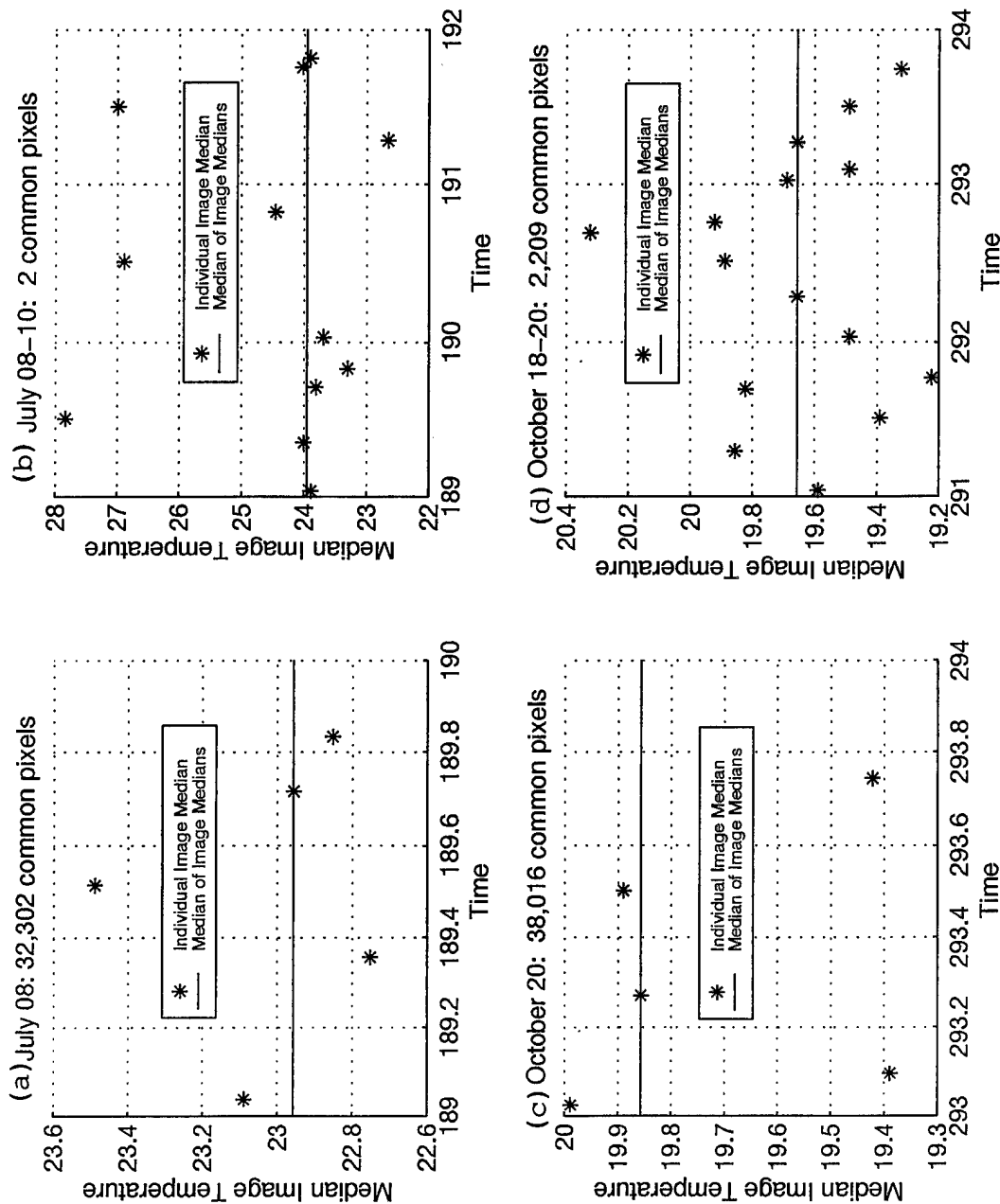


Figure 27. Median temperatures for each of the images (computed over the common pixels only) and "median of medians" temperature during the time periods considered. (a) July 8, 1995, (b) July 8-10, 1995, (c) October 20, 1995, (d) October 18-20, 1995.

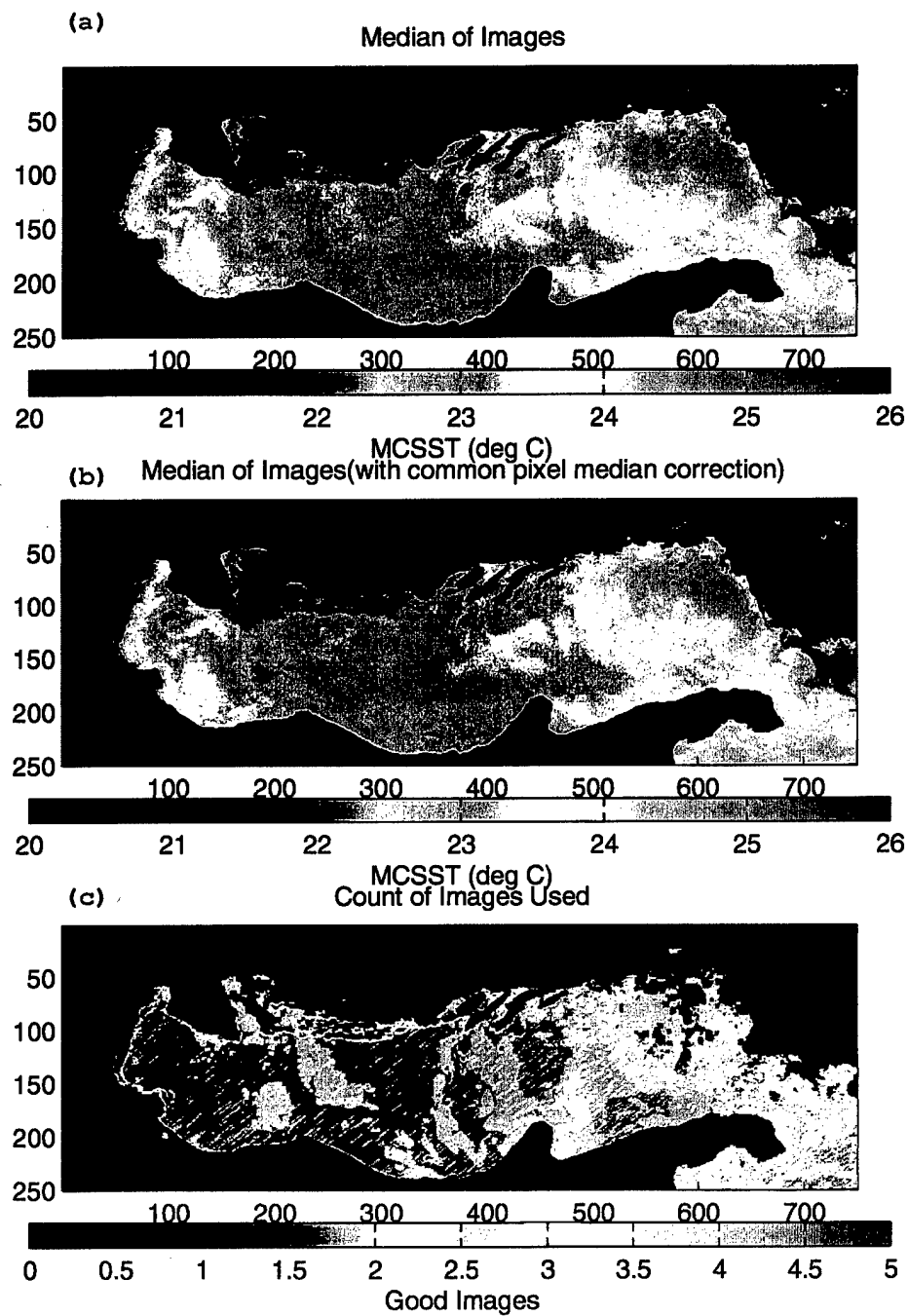


Figure 28. For July 8, 1995; (a) median of satellite corrected images. (b) "Median of medians" correction to (a). (c) Count of images used.

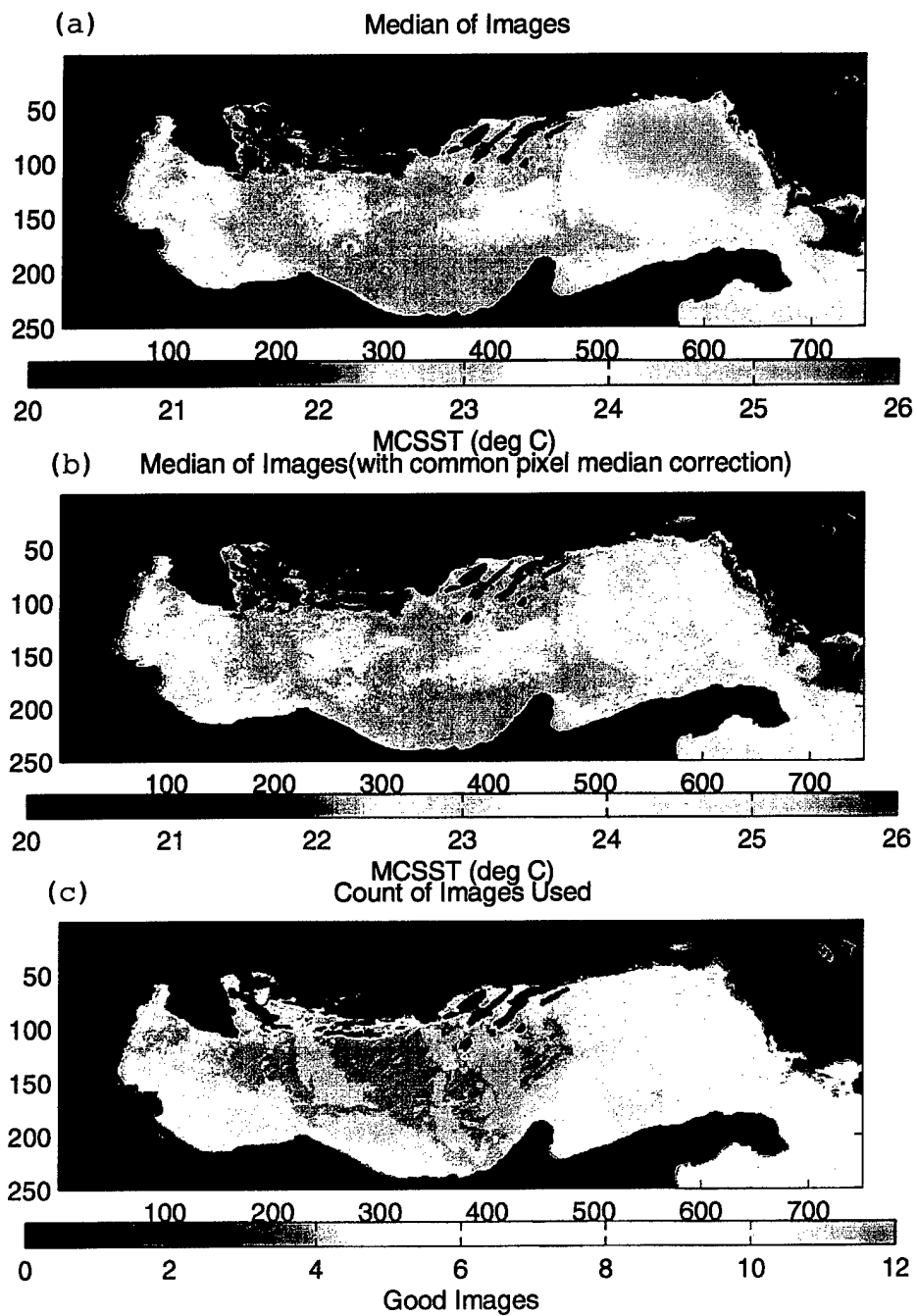


Figure 29. Same as Figure 28, but for three-day period (July 8-10, 1995).

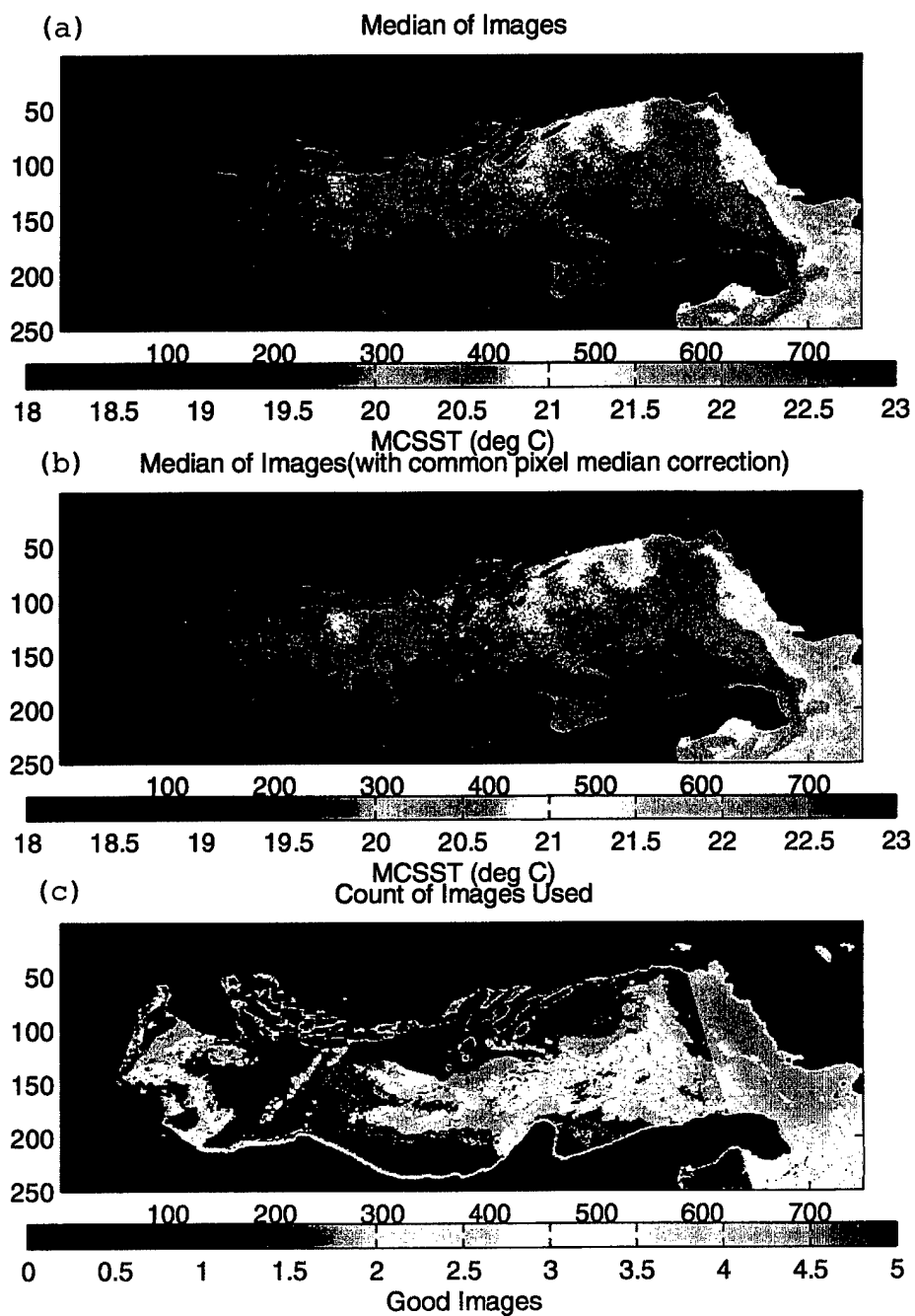


Figure 30. Same as Figure 28, but for October 20, 1995.

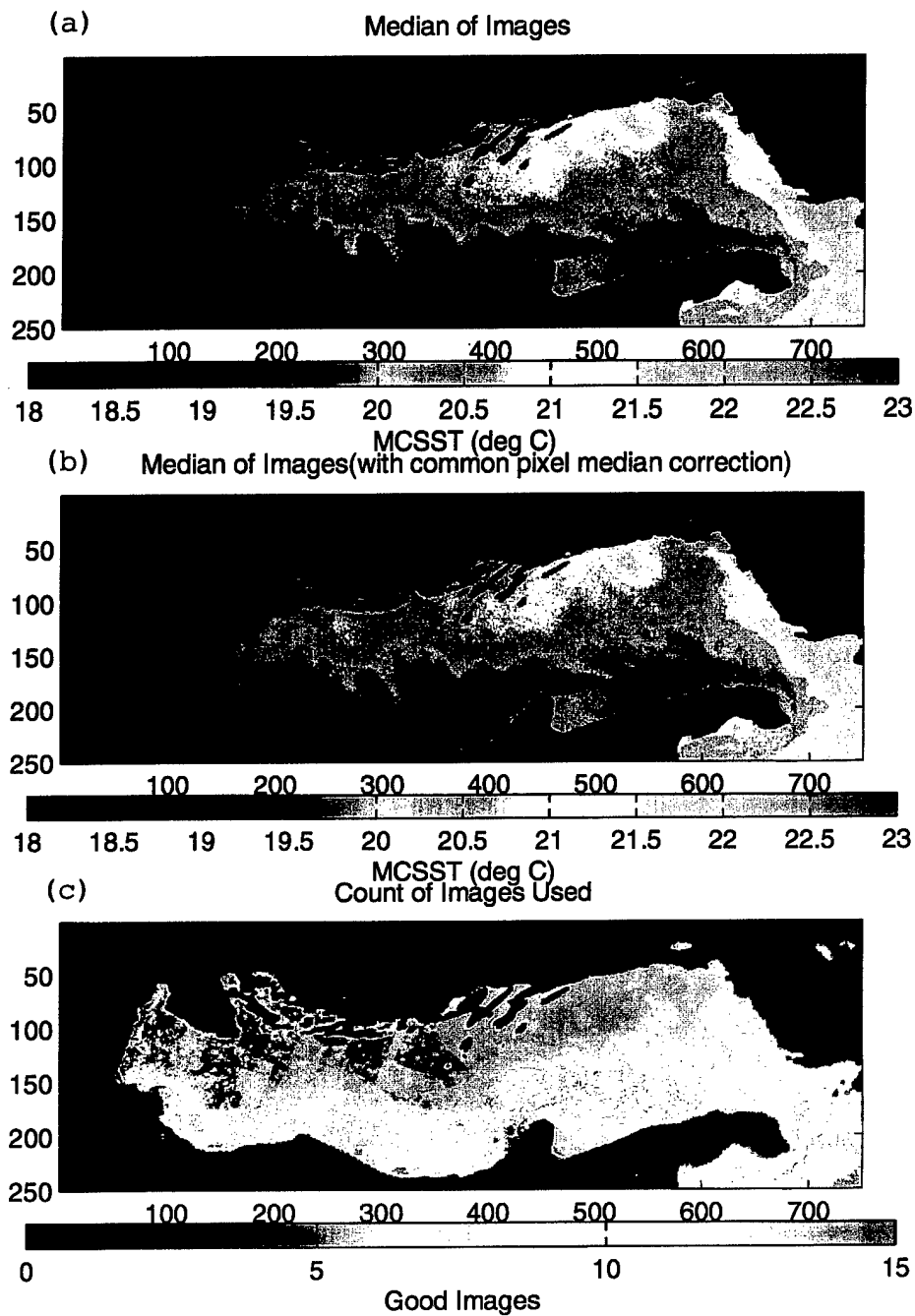


Figure 31. Same as Figure 28, but for three-day period (October 18-20, 1995).

1 and 3 day Image Compositing Flow Diagram

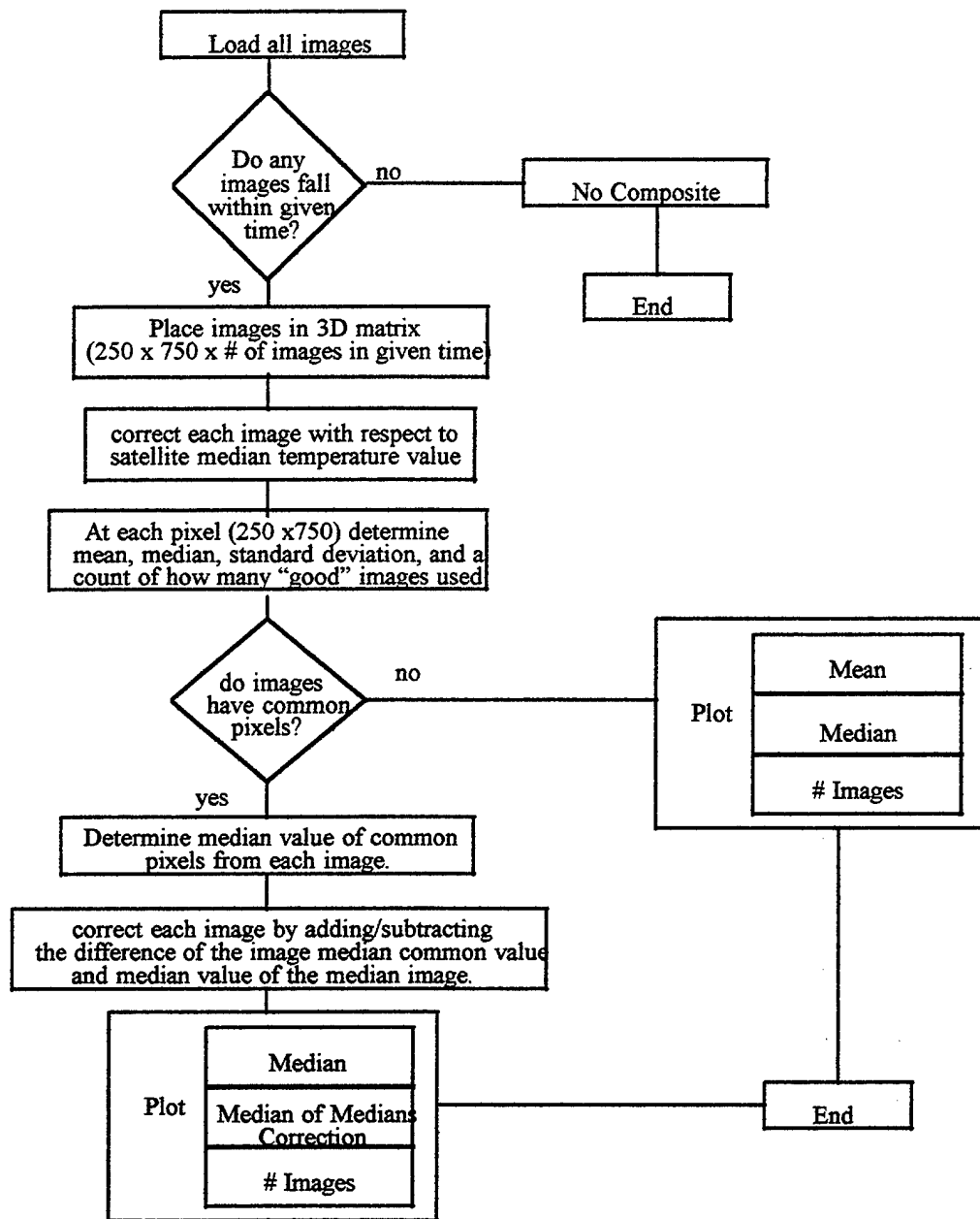


Figure 32. 1 and 3 day composite images flow diagram

Weekly and Monthly Image Compositing Flow Diagram

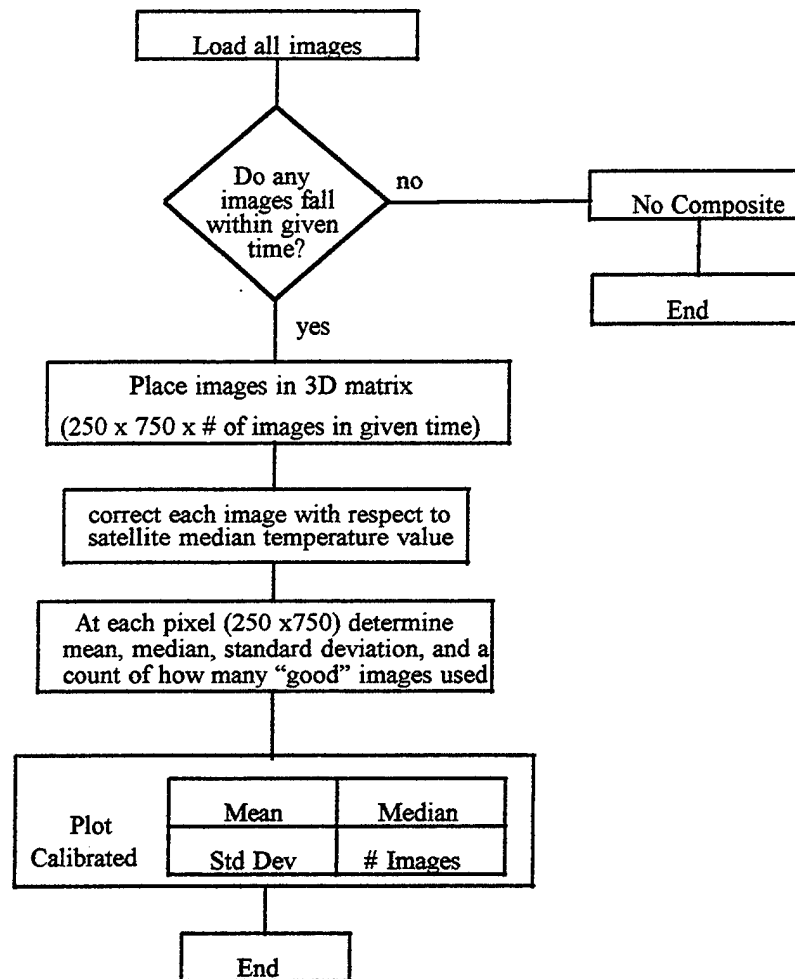


Figure 33. Weekly and monthly composite images flow diagram.

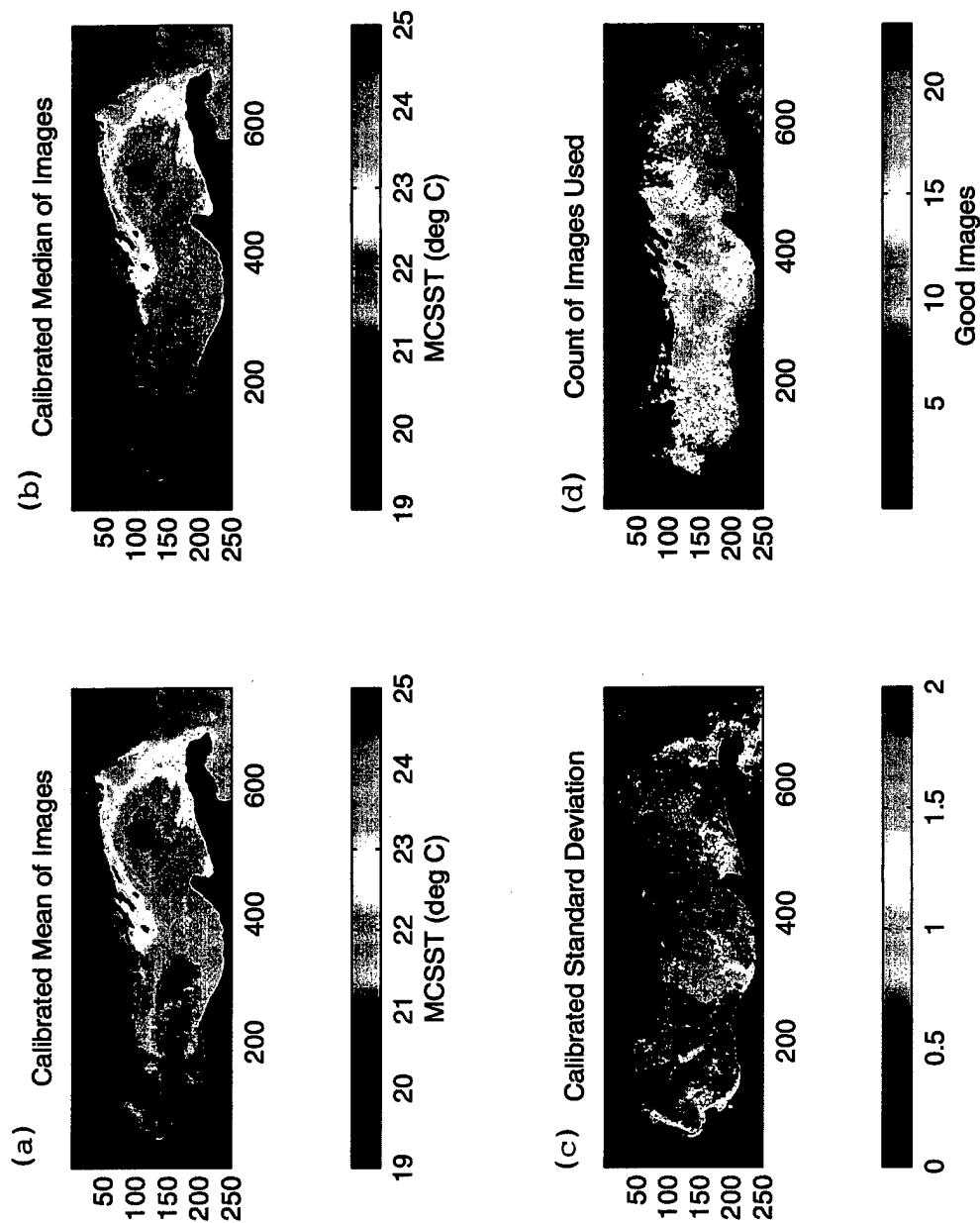


Figure 34. Composite based on data corrected by median difference for September 19-25, 1995; (a) mean, (b) median, (c) Standard deviation, (d) count of images used in composite images.

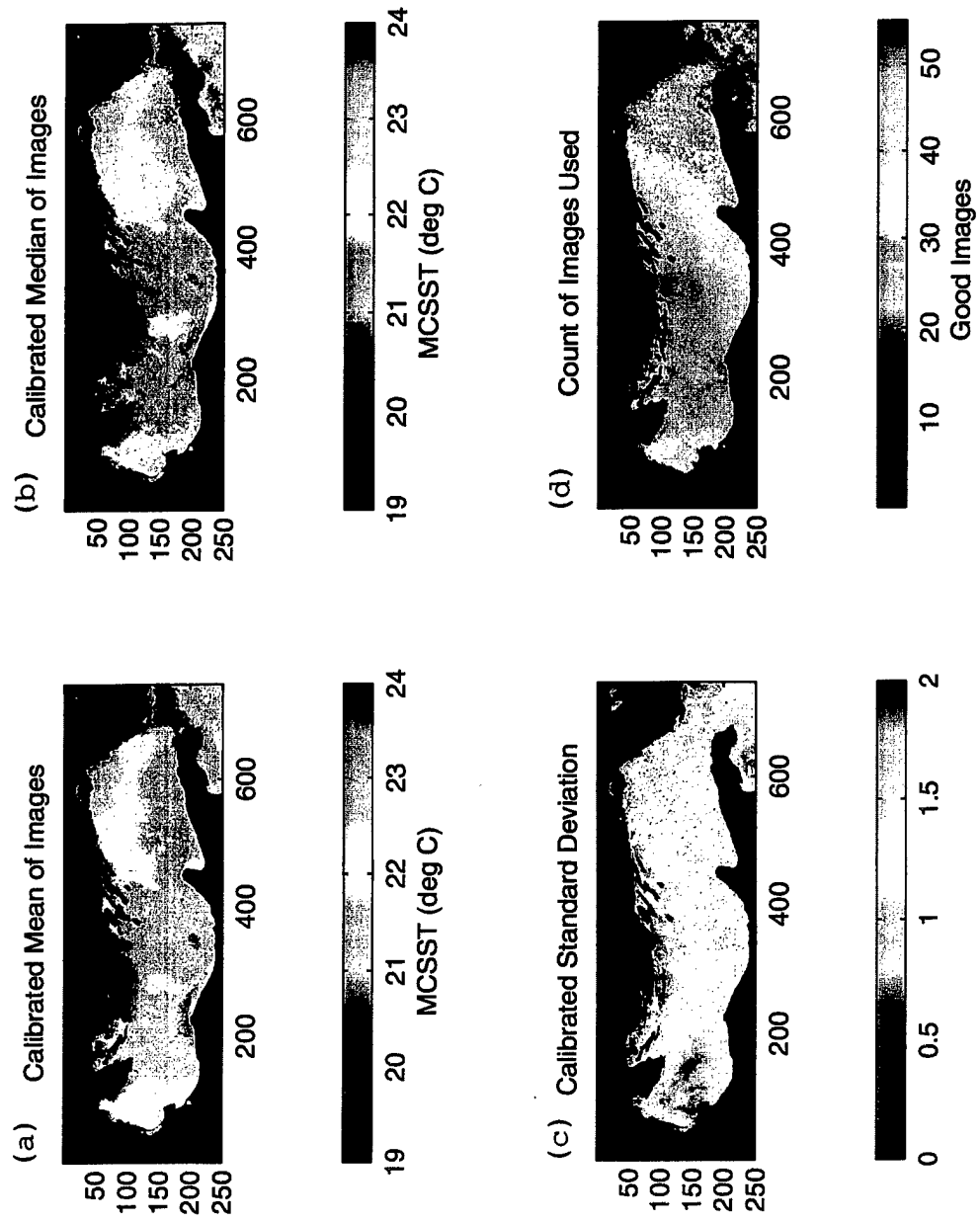


Figure 35. Same as Figure 34, but for June, 1995.

IV. RESULTS

The compositing methods described in Chapter III were applied to many time periods (from one day to one month) between May and October, 1995. Here only selected composite images, eventually augmented with drifter trajectories, are presented to describe the temporal (seasonal) and spatial (basin to meso-scale) variation of the Adriatic Sea surface temperatures.

A. MONTHLY COMPOSITES

The period covered allows a clear look at three of the four seasons similar to those defined in previous studies of the Adriatic, i.e., May and June for spring, July and August and early September for summer, and late September and October reflecting autumn (Artegiani et al.; 1997, Gacic et al., 1997). In each image, the Adriatic SST is represented with a color scale whose minimum and maximum values are adjusted for each month to best exhibit differences in water masses.

Figure 36a demonstrates the spring characteristics in the month of May. The developing warm water region in the Northern Adriatic travels along the Italian coastline while the southern and middle basins remain cold. The eastern shelf in the southern Adriatic grows warmer through the spring, possibly from intrusion from the Ionian Sea. This allows the region along the Albanian coast to maintain higher temperatures than the western coastal waters and the rest of the basin.

As summer progresses from June to August (Figures 36b,c,d) the region in front of the Po river continues to warm and expand to cover most of the northern basin. The temperature range of the basin has risen from an approximate low of 19°C in June to a high of nearly 27°C in July and August. A warm pool that begins in the southern basin grows as the season proceeds, and eventually migrates to the west toward the end of the summer. The exception to this basin wide warming trend occurs along the entire eastern coast. While the majority of the Adriatic SST rises, a narrow region of upwelling becomes apparent during the summer months, keeping the temperatures 2-3°C cooler.

As autumn begins, warmer waters remain along the southern basin near both the eastern and western coastlines while cold water masses develop in the middle and southern Adriatic basins (Figures 36e,f). The temperature matches that of the Ionian Sea, making the possibility of a water mass intrusion from the south a possibility. Concurrently, the

northern end of the basin experiences a heat loss to the atmosphere making it significantly cooler than the rest of the sea. The season change is apparent as the absolute temperatures drop to a range of 17 to 24°C. The beginning of the winter time Po induced cold coastal plume found by Gacic et al. (1997) can also be seen in October (Figure 36f).

Because data were only available from May to October, 1995, there is no representation of the winter season.

B. WEEKLY COMPOSITES WITH DRIFTER TRACKS

The weekly composites representing the 24 weeks of this study are displayed in Figures 37 through 44. For each week, the spatial mean SST was determined and removed from the SST estimates. Variations around this mean were normalized by the standard deviation and were color coded with a fixed color scale over the range -3 to +3. This representation eliminates the mean seasonal variations over the Adriatic basin and provides an optimum enhancement of the images in which thermal gradients are well represented by strong color variations. Additionally, the 7-day long tracks of simultaneous surface drifters were overlaid on the composites to show the direction and strength of the surface currents. Drifters tracks appear as black lines with stars at the start of the week and circles at the end.

The spatial mean and the standard deviation interval of the weekly composite temperatures are plotted in Figure 45. The general warming of the sea is obvious between May and August, followed by a slower cooling from August to October. Maximum warming rates of more than 2°C/week occur at the end of May and in early July. The standard deviation varies from 0.6°C (middle May) to 1.3°C (early September).

The week of May 9-15 (Figure 37a) shows a cold basin in the spring (mean SST = 15.9°C) with reduced variance. However, it is apparent that the northern Adriatic is warming, possibly due to the inflow of the Po river or to local solar heating of the shallow water. Likewise the southern Adriatic is warmer than the mean, but the lack of drifters precludes us from determining the source of the warming, and we can only speculate it is due to springtime solar heating.

May 16-22 (Figure 37b) continues warming the northern coastlines with the Po water as a cyclonic circulation begins to appear in the northern Adriatic. Temperatures continue to rise in the south, where a large number of drifters have been released in the Otranto Strait.

By the end of May (Figure 37c) the mean SST has risen to over 17°C and the warm influence of the Po river is definitely seen working down the western coastline. A cold region remains in the south while the Albanian coast stays several degrees warmer than the mean SST. The drifters in the Otranto Strait released in the previous week are slowly spreading in several directions.

The first indication that the summer season is beginning occurs in the week of May 30 to 5 June (Figure 38a) as many of the Otranto drifters begin to rapidly move north along the eastern coastline as the southern Adriatic warms, due to solar heating. The shallow northern basin also continues to heat up because of a combination of solar heating and warmer Po inputs. This warm pool is separated from the cooler water to the south by a sharp thermal front along which the drifters move rapidly in the northeast and north directions. Again, the mean SST continues to rise to nearly 20°C. A narrow south bound stream can be observed in the vicinity of the Gargano peninsula as seen in the moderate speed of the coast-hugging drifter as compared to the nearby slower north-bound drifter. Throughout May, several drifters have had little motion while other drifters in the vicinity have shown good mobility.

During June 6-12 (Figure 38b), a cold core region is apparent in the middle Adriatic as indicated by the lower temperature anomaly. The temperature gradient along the Albanian coast appears to be intensifying as the drifters have continued to move north along the front with increased velocities.

The drifters that had been progressing north along the Albanian coast appear to stay on the thermal front while moving toward the middle of the southern basin during the week of 13-19 June (Figure 38c).

June 20-26 (Figure 39a) shows the beginning of reversing southbound mean circulation on the Albanian shelf. A high velocity southward-flowing stream affects the drifters off the Po delta in the north. As the summer begins, a lower SST anomaly prevails along the Croatian coast, possibly due to upwelling processes.

Progressing from June to July (Figure 39b), the mean SST remains about 22.2°C, but the higher anomaly temperature regions seem to be growing in the Po river mouth and the Albanian coast, possibly due to warm river inputs and solar heating respectively. The relatively warm waters on the Albanian shelf move southward following an event of

northerly Etesian winds (Poulain, 1999). The drifters along the central and southern Italian coast move to the south.

The period of July 4-10 (Figure 39c) shows a dramatic increase in the narrow, swift current running south along the western coastline. All drifters close to the coast have significantly increased velocities. The SST anomaly shows more signs of upwelling occurring on the eastern shores.

Upwelling becomes a very prominent feature in the week of July 11-17 (Figure 40a), as seen in the low SST anomaly along the eastern coast from Istria to the Otranto strait created by upwelling processes. Cold upwelled waters are on the eastern flank of the Otranto strait due to the effects of the northerly winds. Other drifters in the basin continue to follow the swift outbound current along the southern Italian coast.

As the summer continues into July 18-24 (Figure 40b), the northern basin is significantly warmer than the rest of the Adriatic due to the warm inputs of the Po river. This is evident in the fast southbound drifter along the coast. The warm Po plume can be seen as far as in the central basin where it is limited by an east/west thermal front, also delineated by the drifter tracks. The upwelling now appears to be the prominent feature along the Croatian and Albanian coasts, while the drifters continue to move south in the southwestern Adriatic.

During the week of July 25-31 (Figure 40c) a new set of drifters were deployed in the eastern Otranto Strait. Drifters previously in the basin show the persistent southern flowing current along the Italian coast. The SST anomaly demonstrates strong upwelling north and south of the Istrian peninsula. The cold water is advected off shore and form two plumes or filaments that move across the basin, resulting in strong thermal fronts. Upwelling also dominates in the eastern Otranto Strait.

The upwelling in the eastern Adriatic during the week of August 1-7 (Figure 41a) is by far the dominating forcing. The northern front that began the previous week has now stretched across the entire basin, and the southern basin upwelling controls the paths of the drifters. The upwelled water on the Albanian shelf moves northward on the south and southward on the north side, resulting in a convergence and offshore flowing filament of cold water, ending in a "mushroom" shape near the center of the southern Adriatic. A narrow southbound current continues along the Italian coast. The maximum mean SST is also found during this week, with a temperature of 26.4°C.

August 8-14 (Figure 41b) continues to show the summer upwelling and associated thermal fronts.

Despite an increase in cloud cover with respect to previous weeks, many of the features seen in previous weeks continue to be present during August 15-21 (Figure 41c). The outflow along the Italian coast remains in place and is verified by a coast-hugging drifter, while other drifters show some trace of cyclonic circulation in the southern basin. The mean SST has notably dropped to 24.9°C.

The end of August (22-28) (Figure 42a) shows a new release of drifters in the Otranto Strait which are moving consistently into the Adriatic Sea, demonstrating a fairly strong inflow into the basin. Drifters previously in the basin continue on paths along the coastlines in a cyclonic direction. The SST anomaly appears to be reducing throughout the basin, but this is likely due to the comparison with the relatively warmer, late summer Ionian waters at the Otranto Strait.

Strong currents dominate the Otranto Strait and Albanian shelf during the week of August 29 to September 4 (Figure 42b) as seen by the increased velocities of both the inbound and outbound drifters. We may be seeing a change of season as the upwelling, while still present south of the Istrian peninsula, is less influential on the circulation of the sea. Autumn brings the intrusion of the Ionian waters, pushing not only the drifters, but also a warm stream up the Albanian coast. Late August and early September (Figures 42a,b,c) are characterized by a strong cyclonic gyre circulation in the southern basin. The water near both coasts is relatively warmer than the cold center of the gyre. The relative warming near the southern Italian coast is presumably due to the solar heating of the shallow waters.

During the week of September 5-11 (Figure 42c) drifter velocities maintain high speeds along the coast. The drifters remain caught up in the warmer waters, refusing to cross the front.

The weeks of September 12-18 (Figure 43a) and September 19-25 (Figure 43b) exhibit more of the same circulation, with drifters moving quickly along the Croatian coastline following the warm water intrusion from the Ionian. During this time, the drifters that had been slowly moving around the south basin have now joined the northward flow of the other drifters. The Northern Adriatic appears to continue to cool, and the mean SST is now about 22°C.

By the week of September 26 to October 2 (Figure 43c), the drifters escaped the warmer water and move in several different

directions, as the warm coastal layer is widening. The northern most drifter has turned south along the Italian coast, while others have turned to the west at various locations in the basin. The temperature of Ionian water remains significantly higher, but the basin continues to cool into autumn.

The October 3-9 period (Figure 44a) exhibits two distinct sides to the central and southern Adriatic: a continued warm side along the Albanian and Croatian coasts pushing drifters north, and a colder, wider region taking the center and Italian half of the basin. Many drifters move along the front between the two regions. Into October 10-16 (Figure 44b), the drifters move toward the cooler section and turn south. The cold coastal flow along the Italian coast has intensified and the outflow of the Adriatic is much larger than the outflow of previous months. For the first time in months the mean SST has dropped below 21°C. Additionally, another drifter release occurs in the Otranto Strait during this week.

The final week of this study (October 17-23, Figure 44c) shows a strong shear in the Otranto Strait with warm inflow to the east and a cold outflow to the west. The change of current direction corresponds remarkably to the sharp temperature front near the center of the strait. During October it becomes apparent that the outflow is significant as the warm Ionian water is now being replaced by the colder outflowing Adriatic. The Po river is again influencing the SST, with indications of much colder temperatures appearing in the north and close to the Italian coastline.

Figure 46 compares the weekly mean temperature at specific points throughout the Adriatic basin. The Po river mouth, near the Istria peninsula, near the Gargano Peninsula, off the Albanian coast, and both the east and west sides of the Otranto Strait are observed (Figure 46a) in presentations grouped by the north, middle, and extreme southern Adriatic. The Po river is warmer than the northern basin for much of the spring and summer, as seen in Figure 46b. However, as autumn begins the colder inputs of the river drop the temperature below the values encountered near the Istria peninsula. Likewise, the temperatures at the Gargano peninsula and Albanian coast fluctuate with season (Figure 46c). The Albanian coast is warmer in the spring (solar heating) and autumn (Ionian inflow), but much cooler than the Gargano peninsula waters during the summer due to the upwelling along the eastern side of the Adriatic. The temperature differences across the Otranto Strait can

be attributed to upwelling events along the eastern coast and to the shear between the surface flows in and out of the Adriatic. Like the Gargano/Albania comparison, the east side is warmer in the spring and autumn due to local heating and Ionian inputs, but the summer months bring colder upwelled waters that decrease temperature below that of the west side of the Otranto Strait.

C. SELECTED 3 DAY AND 1 DAY COMPOSITES WITH DRIFTER TRACKS

The composite satellite images were used along with the drifter data to describe the mesoscale surface variability in the southern Adriatic and Otranto Strait areas. Two periods with drastically different regimes were chosen, one in July dominated by upwelling processes near the eastern coast and one in October in which the inbound and outbound transports through the Otranto Strait are substantial. In order to provide the most accurate thermal fields during the periods considered, the satellite composite images were offset so as to minimize the difference between the satellite and smoothed drifter temperatures over the periods. Even though the images were already corrected (see Chapter III E) based on global statistics, a better calibration of the composite temperature values can be obtained by a local analysis. For the periods considered (either 1 or 3 days) and for the southern Adriatic and Otranto Strait region, the low-passed filtered drifter temperatures were compared to composite values at the drifter positions. The comparison statistics are presented in Table 4. The images presented in Figures 47 through 54 have been corrected by the mean difference.

Period	Number of drifter observations(6hr)	Mean SST diff (Sat-Drifter) (°C)	Standard dev of SST difference(°C)
8 July	29	0.00	0.25
9 July	35	0.00	0.28
10 July	37	-0.44	0.36
8-10 July	91	-0.36	0.57
17 October	60	-0.31	0.21
18 October	62	-0.47	0.35
19 October	64	-0.37	0.30
17-19 October	160	-0.37	0.24

Table 4. Comparison statistics between smoothed drifter and composite satellite SSTs in the southern Adriatic and Otranto Strait region.

1. Period 8-10 July 1995

The daily (Figures 47 to 49) and the 3-day (Figure 50) composite thermal images reveal a situation dominated by strong upwelling events along the Albanian coast. The cold ($19-20^{\circ}\text{C}$) upwelled water progresses offshore in the form of filaments extending westward or southward from specific fixed locations along the coast. These locations generally correspond to capes and peninsulas where the upwelling dynamics are favored. Northerly winds (mostly Etesian) are triggering these events. The daily sequence of images and the corresponding drifter displacements show the evolution of the mesoscale structure of two cold filaments in the Otranto Strait. In particular the southernmost filament develops a mushroom shape in a few days. Extended upwelling is seen to develop on 10 July (Figure 48) further to the north on the Albanian shelf. The cloud cover on the subsequent day preclude the description of its evolution.

On the other side of the basin, rather strong southeastward currents carry the relatively warm surface Adriatic water along the Italian coast and out of the basin on the western side of the Otranto strait. The surface temperature is about $24-25^{\circ}\text{C}$. No structural difference is seen over the 3-day sequence.

The 3-day image (Figure 50) is a mean representation of the above structures. The outflow of warm water is obvious along the Italian coast and through the western flank of the Otranto Strait. The cold upwelling structures near the southern Albanian coast (eastern Otranto Strait) are also well represented. In contrast, the sudden upwelling occurring on 10 July to the north is blended with the warmer conditions of the previous days. This is a situation in which daily images are necessary to describe the mesoscale structure of these rapidly evolving phenomena.

2. Period 17-19 October 1995

The surface thermal field for the period 17-19 October (Figures 51 to 54) is somehow reversed with respect to the July situation. Relatively cold ($\sim 20^{\circ}\text{C}$) water is outflowing along the Italian coast and through the western Otranto Strait. Speeds are of the same order of magnitude as in July (about 25 km per day or about 20-30 cm/s). On the other side of the Strait and on the Albanian shelf there is a strong inflow of warm Ionian surface water. The horizontal transport of surface waters across the strait is thus substantial and highly sheared.

The daily sequence of images discloses the evolution of mesoscale instability features across the thermal front separating the warm Ionian and cold Adriatic waters. On 17 October (Figure 51), some of the drifters show a cyclonic (counter-clockwise) movement around a small (~10 km) cold eddy that had probably pinched off from a frontal instability at previous times and had penetrated the warm waters. Just to the south, we see the birth of a new instability with intrusion of cold water into the warm environment. On subsequent days (Figures 52 and 53), the meander develops into a parcel of cold water that eventually will detach from the front. On 19 October, a second meander has formed just north of the parcel. The drifter motion in the vicinity indicates strong shear of the horizontal currents, necessary conditions to create meanders and parcels through barotropic instability of the mean circulation.

A warm feature is apparent in the northeast of the southern Adriatic off the Montenegro coast. Although its formation mechanisms are unclear, the feature is seen to propagate to the northwest with the prevailing mean surface circulation.

The 3-day composite image (Figure 54) delineates the main features of the surface thermal fields, but the details of the fast evolving instabilities are blurred. This is a further evidence that, to describe the mesoscale features in the Adriatic, full spatial resolution and temporal averaging over a maximum of one day are necessary.

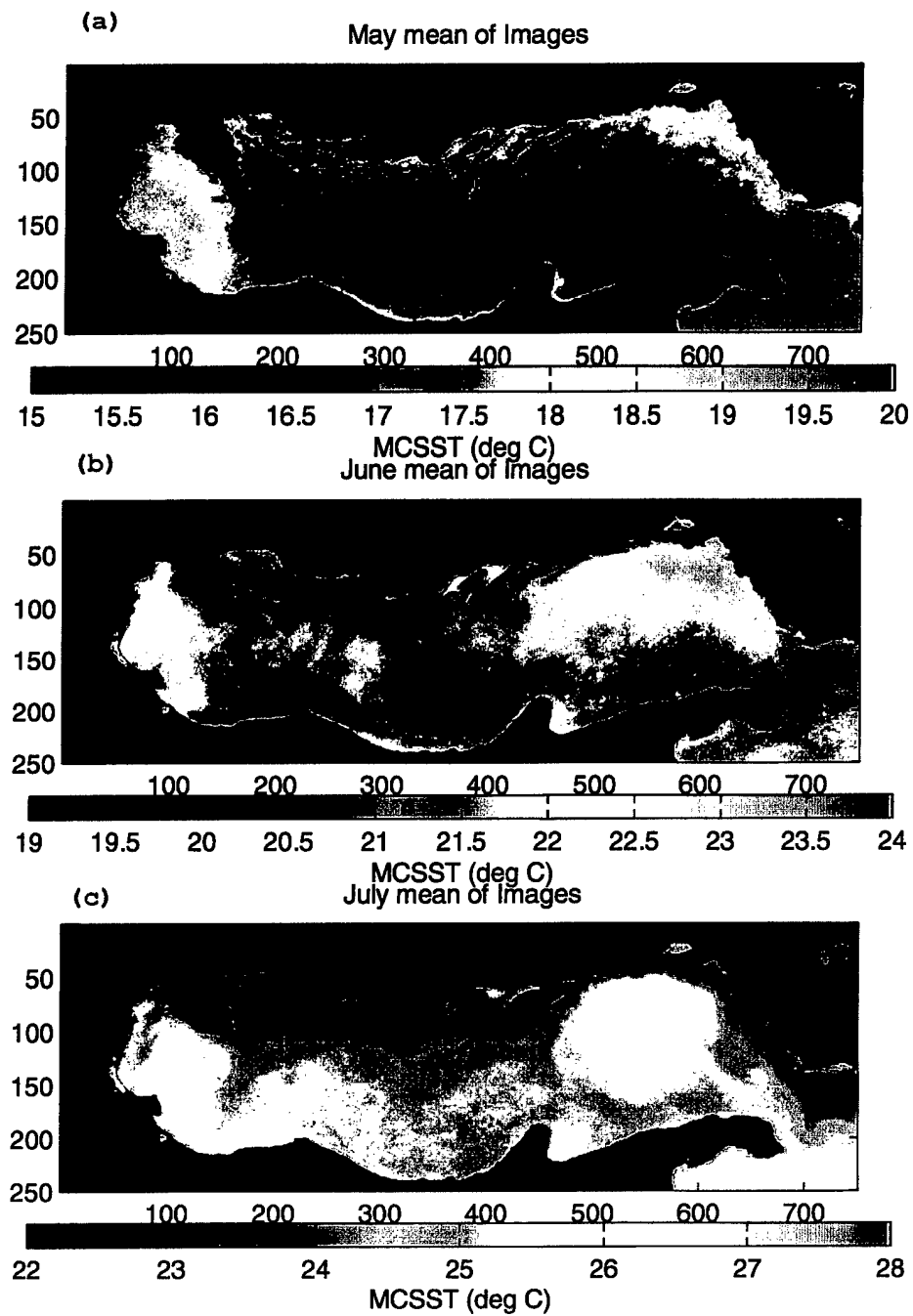


Figure 36. SST composite images for (a) May, 1995, (b) June, 1995, (c) July, 1995.

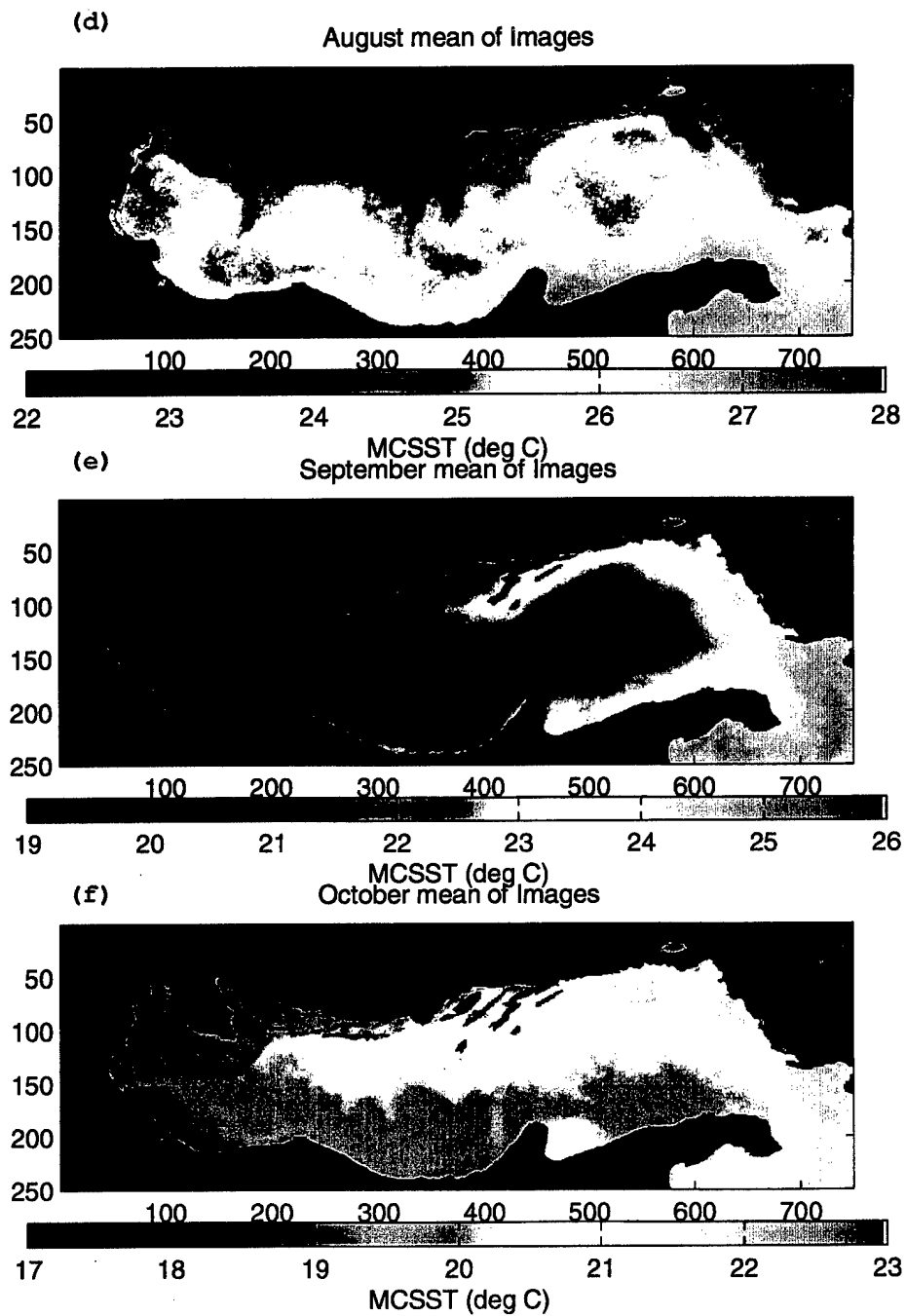


Figure 36 continued. SST composite images for (d) August, 1995, (e) September, 1995, (f) October, 1995.

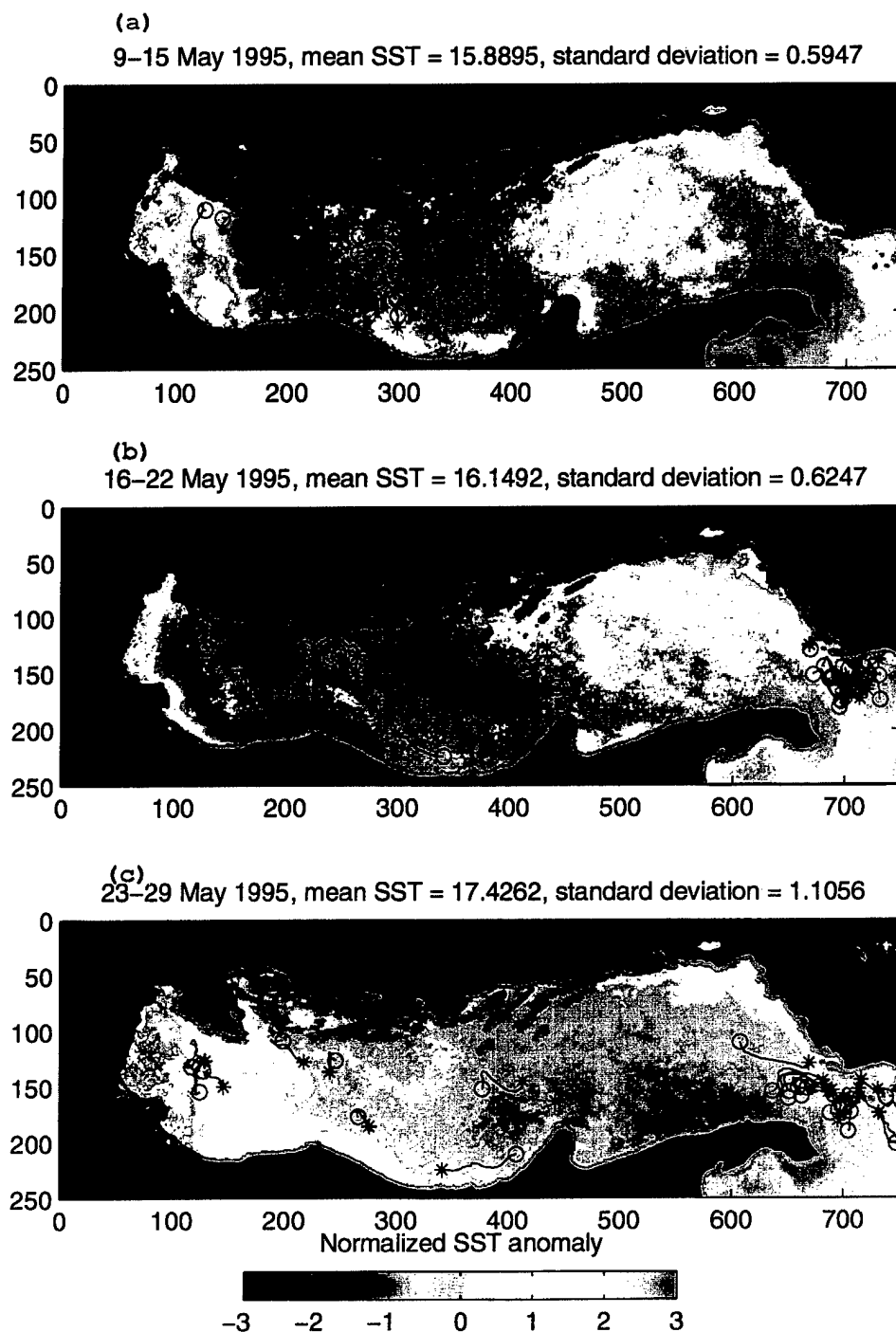


Figure 37. Weekly composite images for (a) May 9-15, 1995, (b) May 16-22, 1995, (c) May 23-29, 1995. The spatial mean was removed and the SST anomaly was normalized by the standard deviation. Weekly drifter trajectories are superimposed, with star (circle) symbols at beginning (end).

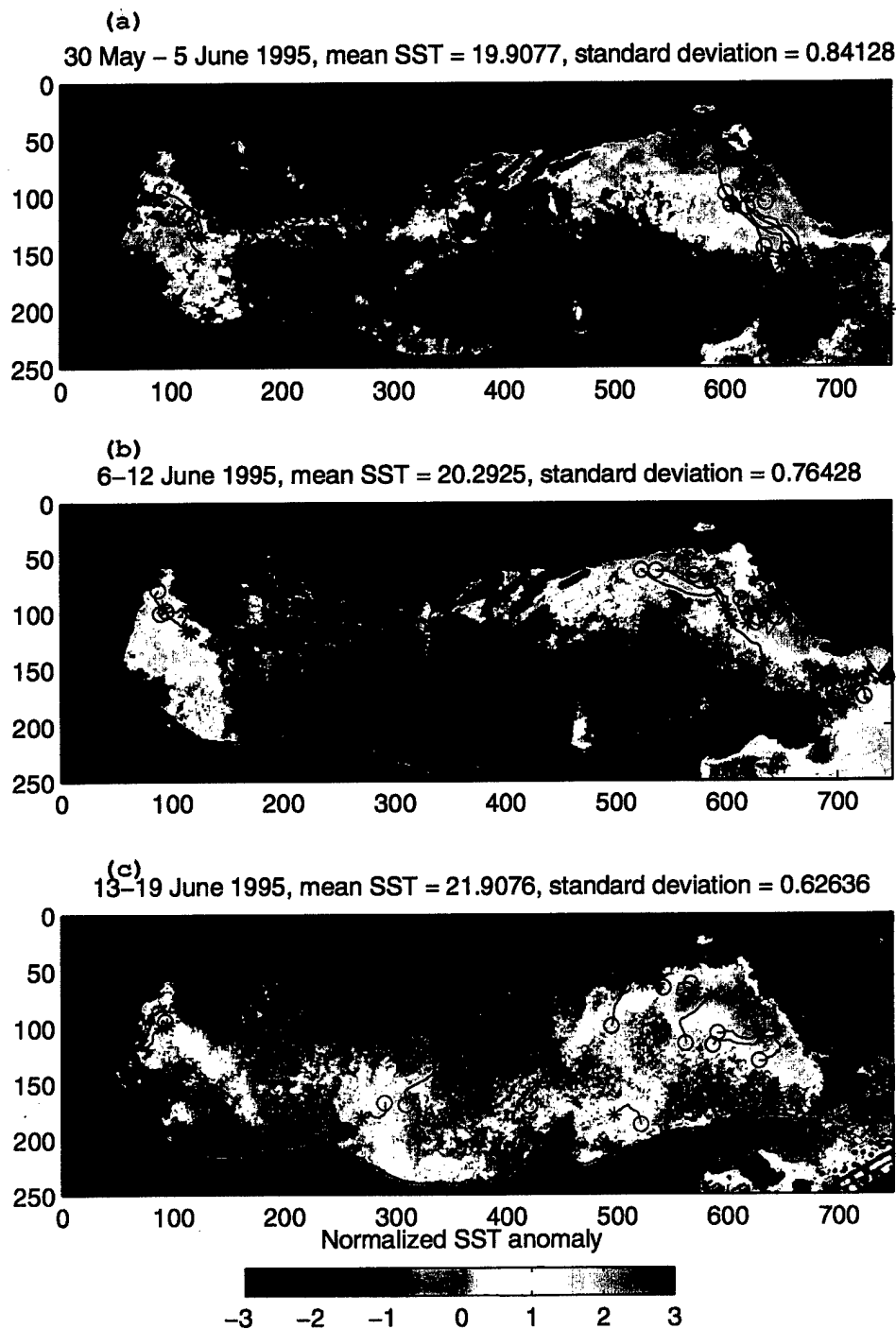


Figure 38. Same as Figure 37, but for (a) May 30 - June 5, 1995, (b) June 6-12, 1995, (c) June 13-19, 1995.

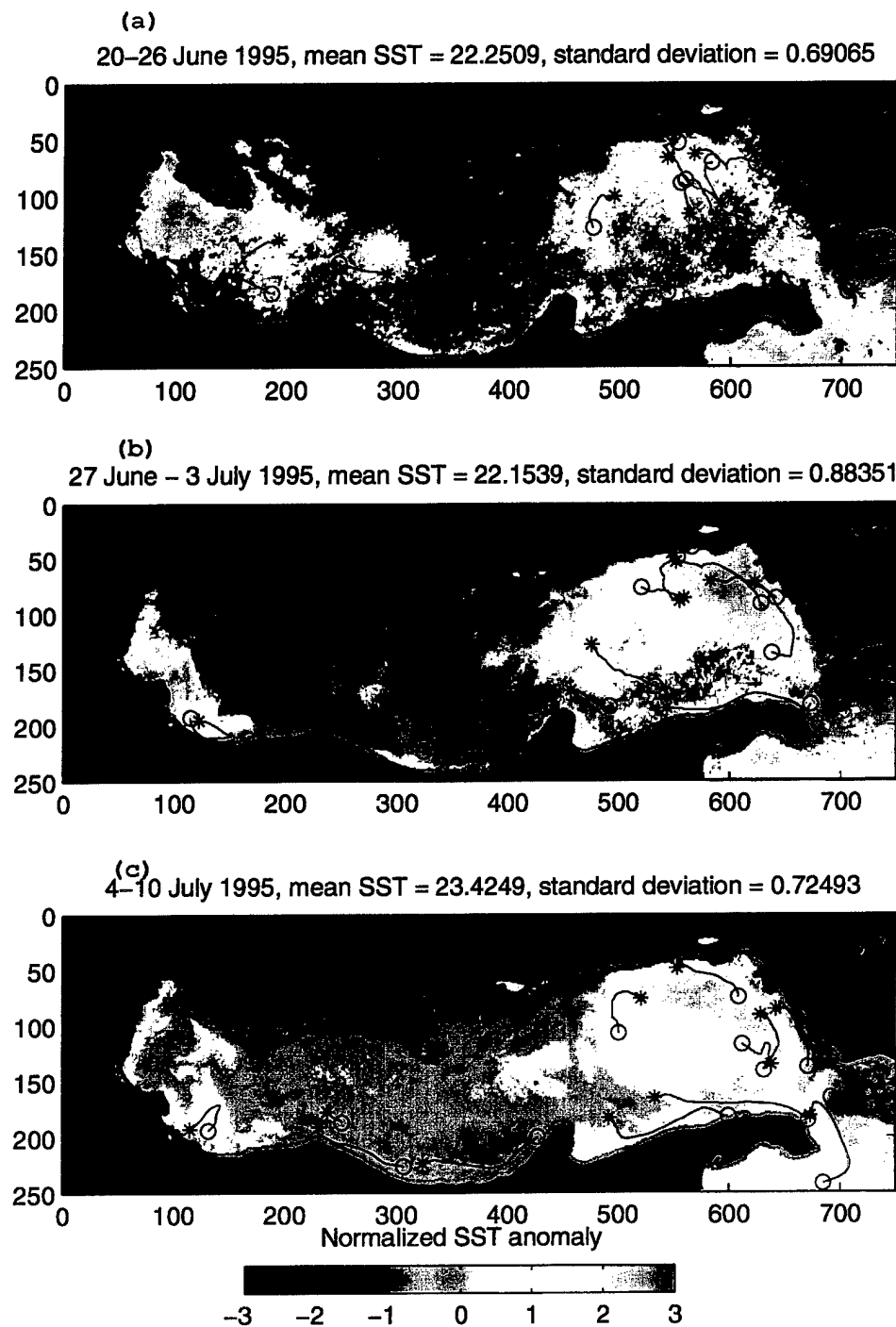


Figure 39. Same as Figure 37, but for (a) June 20-26, 1995, (b) June 27 - July 3, 1995, (c) July 4-10, 1995.

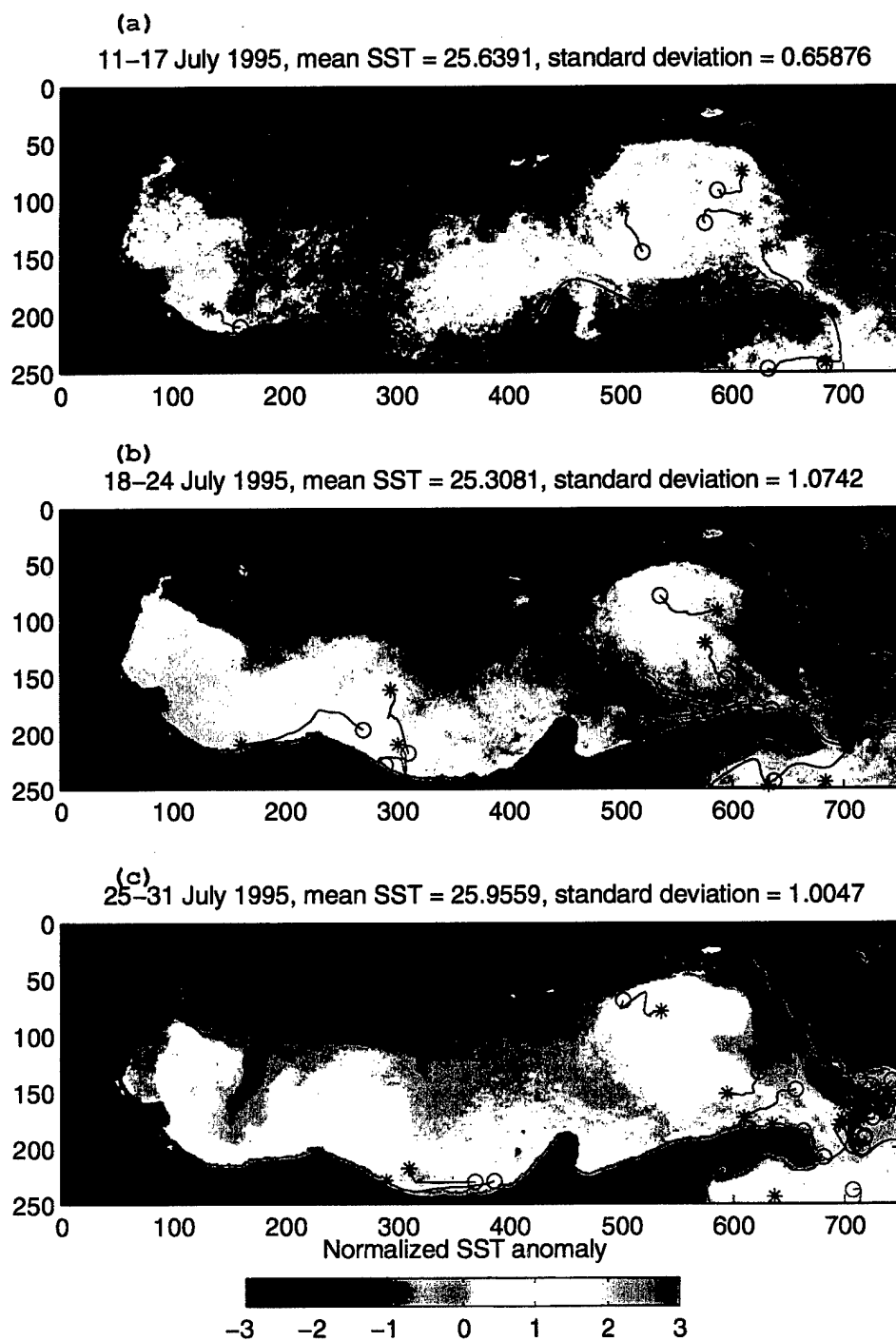


Figure 40. Same as Figure 37, but for (a) July 11-17, 1995, (b) July 18-24, 1995, (c) July 25-31, 1995.

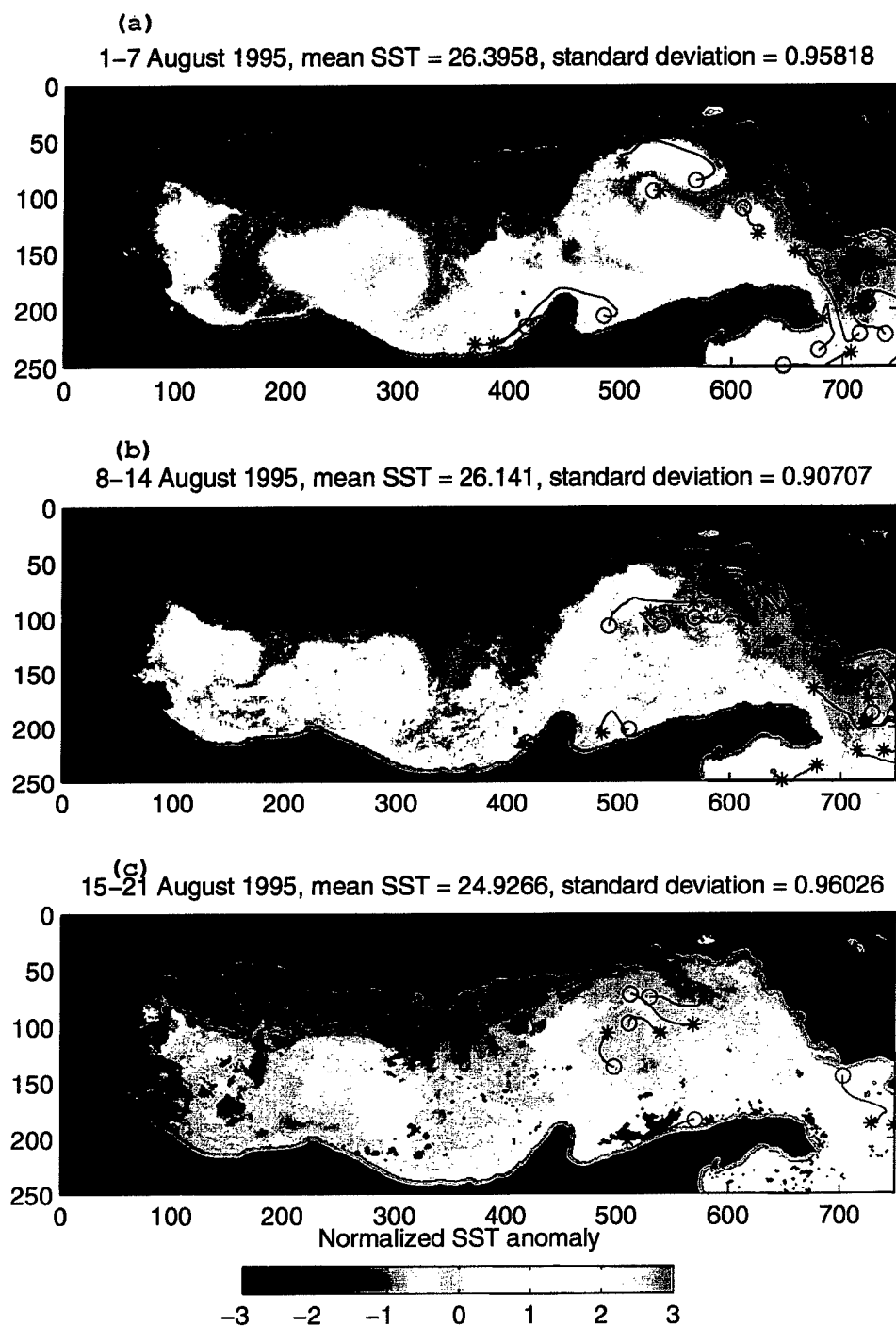


Figure 41. Same as Figure 37, but for (a) August 1-7, 1995, (b) August 8-14, 1995, (c) August 15-21, 1995.

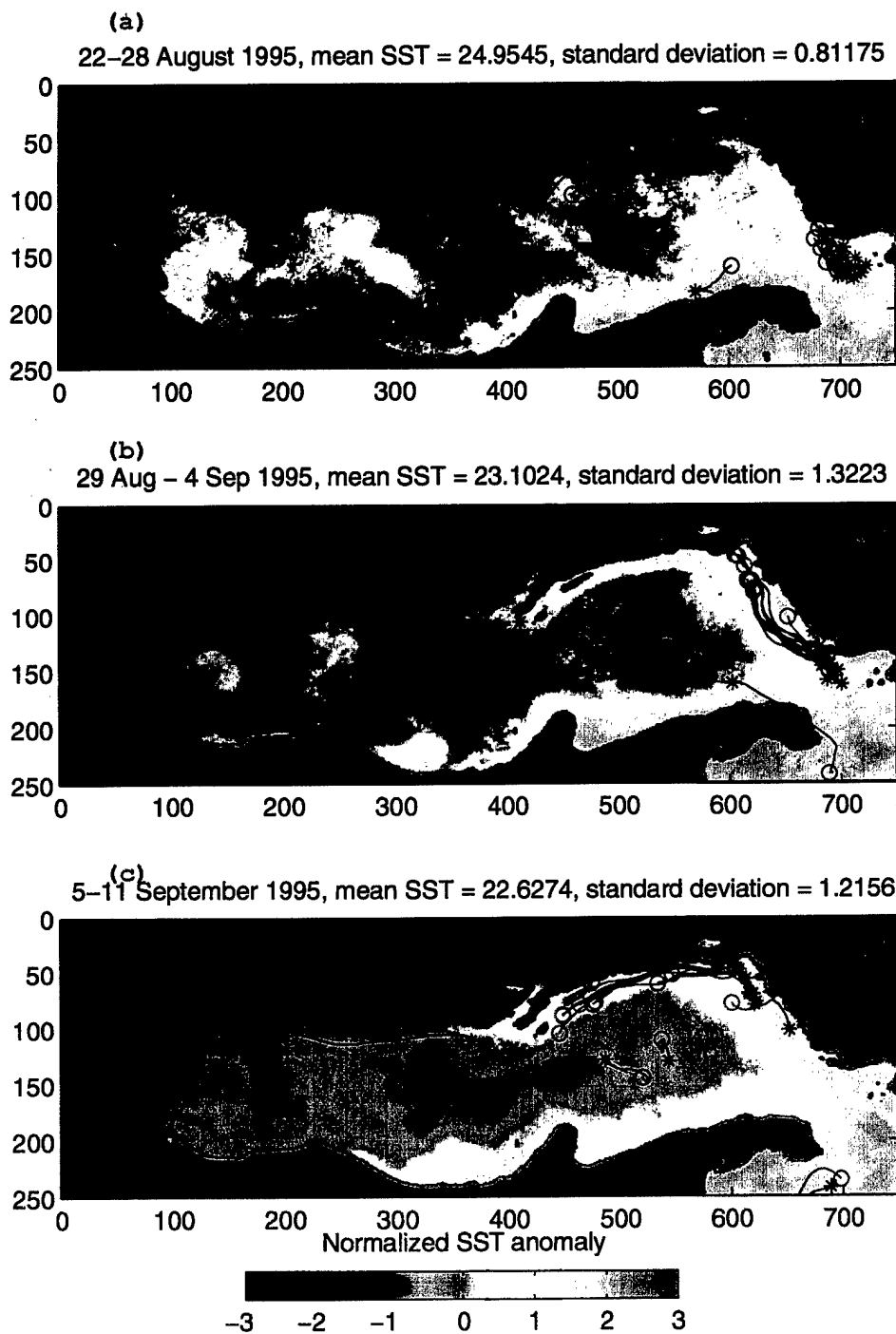


Figure 42. Same as Figure 37, but for (a) August 22-28, 1995, (b) August 29 - September 4, 1995, (c) September 5-11, 1995.

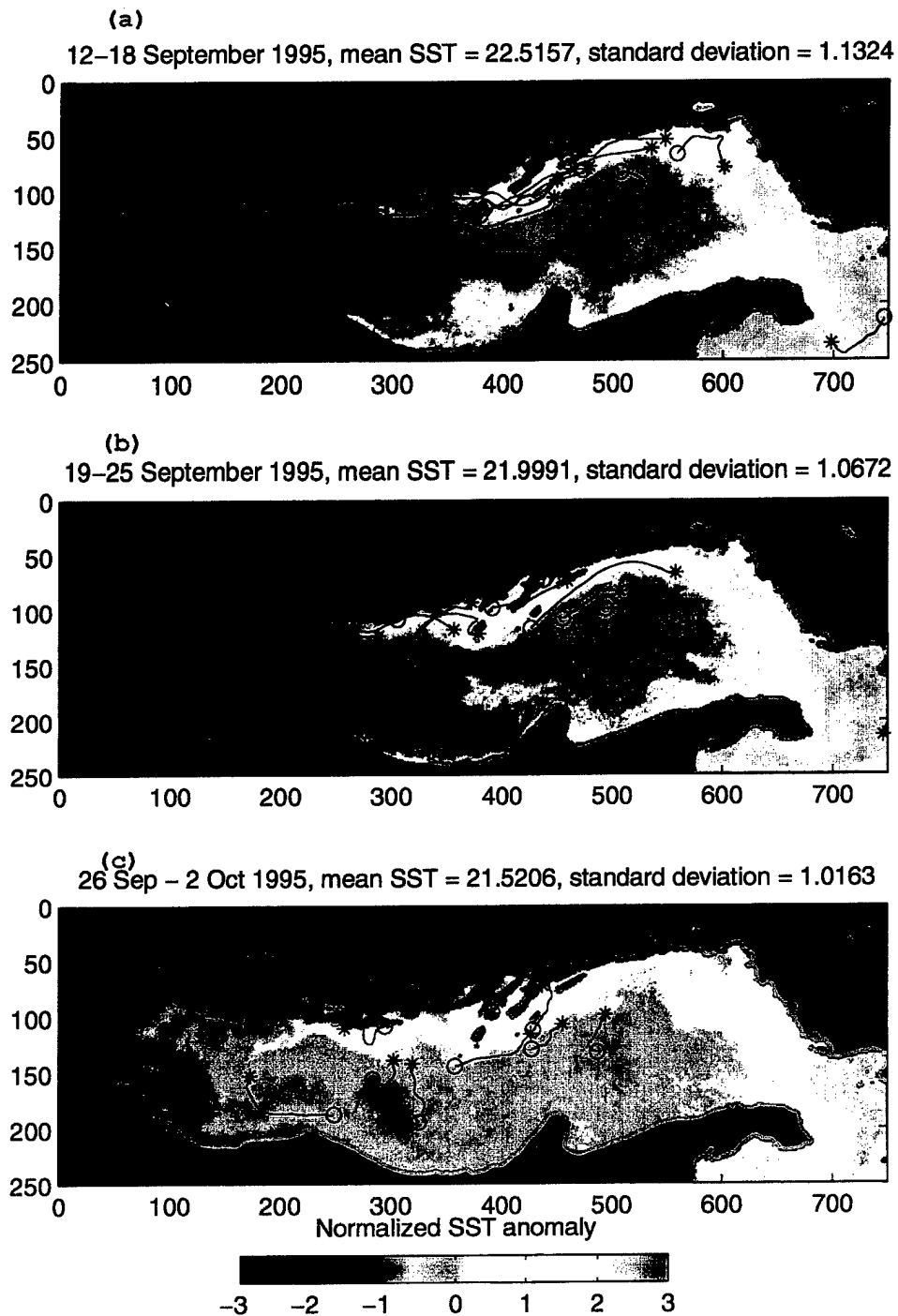


Figure 43. Same as Figure 37, but for (a) September 12-18, 1995, (b) September 19-25, 1995, (c) September 26 - October 2, 1995.

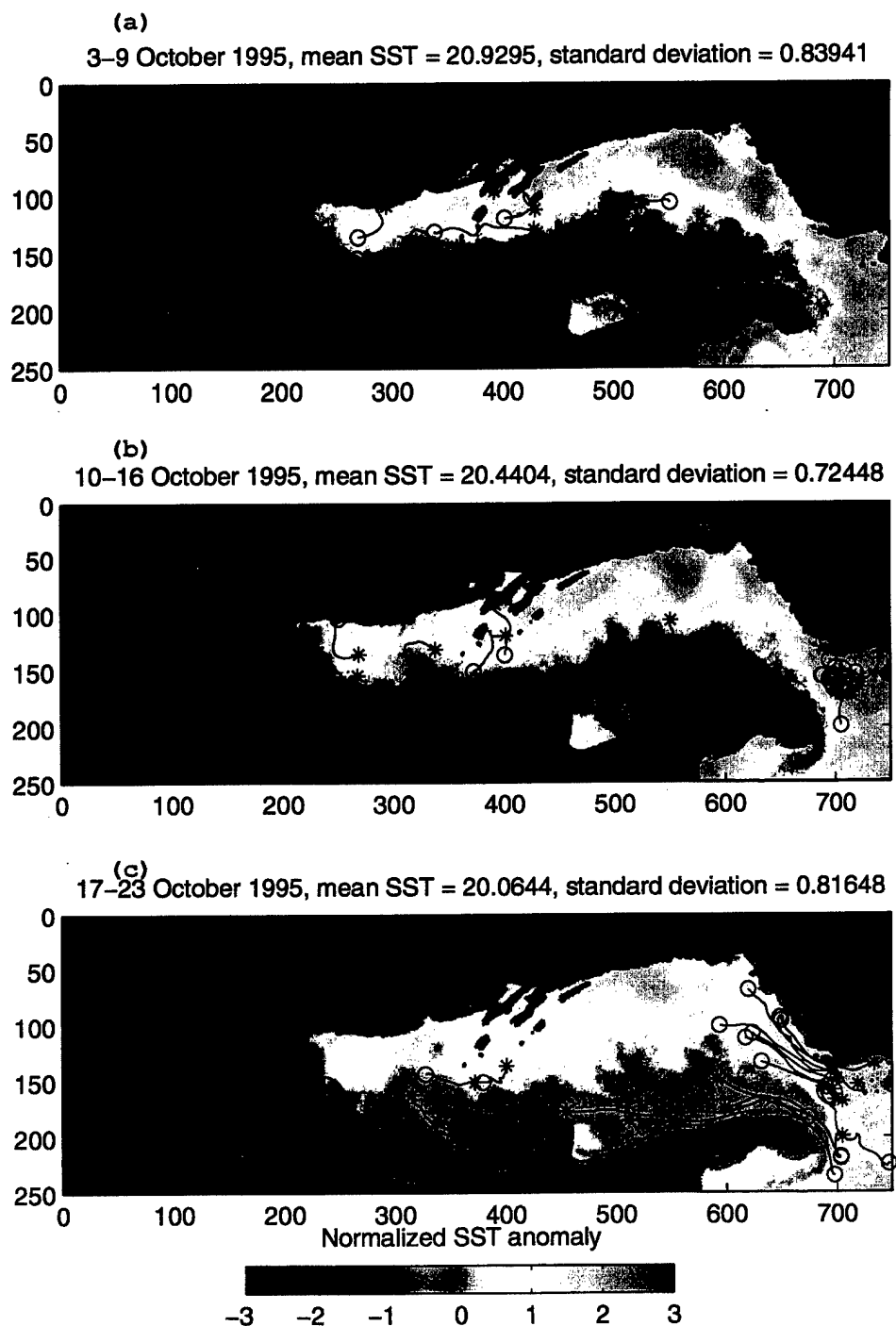


Figure 44. Same as Figure 37, but for (a) October 3-9, 1995, (b) October 10-16, 1995, (c) October 17-23, 1995.

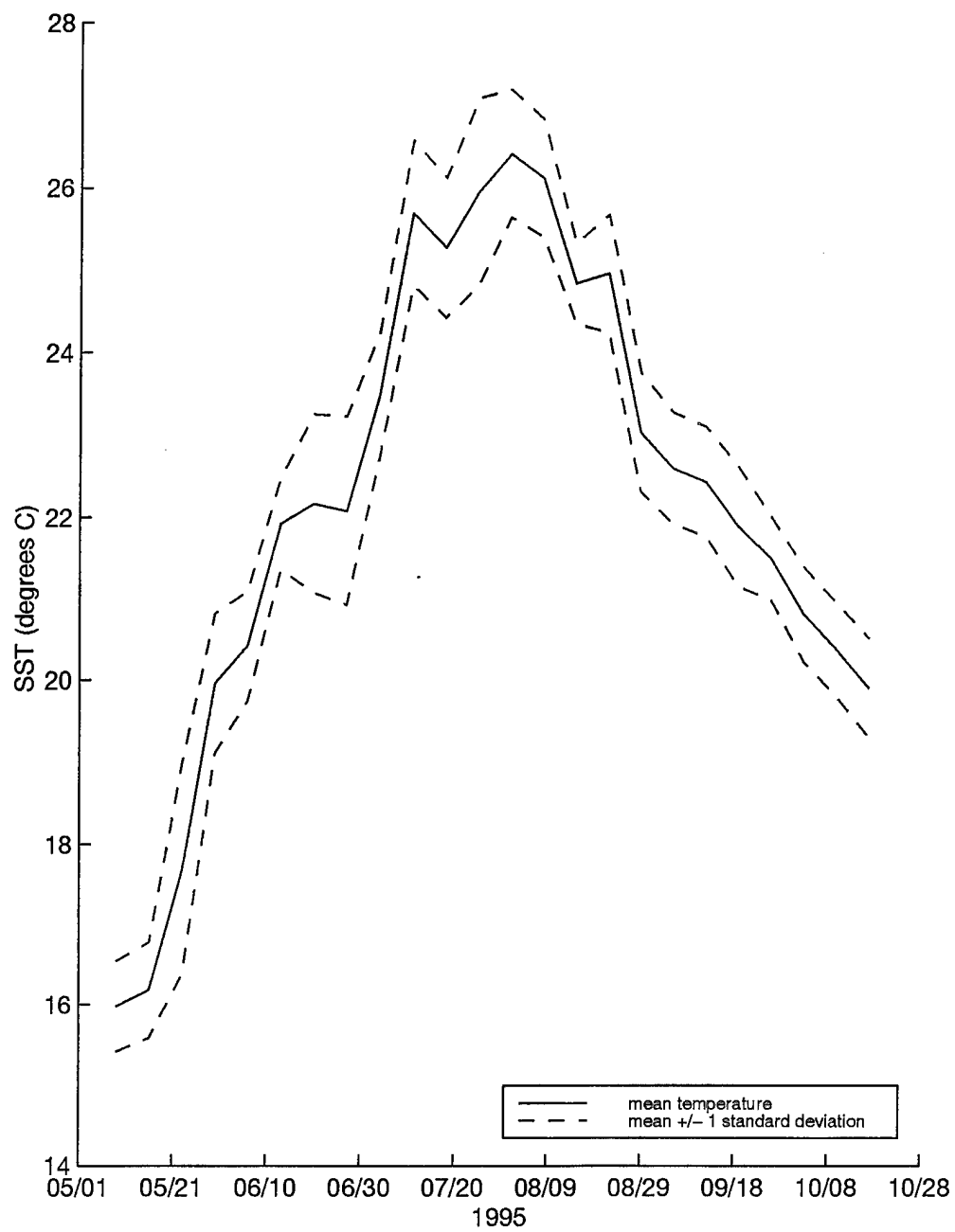


Figure 45. Spatial mean and standard deviation interval of the weekly temperature composites over the Adriatic Sea.

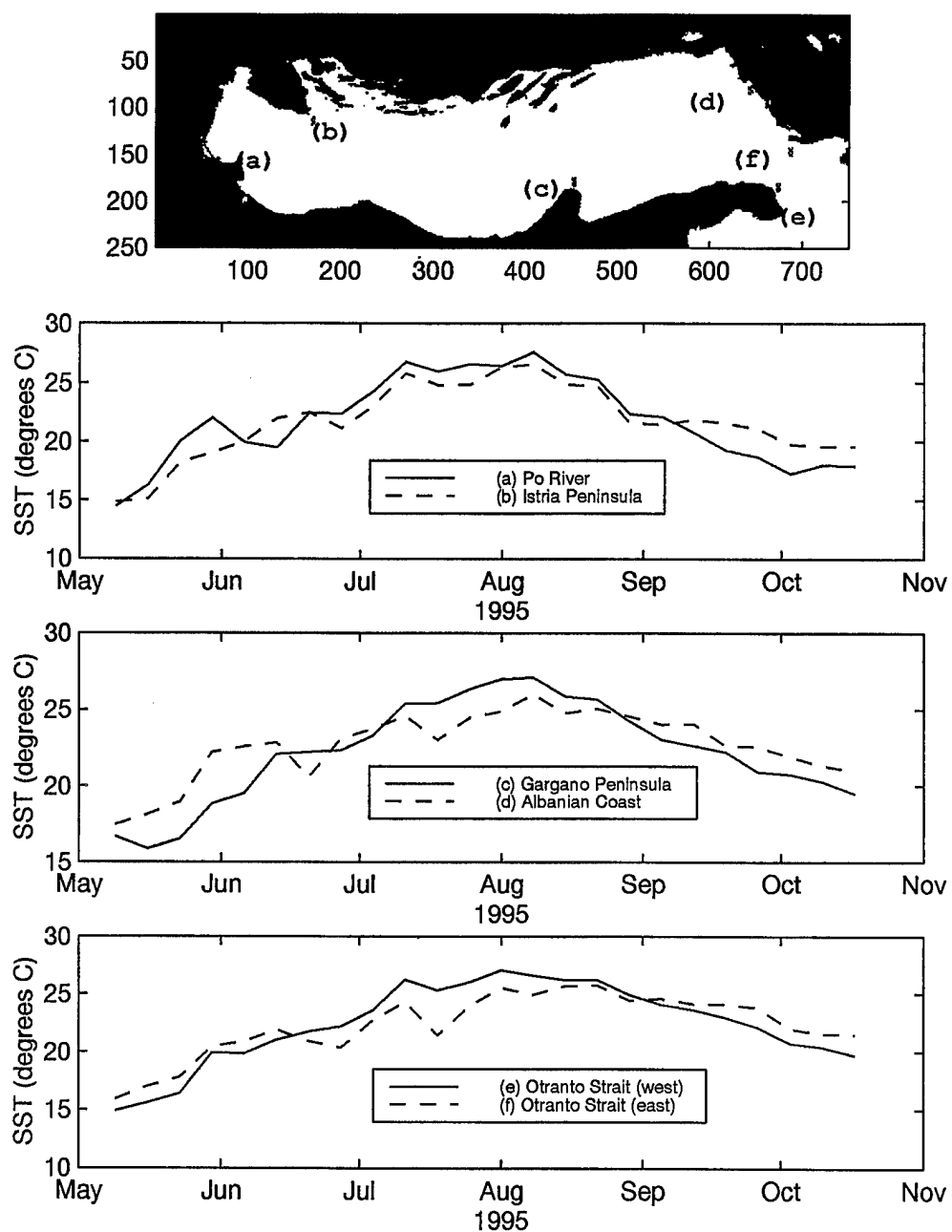


Figure 46. Comparison of weekly mean temperatures at (a) Po River, (b) Istria Peninsula, (c) Gargano Peninsula, (d) Albanian Coast, (e) Otranto Strait (western boundary), (f) Otranto Strait (eastern boundary).

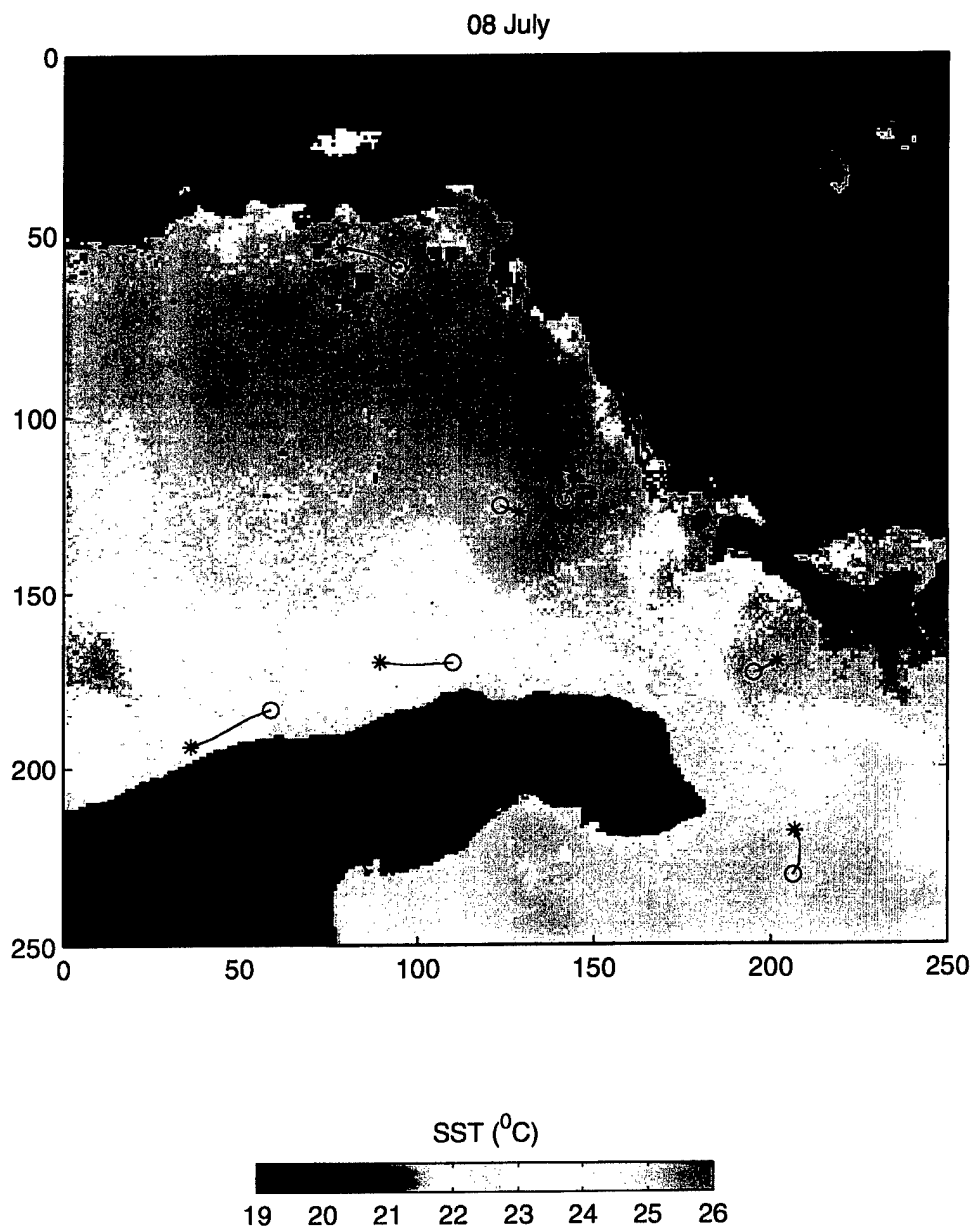


Figure 47. "Median of medians" composite in the southern Adriatic and Otranto Strait region with simultaneous drifters overlaid for period July 8, 1995. Drifter tracks over the same time are overlaid, with star (circle) symbols at beginning (end).

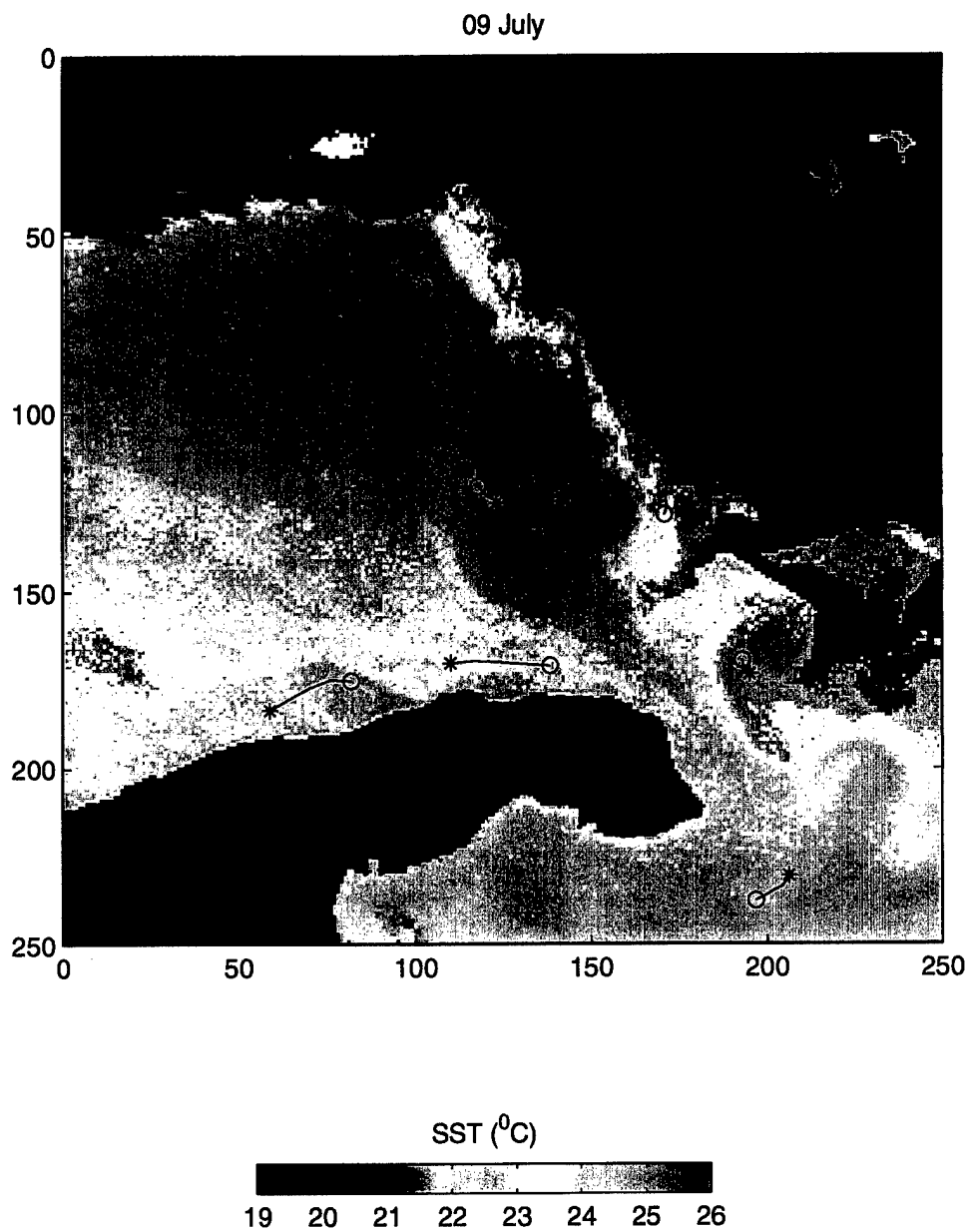


Figure 48. Same as Figure 47, but for July 9, 1995.

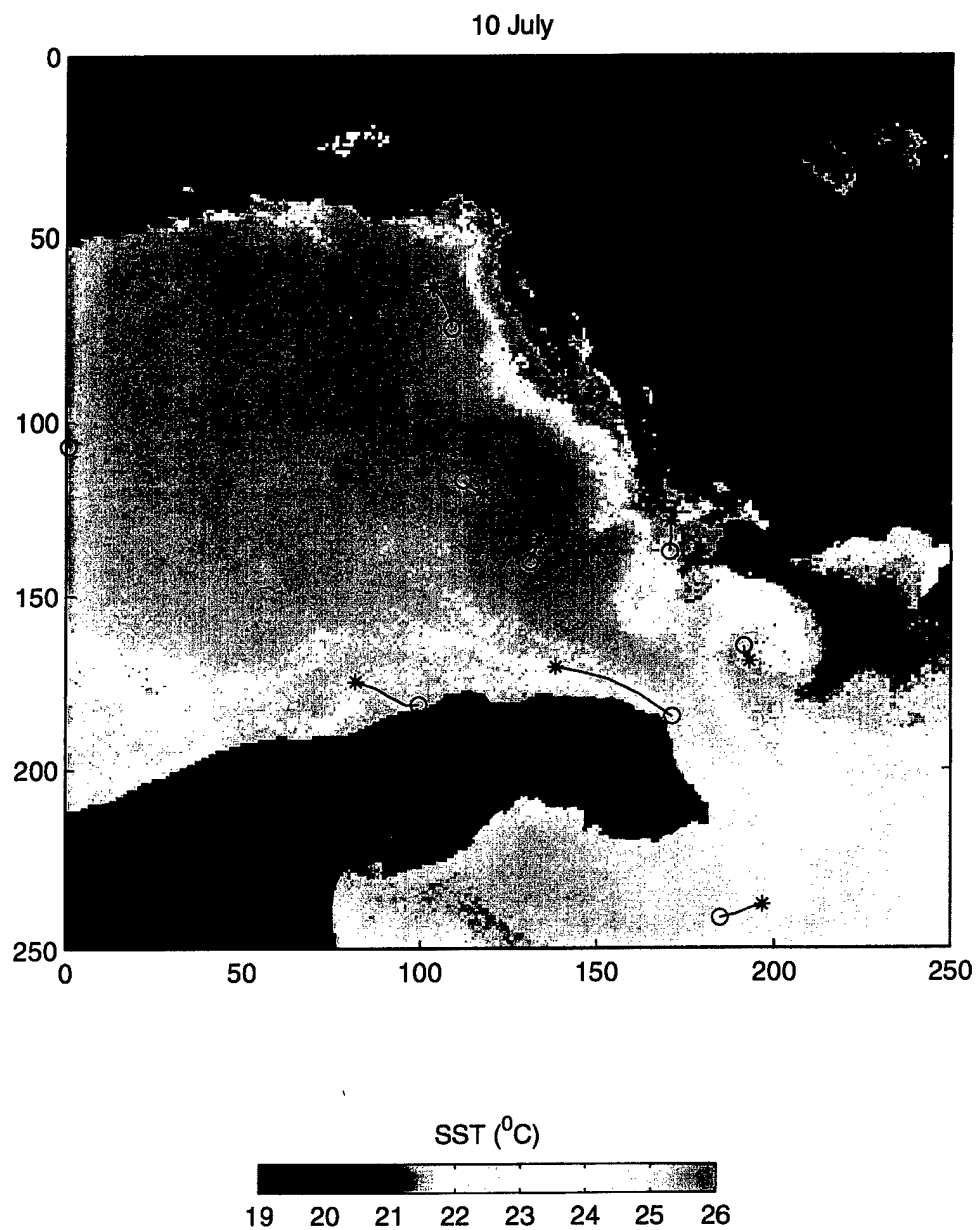


Figure 49. Same as Figure 47, but for July 10, 1995.

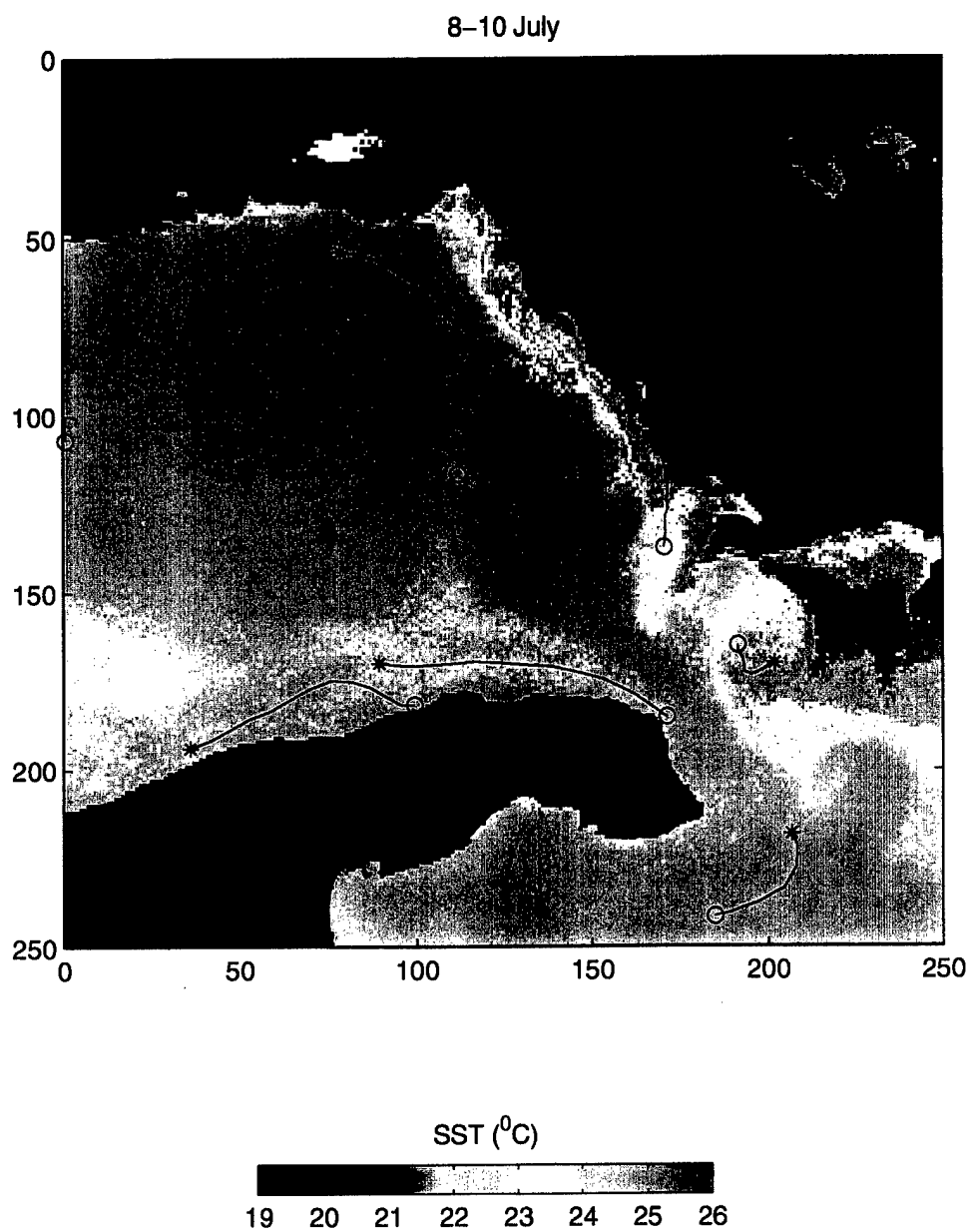


Figure 50. Same as Figure 47, but for July 8-10, 1995.

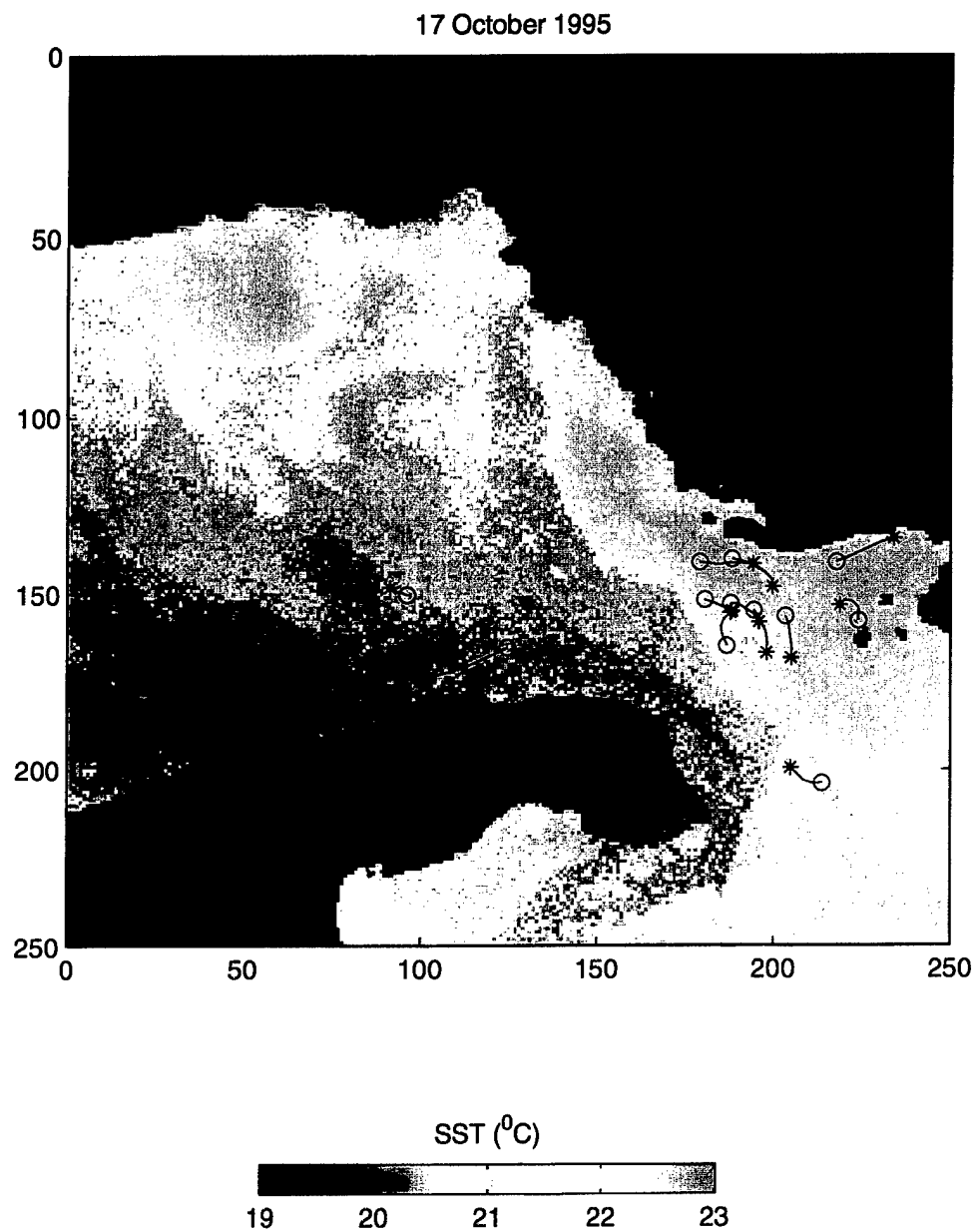


Figure 51. Same as Figure 47, but for October 17, 1995.

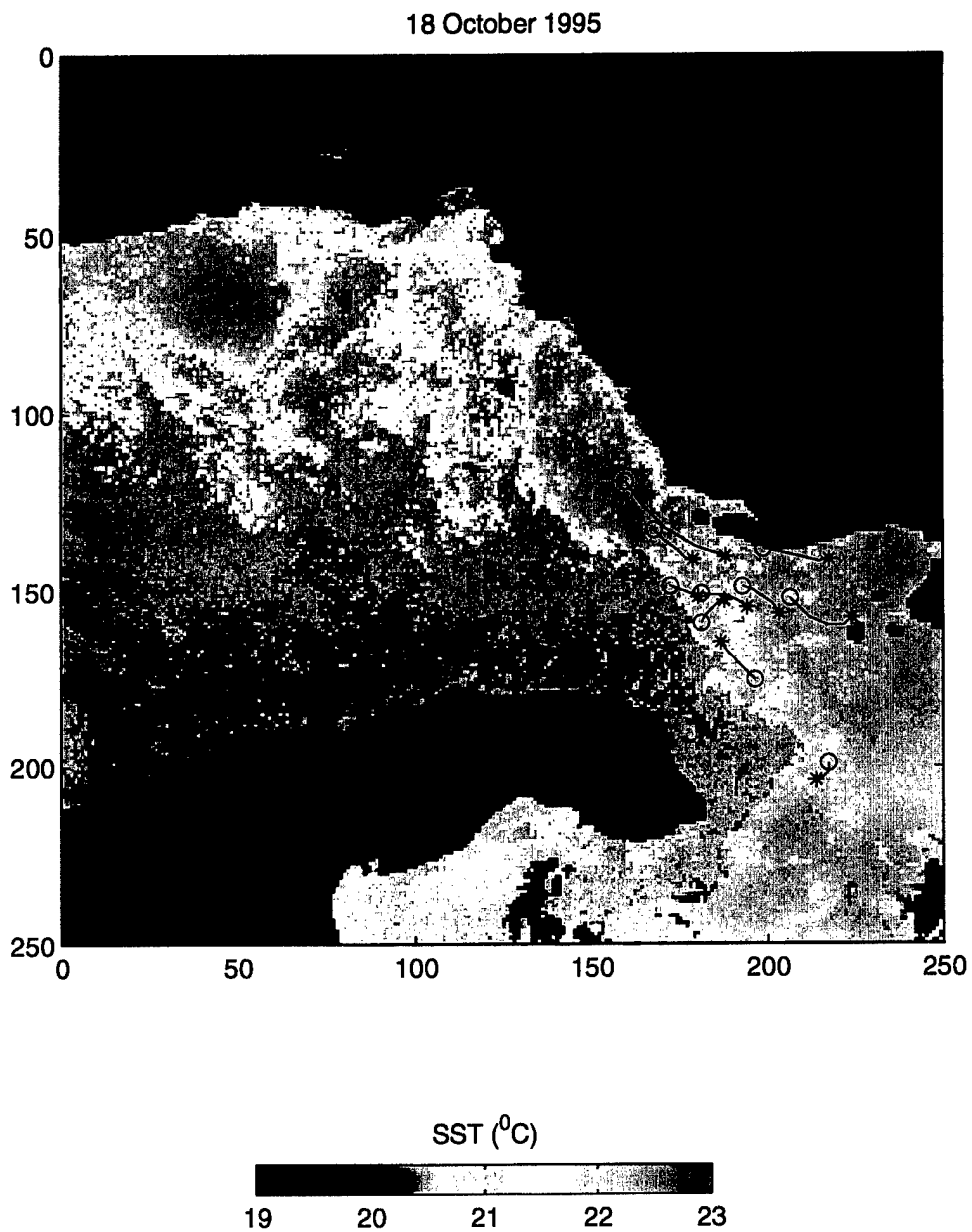


Figure 52. Same as Figure 47, but for October 18, 1995.

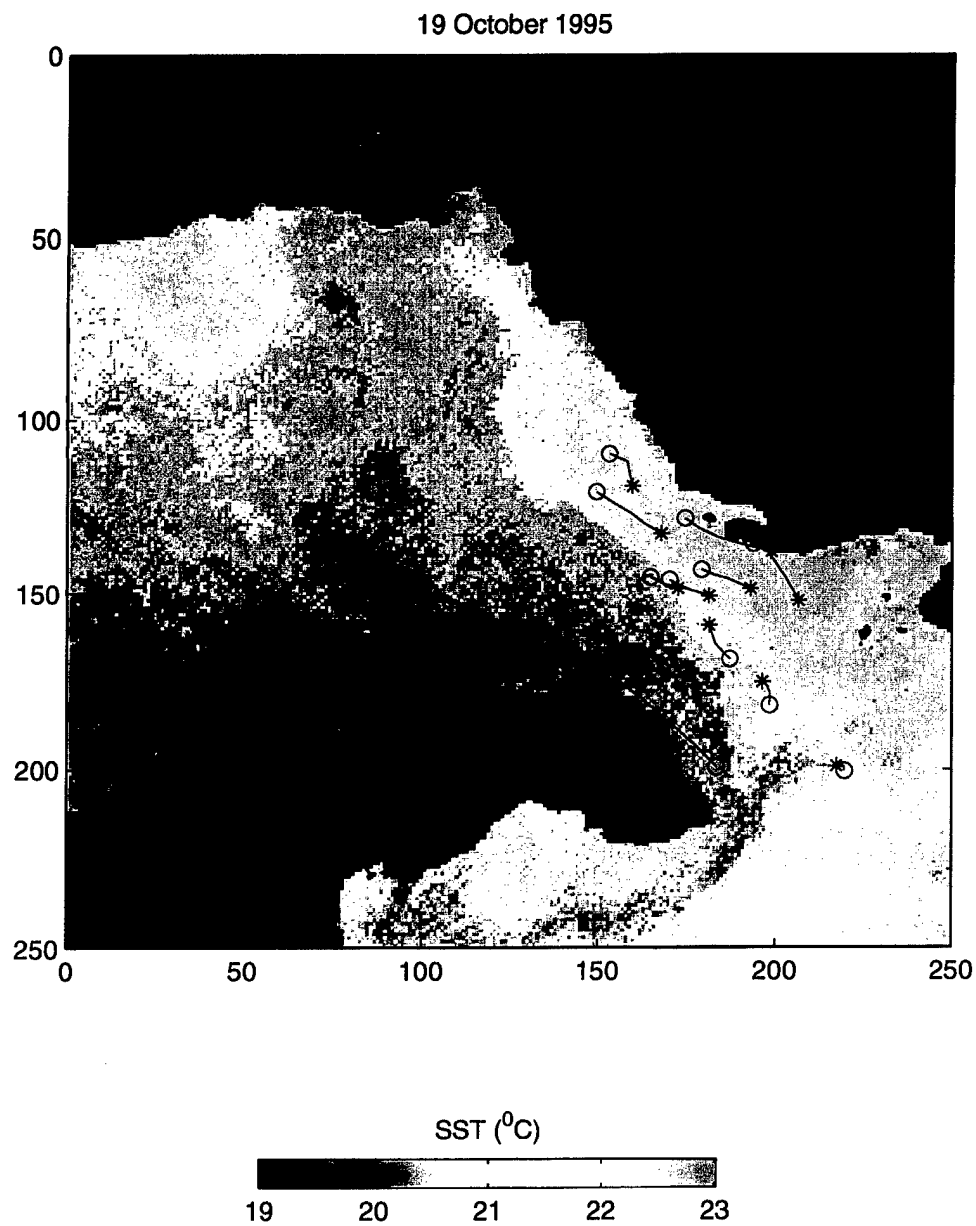


Figure 53. Same as Figure 47, but for October 19, 1995.

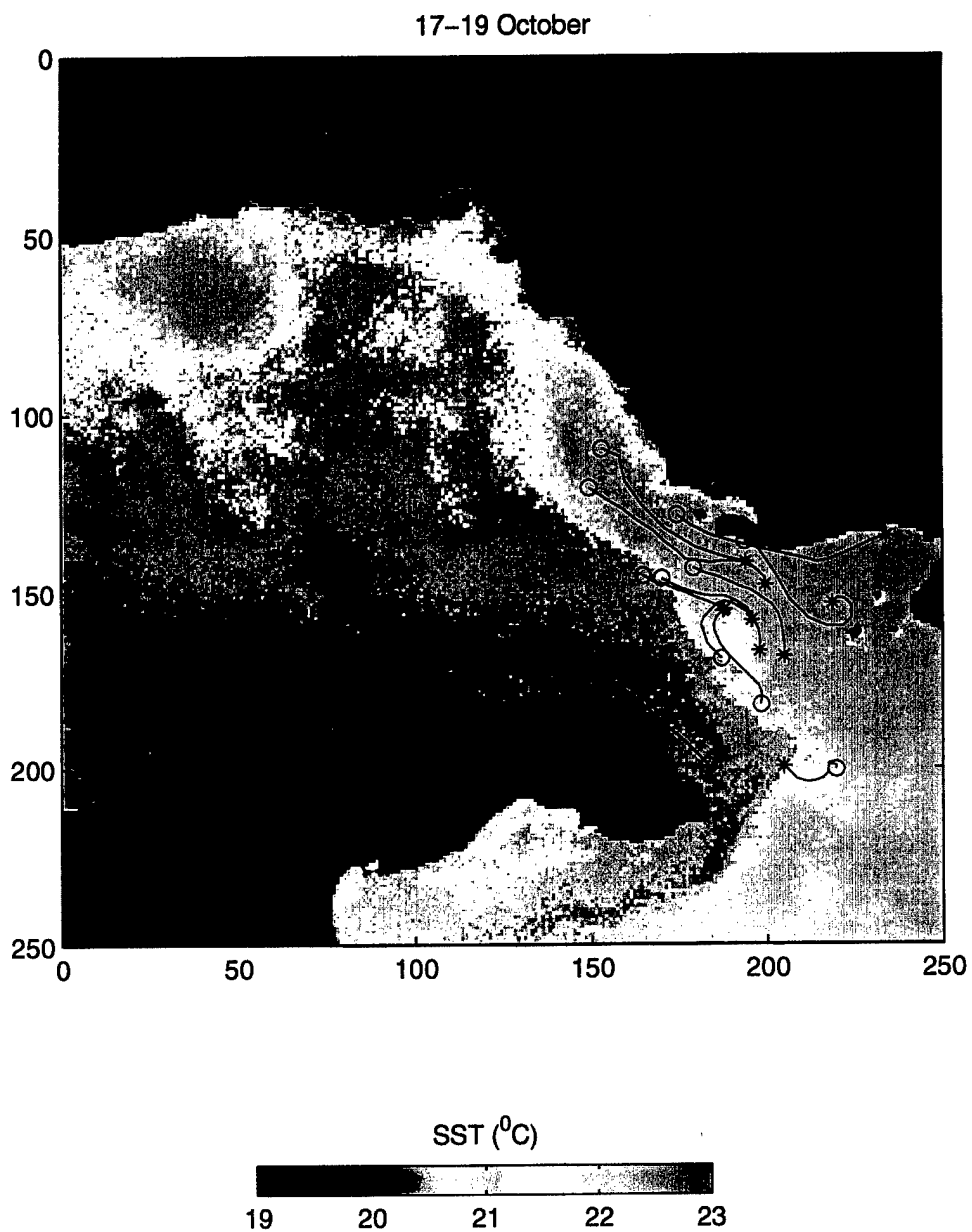


Figure 54. Same as Figure 47, but for October 17-19, 1995.

V. DISCUSSION AND CONCLUSIONS

This study has focused on a period of 6 months (May to October, 1995) in which the full resolution (1.25x1.25 km) satellite AVHRR images were used to describe and study the variability of the Adriatic sea surface temperature and circulation from meso- (days) to seasonal (months) scales. The satellite infrared temperatures were compared to simultaneous and collocated in situ drifter temperature measurements. They were corrected by removing biases obtained by regression analysis. The corrected images were used to produce maps representing daily, three-day, weekly and monthly Adriatic SSTs. Selected composites augmented by drifter overlays disclosed important quantitative features of the Adriatic.

For the period of May to October, 1995, the seasonal characteristics found were similar to those discovered in previous studies. The warming in springtime of the Po river area and along the Albanian coastline is consistent with Gacic et al.(1997). However, Gacic et al. reported a warm gyre over the middle Adriatic that is not apparent in this study, possibly due to the short duration (6 months) of this study compared to the 8 year study previously undertaken. Similarly, the summer season finds features discovered in previous studies present in our own data, with colder waters upwelling along the eastern coastlines and cyclonic gyres forming in the middle and southern Adriatic as summer and autumn progress. While the majority of the seasonal features persist between studies, the timing varies from one to another. Artegiani et al.(1997) determines the summer season lasts July to October while Gacic et al.(1997) concludes July, August and September comprise the summer. As the features change with season, our results suggest seasons consisting of a spring that lasts from May to June, a summer from July to only the end of August, and autumn commencing in September. This may be a conclusion unique to this study because only 6 months of data were used. Transition from the summer regime with warm water to the west and cold water to the east to the autumn/winter regime with opposite thermal gradients occurs between September and October, a month earlier than the results of Gacic et al.(1997). A temperature minimum is evident in the center of the southern Adriatic in September. The middle and southern basins are already split by a longitudinal thermal gradient in October (vs. in November in Gacic et al., 1997). The maximum temperature in the Jabuka Pit area in spring is not

substantiated by our observations. However, the warm (anti-cyclonic) feature north of the Jabuka Pit is evident in October in both Gacic et al.'s (1997) and our results.

Weekly composites, augmented with surface trajectories, reveal sub-basin and mesoscale features in the surface waters of the Adriatic. The combination of SST anomaly and drifters demonstrated such features as coastal upwelling, thermal fronts, river runoff, sub-basin gyres, and frontal meanders. While these features may have been found by either method of observation, they were enhanced by the combination of SST composites and drifters.

Mesoscale structures require short time (1 to 3 day) averaging combined with full spatial resolution. Comparison of 1-day and 3-day composites to weekly composites show the difference short term compositing can make in the evolution of features. Weekly and monthly composites show upwelling is the primary event occurring in the southern Adriatic during the month of July, but without the relatively small time period, features such as cold upwelling filaments extending into the Otranto Strait would be missed as individual thermal events. Drifter displacements confirm the uniqueness of the filaments and their progression over short times. Likewise, the southbound cold water parcel is invisible in October monthly and weekly composites, demonstrating the necessity of short term (1 to 3 day) compositing to study mesoscale structures.

Blending of satellite thermal data and in situ drifter measurements provide an optimum representation of the surface temperature and circulation fields. The drifter data used in this study enabled us to correct (or calibrate) the satellite infrared temperatures allowing the creation of thermal maps with no systematic bias and a RMS accuracy of less than 1°C. On the other hand, the shape and evolution of the SST patterns provides a qualitative spatial extension of the drifters current measurements, supporting the observation that temperature can be considered as a tracer that is advected by the currents. This is apparent in the remarkable agreement between drifter displacements and the evolution of surface thermal features.

VI. RECOMMENDATIONS

Application of similar AVHRR image processing for a longer period of time in the Adriatic and other regions of the Mediterranean Sea is in order. Extending the time period covered to a year and even multi-years, this method will provide the most accurate description of the Adriatic surface dynamics at scales ranging from tens of km and days (mesoscale) to the basin size (hundreds of km) and years.

Additionally, it is recommended that future studies calibrate satellite images with contemporaneous/collocated drifter data in other semi-enclosed seas to improve accuracy of the surface thermal fields.

LIST OF REFERENCES

- Artegiani, A., D. Bregant, E. Paschini, N. Pinardi, F. Raicich, and A. Russo, "The Adriatic Sea general circulation, Part II", *J. Phys. Oceanogr.*, 27: 1515-1534, 1997.
- Davis, R.E., "Drifter observations of coastal currents during CODE, 1985. The method and descriptive view," *J. Geophys. Res.*, 90: 4741-4755, 1985.
- Gacic, M., S. Marullo, R. Santoleri, and A. Bergamasco, "Analysis of the seasonal and interannual variability of the sea surface temperature field in the Adriatic Sea from AVHRR data (1984-1992)," *J. Geophys. Res.*, 102(C10), 22937-22946, 1997.
- Hansen, D.V. and P.-M. Poulain, "Processing of WOCE/TOGA drifter data," *J. Atmos. Oceanic Technol.*, 13:900-909, 1996.
- McClain, E.P., W.G. Pichel, and C.C. Walton, "Comparative performance of AVHRR-based multichannel sea surface temperature," *J. Geophys. Res.*, 90(C6), 11,587-11,601, 1985.
- Orlic, M., M. Gacic, P.E. La Violette, "The currents and circulation of the Adriatic Sea," *Oceanol. Acta*, 15: 109-124, 1992.
- Poulain, P.-M., P. Zanasca and A. Warn-Varnas, "Drifter observations in the Nordic Seas (1991-1995) - Data report," *SACLANTCEN Memorandum*, SM-299, Saclant Undersea Research Centre, La Spezia, Italy, pp. 95, 1996.
- Poulain, P.-M., E. Nacini, S. Pouliquen, P. Flament, "Adriatic Sea; Sea Surface Temperature Images from the NOAA Advanced Very High Resolution Radiometer 9 May to 22 October," *IFREMER CD-ROM*, 1998.
- Poulain, P.-M., "Drifter Observations of Surface Circulation in the Adriatic Sea," 1999, in press.

Strong, A.E. and E.P. McClain, "Improved ocean surface temperatures from space-comparisons with drifting buoys," Bull. Amer. Meteor. Soc., vol. 65, pp. 138-142, 1984.

INITIAL DISTRIBUTION LIST

1. Defense Technical Information Center 2
8725 John J. Kingman Road, STE 0944
Ft. Belvoir, Virginia 22060-6218
2. Dudley Knox Library 2
Naval Postgraduate School
411 Dyer Rd.
Monterey, California 93943-5101
3. Chairman, Code OC 1
Department of Oceanography
Naval Postgraduate School
833 Dyer Rd. Room 328
Monterey, California 93943-5122
4. Professor Pierre-Marie Poulain (Code OC/PN) 4
Department of Oceanography
Naval Postgraduate School
833 Dyer Rd. Room 328
Monterey, California 93943-5122
5. Professor Philip A. Durkee (Code MR/DE) 1
Department of Meteorology
Naval Postgraduate School
Monterey, California 93943
6. Professor Pierre Flament 1
Department of Oceanography
University of Hawaii
1000 Pope Road
Honolulu, Hawaii 96822
7. Director 1
SACLANT Undersea Research Centre
SACLANTCEN CMR 426
APO-AE 09613-5000
8. LT Jason A. Vogt 2
9927 Milda Drive
Houston, Texas 77088